Chemical re-equilibration and dynamic recrystallization of minerals in the Almklovdalen Peridotite Massif, SW Norway.

MSc thesis by: Marc Breddels
Supervisors: dr. H.L.M. van Roermund & prof. dr. M.R. Drury
Utrecht University
14-08-2015

Abstract

The Western Gneiss Region (WGR) of SW Norway is characterized by the occurrence of numerous garnet peridotite bodies that were emplaced from the hanging-wall mantle into the subducted country rock gneisses of the Baltic basement by continental collision during the Scandian phase of the Caledonian orogeny (430-390 Ma). The Almklovdalen Peridotite Massif (APM) is one of such garnet peridotite bodies. The main objective of this Msc thesis is to determine the physical conditions (in terms of pressure and temperature) under which mantle rocks of the APM were emplaced into the subducting continental crust, when the coarse grained mantle wedge M1 porphyroclast assemblage recrystallized into a finer grained M2 assemblage. This is done by electron microprobe (EMP) analyses on samples/minerals from the APM and the application of geothermobarometric calculations to the results of the EMP analyses. The EMP analyses on minerals from the M1 porphyroclast assemblage yield homogeneous chemical profiles (linescans) for the most abundant elements interpreted to be a result of chemical re-equilibration by solid state diffusion during Scandian metamorphism. The contents of less mobile elements like Al in orthopyroxene and Cr in garnet are however lower in minerals from the M2 assemblage than in minerals from the M1 assemblage and have not completely re-equilibrated. Cr in garnet allowed the distinction between high-Cr M1 garnet porphyroclasts and low-Cr M2 garnet, which recrystallized together with M2 Cr-spinel during Scandian deformation/metamorphism. Geothermobarometry results yield similar temperature estimates for the M1 and M2 assemblage near 750 °C at 35 kbar when using the geothermometer/ geobarometer combination of T[OpxBK90] and p[NimisTaylor00], but an underestimation in PT conditions occurs for the M1 assemblage when the combination of T[OpxBK90] and p[BKN90] are used due to the high Al content of M1 orthopyroxene. The lower amount of Al in M2 orthopyroxene, together with the higher pressure estimate for the M2 assemblage from geothermobarometery suggest that the Scandian crustal emplacement of the APM may have involved prograde metamorphism.

Contents

1. Introduction

The bedrock of the Western Gneiss complex (WGC) exposed within the Western Gneiss Region (WGR) of SW Norway, represents an ancient exhumed continent-continent collision zone, which records the deep Caledonian subduction of the Baltica continental margin beneath the Laurentian continental margin resulting in deformation and metamorphism under high-pressure (HP) and ultrahigh-pressure (UHP) conditions (Krogh, 1977). The subduction/collision was soon followed by buoyancy-driven exhumation, which occurred during the Scandian phase of the Caledonian orogeny around 430-390 Ma (Carswell et al., 2003; Brueckner & Van Roermund, 2004; Spengler et al., 2009; Hacker et al., 2010). Evidence for subduction down to UHP conditions is given by the discovery of microdiamonds in the Baltica basement gneisses found in the NW part of the WGR (Dobrzhinetskaya, 1995), microdiamonds in megacrystic garnet websterite/peridotite in the NW WGR (Van Roermund et al., 2002; Vrijmoed et al., 2006), microdiamond in eclogites in the SW part of the WGR (Smith and Godard, 2013) and the presence of majoritic garnet in garnet peridotite bodies (Van Roermund and Drury, 1998; Van Roermund, 2009b). The discovery of UHP-stable minerals is in agreement with thermobarometric calculations on grt-omph-ky-phen-coe/qtz in eclogite (Ravna & Terry, 2004).

A unique feature of the WGR is the occurrence of numerous ultramafic bodies, consisting of garnet peridotite, garnet pyroxenite and chlorite peridotite that are enclosed in the basement gneisses (Van Roermund, 2009a,b). The garnet peridotites are composed of variable amounts of garnet, olivine, orthopyroxene and clinopyroxene. Two types of these orogenic garnet peridotites can be distinguished: Mantle wedge garnet peridotites (MWGP) and subduction zone garnet peridotites (SZGP) (Van Roermund, 2009b). The MWGP were emplaced by deformation and density driven sinking of pre-Caledonian peridotite from the sub-Laurentian mantle wedge into the subducting continental crust of Baltica during the Scandian orogeny (Brueckner, 1998; Brueckner and Van Roermund, 2004; Van Roermund 2009b; Brueckner et al., 2010). An emplacement model for intruding peridotites into subducting slabs of continental crust is given by Brueckner (1998) (Fig. 1.1). For MWGP crustal emplacement must have occurred from the garnet-olivine stability field of the overlying subcontinental lithospheric mantle. Exhumation of the subducted continental crust of Baltica with its mantle-derived peridotite/pyroxenite cargo occurred in the late Scandian after slab detachment, leading to rapid buoyant exhumation of the less dense subducted crustal rocks with respect to the surrounding mantle rocks (Brueckner, 1998; Brueckner and Van Roermund, 2004; Brueckner et al., 2010).

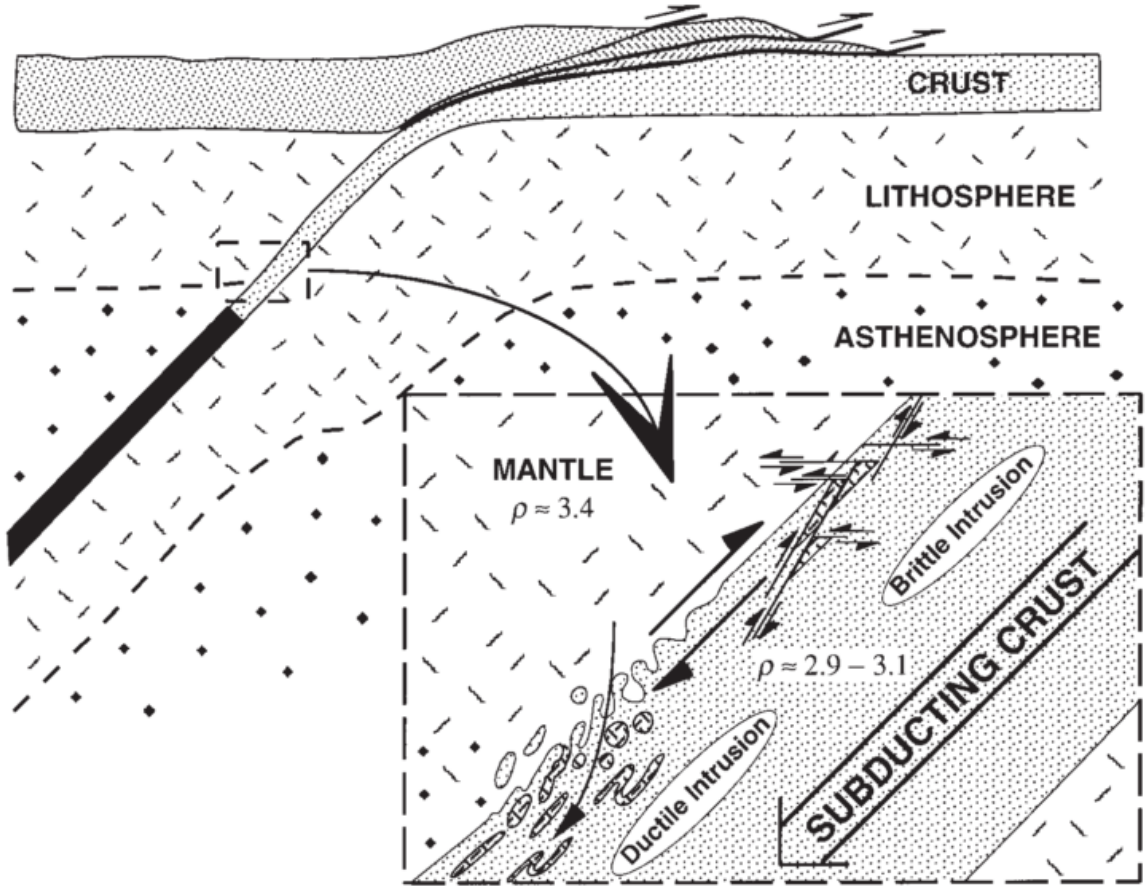

Figure 1.1: ***Brueckner, 1998.*** **Emplacement model for intruding peridotites into subducting slabs of continental crust. Ductile and brittle intrusion of mantle material into the subducting continental crust driven by density contrast is illustrated. (Brueckner, 1998).**

SZGP is formed by prograde metamorphism of low-pressure protoliths like serpentinites or spinel peridotites to (ultra-) high pressure garnet peridotite/garnet pyroxenite/eclogite (Van Roermund, 2009b). The prograde metamorphism occurred by deep continental subduction below the spinel-garnet phase transition in the mantle during the Scandian orogeny (Spengler et al., 2009). The main difference between MWGP and SZGP is that MWGP can have UHP garnet-olivine assemblages of pre-Scandian (Archean and Proterozoic) age, while SZGP only contains Scandian age UHP garnet-olivine assemblages (Van Roermund, 2009b). This difference is illustrated in the paragenetic diagram by Van Roermund (2009b) (Fig. 1.2). The garnet-olivine assamblages in MWGP may have formed in the stages M1 (Archean) and/or M2 (Proterozoic), while the garnet-olivine assemblages in SZGP have formed in stage M3a (Scandian) (Fig 1.2).

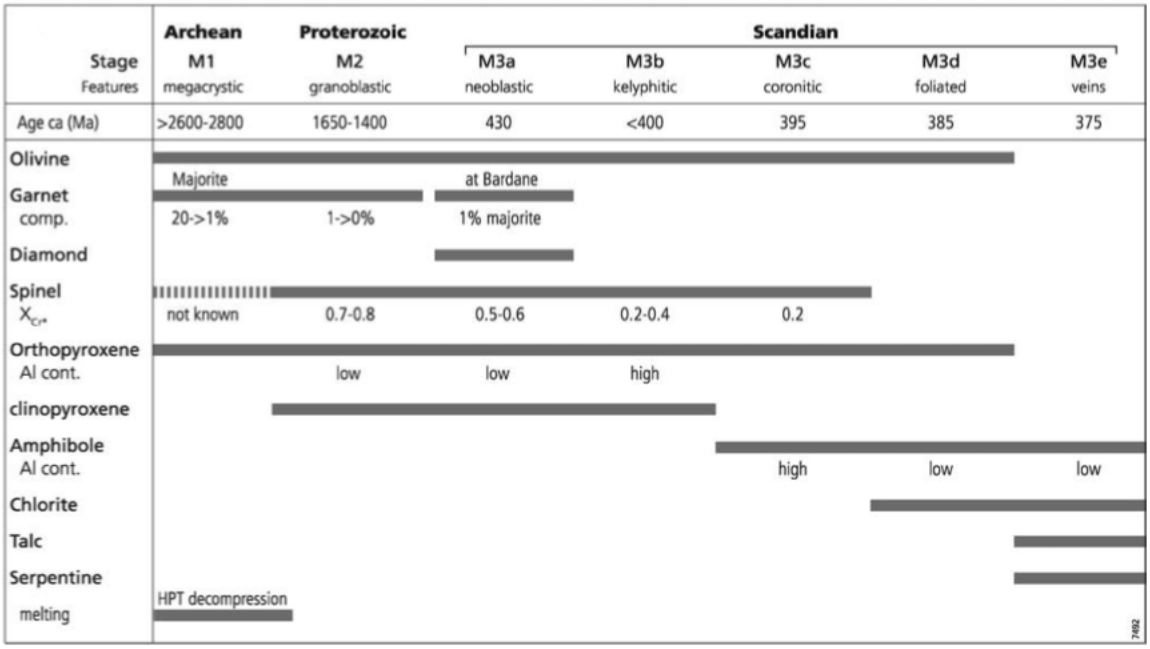

Figure 1.2: *Van Roermund, 2009b.* Paragenetic diagram for mantle derived garnet-bearing peridotites in the Northern UHPM terrain, Western Gneiss Region, Norway (Van Roermund, 2009b). The garnet-olivine assamblages in MWGP may have formed in the stages M1 (Archean) and/or M2 (Proterozoic), while the garnet-olivine assemblages in SZGP have formed in stage M3a (Scandian).

The garnet peridotite bodies and eclogites in the WGR have been the subject of numerous studies over the last decades. Such studies involve for example: 1) The dating of the pre-Caledonian mantle mineral assemblages (Brueckner et al., 2010; Beyer et al., 2012) and/or the Scandian UHP assemblages (Carswell et al., 2003; Hacker, 2007). 2) Estimating pressure and temperature conditions of pre-Caledonian mantle mineral assemblages and/or Scandian UHP assemblages (Carswell, 1986; Van Roermund, 1998, 2009a; Spengler et al., 2009). 3). Estimating pressure and temperature conditions of country rock eclogite and gneisses (Ravna & Terry, 2004). Combining the results of these studies allows the formation of Scandian peak metamorphic temperature and pressure contour map across the WGR (Fig 1.3) (Griffin et al., 1985; Wang et al., 2013). On this map an increase in Scandian peak metamorphic temperature can be seen from the SE part of the WGR towards the NW with three UHP domains along the West-coast (Fig. 1.3). The highest PT conditions for Scandian metamorphism in the WGR are found for samples from the North-Western UHP domain (the Fjørtroft, Flemsøy, Otrøy region), where pressures near 6 GPa and temperatures between 850-950 °C are reported (Van Roermund, 2009a; Spengler et al., 2010).
In figure 1.3 the occurrences of Mg-Cr type garnet peridotite, Fe-Ti type garnet peridotie, UHP eclogite, coesite, microdiamond and majoritic garnet in the WGR are indicated. One of the locations where Mg-Cr type garnet peridotite occurs is at Almklovdalen, a village located inside the SW UHP domain (Fig. 1.3). At Almklovdalen a large ultramafic body is situated mainly consisting of dunite with local occurrences of garnet peridotite, garnet pyroxenite and eclogite. The Almklovdalen peridotite massif (APM) will be the topic of the present study.

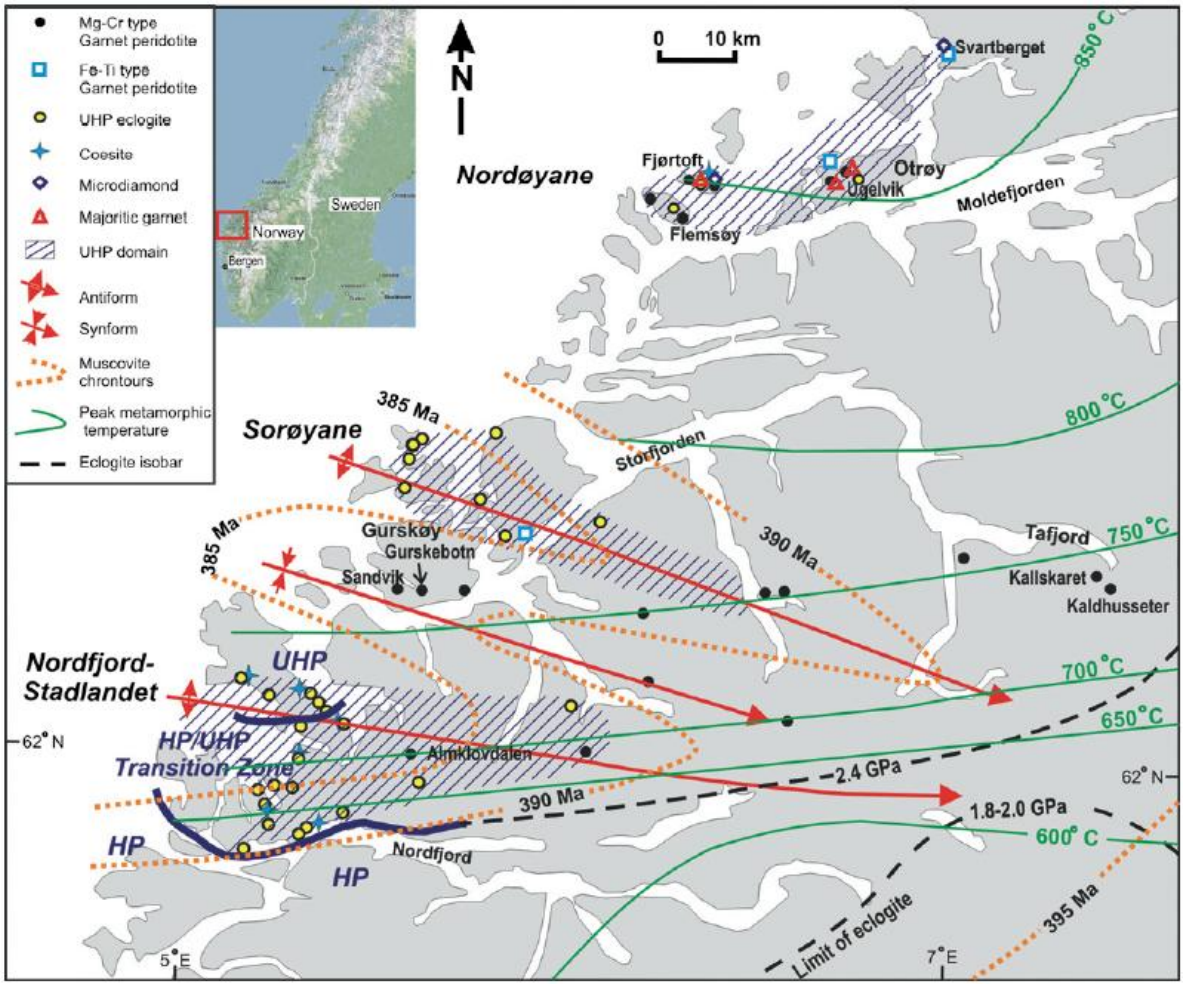

Figure 1.3: Overview of pressure and temperature estimates for the Scandian peak metamorphism from earlier studies in the Western Gneiss region as well as age estimates for muscovite, major fold axes, HP and UHP domains and coesite, microdiamond, majoritic garnet locations (Wang et al., 2013 and references therein).

The APM is of the mantle wedge garnet peridotite type and therefore incorporated in the continental crust during the collision between Laurentia and Baltica during the Scandian phase of the Caledonian orogeny (Brueckner et al., 2010). The pre-Scandian evolution of the APM is thought to consist of large scale depletion by decompression melting during the Archean (M1 in Fig. 1.2), resulting in high amounts of depleted dunite (Mg# 92-93) (Beyer et al., 2006; Brueckner et al., 2010). Dating of the melt extraction was done by Re-Os dating applied to dunite samples (Spengler, 2006; Beyer et al., 2006; Brueckner et al., 2010). After the Archean, refertilization (M2 in Fig 1.2) occurred by intrusion of mafic melts during one or multiple refertilization events, illustrated by veins and dikes of garnet peridotite, garnet pyroxenite and eclogite inside the depleted dunite (Beyer et al., 2006; Brueckner et al., 2010). Dating of the refertilization events gives Sm-Nd mineral isochron ages between 1.8 and 1.65 Ga (Gothian) as well as between 1.3 and 0.8 Ga (Sveconorwegian) (Brueckner et al., 2010). A final refertillization event is related to the Caledonian orogenic cycle. This event caused Fe-Ti tholeitic dikes to intrude the APM, which were subsequently metamorphosed

into eclogite by prograde UHP metamorphism (Griffin & Qvale, 1985).

No prograde metamorphic path has been reported for the peridotites of the APM, but are instead incorporated in the subducting continental slab of Baltica when it was exhumed back towards the surface (Brueckner et al., 2010). This is backed up by geothermobarometric results from Pijpers (2012), in which Electron Microprobe (EMP) mineral chemical data of M1 mineral assemblages of peridotites and pyroxenites from different localities within the APM are used to estimate pressure and temperature conditions during crustal incorporation (Fig. 1.4). The mineral chemical data from other localities than Gusdal Quarry used by Pijpers (2012) are from earlier studies by: Lappin (1974), Medaris (1980), Carswell (1981). The PT results illustrated in figure 1.4 are for the porphyroclast assemblage, representing the mantle mineral assemblage present within the hanging wall during the proterozoic before the onset of Caledonian suduction (Pijpers, 2012). 2 sets of geothermeters and barometers were used to estimate the temperature conditions for the APM illustrated in figure 1.4. These estimated temperature conditions range between 695 °C and 778 °C, which is in agreement with the temperature contours over Almklovdalen from previous studies (Fig 1.3). The pressure estimates range from 22 to 35 kbar (Fig 1.4). The geothermobarometric calculations done by Pijpers (2012) yield similar PT conditions for the recrystallized Caledonian assemblage. This suggests that chemical re-equilibration by intracrystalline diffusion took place during the crustal emplacement of the APM (Pijpers, 2012).

$T_{Powell85}$ + $P_{NimisTaylor00}$		
Locality	**Temperature (°C)**	**Pressure (kbar)**
Gusdal Quarry	712 ± 17	31 ± 2
Lien (core)	750	28
Lien (rim)	700	33
Rødhaugen (core)	747 ± 7	22,5
Rødhaugen (rim)	695 ± 5	22 ± 1
T_{EG79} + $P_{NimisTaylor00}$		
Locality	**Temperature (°C)**	**Pressure (kbar)**
Gusdal Quarry	740 ± 20	32 ± 3
Lien (core)	778	30
Lien (rim)	728	35
Rødhaugen (core)	775 ± 7	23,5
Rødhaugen (rim)	725 ± 8	23 ± 1

Figure 1.4: Geothermobarometric results for different localities within the Almklovdalen peridotite massif (Pijpers, 2012). The chemical EMP data used is from the homogenized pre-Caledonian porphyroclast assemblage.

The APM also contains boudinaged lenses of eclogite within the massif, which are classified as 'internal' eclogites, due to their location within a peridotite massif (Griffin & Qvale, 1985; Van Roermund, 2009a). The occurrences of eclogites within the country rock gneisses are classified as 'external' eclogites (Griffin & Qvale, 1985; Van Roermund 2009a). The external eclogites are Fe-rich and thought to have originated by Scandian prograde metamorphism of amphibolites and/or basalt/gabbros, because these eclogites reveal prograde mineral zoning in garnet (Griffin & Qvale, 1985; Van Roermund, 2009a).

According to the temperature contours constrained from earlier studies throughout the WGR (Fig. 1.3), the APM is located at 700 °C for the Scandian peak metamorphic temperature, with a pressure in the HP/UHP transition zone (Wang et al., 2013). The main objective in this MSc thesis is to estimate the physical conditions under which the (dynamic) recrystallization of the M1 porphyroclast crystals at the APM took place. This is done to say something about the physical conditions (in terms of pressure and temperature) operating in the mantle rocks during crustal emplacement, when the coarse grained mantle wedge M1 porphyroclast assemblage recrystallized into a finer grained M2 assemblage. An additional objective is to investigate the degree of chemical homogenization by intragranular diffusion during prograde and retrograde metamorphism within the APM. To answer the above questions, garnet periodotite/pyroxenite and eclogite samples were taken from the Gusdal quarry locality within the APM. Different garnet peridotite/pyroxenite samples from Gusdal quarry were previously studied by J. Pijpers (2012), but those samples did not include internal eclogites. The eclogites that were sampled at the Gusdal Quarry will be compared to garnet peridotite/pyroxenite in terms of microstructure and chemical composition.

2. Geological setting and methods

2.1. Geological Setting

The Scandinavian Caledonides, now exposed as a deeply eroded mountain belt that stretches 1800 km along the coast of Norway (Fig. 2.1), formed as a result of a series of collisional events during the convergence and ultimately collision between the Baltic and Laurentian plates in the early Paleozoic (Roberts, 2003). The collision occurred during the 430-390 Ma Scandian orogeny and led to the final closure of the Iapetus ocean, the deep subduction of the crystalline basement rocks of the Baltic shield and the South-Eastward thrusting of allochthonous nappes over the basement rocks of the Baltic shield (Brueckner et al., 2010; Hacker & Andersen, 2010). The allochthons were thrusted up to several hundreds of kilometers towards the SE over the Baltic shield and can be divided into four main tectonostratigraphic units: The lower, middle, upper and uppermost allochthons (Fig.2.1) (Roberts, 2003; Gee et al., 2008). The lower and middle allochthons consist of shelf and continental rise successions originating from the western margin of Baltica (Roberts, 2003). The upper allochton consists of oceanic and magmatic arc associations from the Iapetus ocean (Roberts, 2003). The uppermost allochton is thought to consist of rocks of Laurentian affinity (Roberts, 2003). The lowermost tectonostratigraphic unit in the Scandinavian Caledonides is the un-reworked autochthonous crystalline basement of the Baltic shield, exposed east of the Caledonian thrust front (Beyer et al., 2006). A large exposure of this basement, interpreted to be the outermost western part of the basement that was reworked during the Caledonian, can be found in the Western Gneiss Region (WGR) of Western Norway (Beyer et al., 2006).

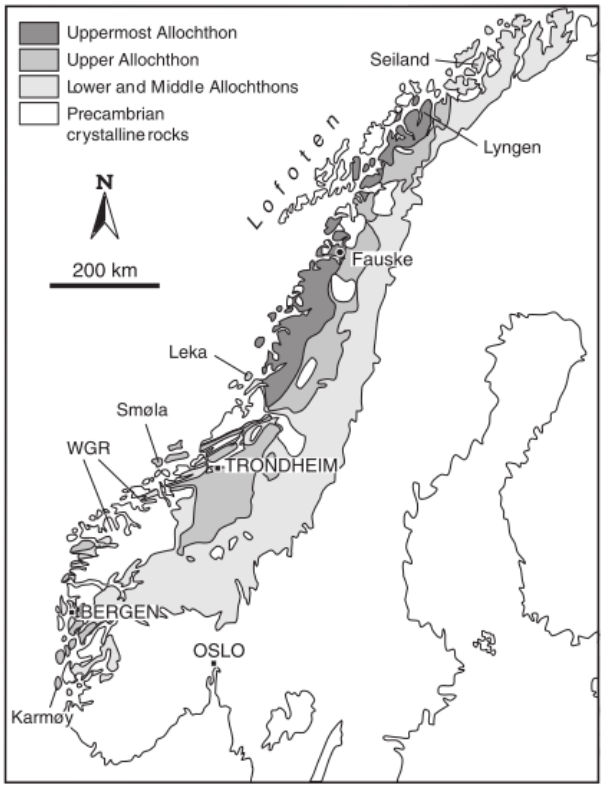

Figure 2.1: Tectonostratigraphy of the Scandinavian Caledonides (Roberts, 2003).

The rocks in the WGR mainly consist of orthogneisses that formed by magmatism during the mid to late proterozoic and are often referred to as the Western Gneiss Complex (WGC) (Brueckner et al., 2010; Hacker & Andersen, 2010). The WGC is thought to be the Western part of Baltica during the final collision with Laurentia and therefore subducted deeply beneath Laurentia during the Scandian orogeny (Brueckner et al., 2010). The intensity of Scandian deformation and metamorphism increases throughout the WGC from the SE towards the NW as is evident from the temperature contour map illustrated in Fig. 1.3 and the presence of UHP metamorphic domains present in the Western parts of the WGC (Hacker et al., 2010;Wang et al., 2013). The increase in intensity of deformation and metamorphism from SE to NW in the WGC is thought to reflect deeper subduction towards the NW during the Scandian (Carswell et al., 2003; Van Roermund,2009a,b; Hacker et al.,2010; Wang et al., 2013). Retrograde metamorphism during the exhumation of the WGC occurred under amphibolite and greenschist facies conditions and is partly associated with hydration (Cordellier et al., 1981; Kostenko et al., 2002).

Within the gneisses of the WGC, abundant boudins of eclogite can be found, consisting of HP-quartz stable and UHP-coesite/diamond stable eclogites (Brueckner et al., 2010; Hacker et al.,2010). Additionally, peridotite bodies composed of Mg-Cr peridotite and Fe-Ti peridotite occur in the WGR (Fig. 1.3). One of the largest peridotite bodies in the WGR of Norway is the Almklovdalen Peridotite Massif (APM), located about 5km to the SE of the

village of Åheim (Fig. 2.2). This peridotite body outcrops over an area of 8.0 km^2 and is intensely deformed by multiple orogenic events (Cordellier et al., 1981; Osland, 1997). The core of the APM consists of layered dunites and chlorite-bearing dunites, with increasing serpentinization towards the contact with the surrounding gneisses (Fig. 2.2) (Cordellier et al., 1981; Osland, 1997). The dunites at Almklovdalen/Sunndalen are remarkably fresh and mined for their high olivine Mg# (92-93) used for applications in the steel industry (Osland, 1997). Mining was formerly done by A/S olivine and presently by the Sibelco mining group. The zone of serpentinization is up to 150 m thick along the Northern zone and 300 m thick along the Southern zone (Osland, 1997). Near the Northern contact at the Gusdal quarry locality, eclogite boudins occur that are up to 2 m thick and 20 m long (Osland, 1997). The eclogite boudins can be found for 300 m along strike near the Northern contact (Fig. 2.2) and vary from unaltered eclogite to amphibolite with remnants of an eclogitic structure (Osland, 1997). Garnet peridotite and garnet websterite occur in several localities within the APM (Fig.2.2) along the strike of the compositional layering (Cordellier et al., 1981; Osland, 1997). The peridotites occur as layers of several decimeters thick with alternations of garnet-rich and garnet-poor rocks (Medaris, 1980). At locations of increased shearing near the boundaries of garnet-peridotite layers, increasing amounts of chlorite and amphibole occur, as well as kelyphitic rims around garnet (Medaris, 1980; Cordellier et al., 1981; Osland, 1997). The garnet-rich layers inside the APM are thought to have formed by refertilization of the strongly depleted dunite during the mid and/or late Proterozoic due to intrusion of asthenospere derived melts (Beyer et al., 2006).

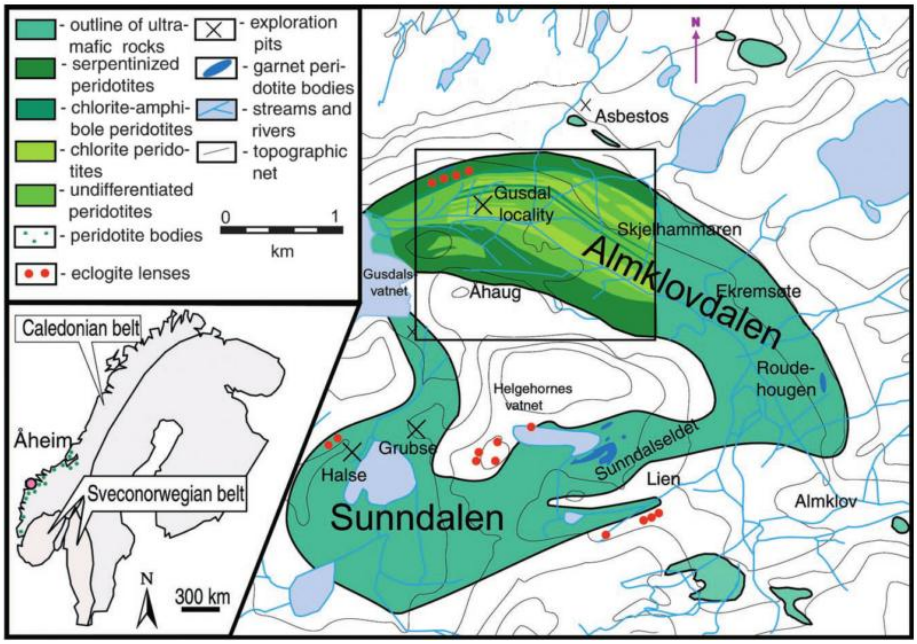

Figure 2.2: A map of the Almklovdalen peridotite massif near Åheim, Western Gneiss Region, Norway including the compositional layering at the Gusdal quarry location (Kostenko et al., 2002).

A structural study of the APM done by Cordellier et al., (1981) resulted in the recognition of 4 main deformation events. The compositional banding (S_0) is defined by dm-scale layers of garnet-peridotite and garnet-websterite, which represent the remnants of a M_1 mantle wedge assemblage (Fig. 2.3)(Cordellier et al., 1981; Osland, 1991; Prelicz, 2005). The oldest deformation phase (D_1) involves isoclinal folding of the compositional banding (S_0) (Cordellier et al., 1981). The first deformation phase (D1) is inferred to be of proterozoic age and is defined by the shape and/or crystallographic preferred orientation of the major HP/UHP rock forming minerals (Van Roermund, 2009b). A second deformation phase (D_2) (inferred to be of Scandian age) is associated with chloritization of garnet and shear zone generation, producing a S_2 foliation and bounding the garnet peridotite lenses (Fig. 2.3)(Cordellier et al., 1981). A third retrograde deformation phase (D_3) produced a S_3 foliation and is preserved in the major part of the peridotite body (Fig. 2.3)(Cordellier et al., 1981). S_2 and S_3 represent retrograde Scandian foliations and therefore represent the M_2 and M_3 microstructural sequence. The fourth and last deformation phase (D_4) is responsible for the large scale folding of the APM, deforming the S_3 foliation and producing an E-W striking S_4 foliation in the surrounding gneisses (Fig. 2.3)(Cordellier et al., 1981). Although four deformation stages were identified, a continuous retrograde deformation path evolving from the garnet-peridotite facies to the amphibolite facies is suggested (Cordellier et al., 1981). Retrograde deformation was also accompanied by the introduction of fluids (Cordellier et al., 1981).

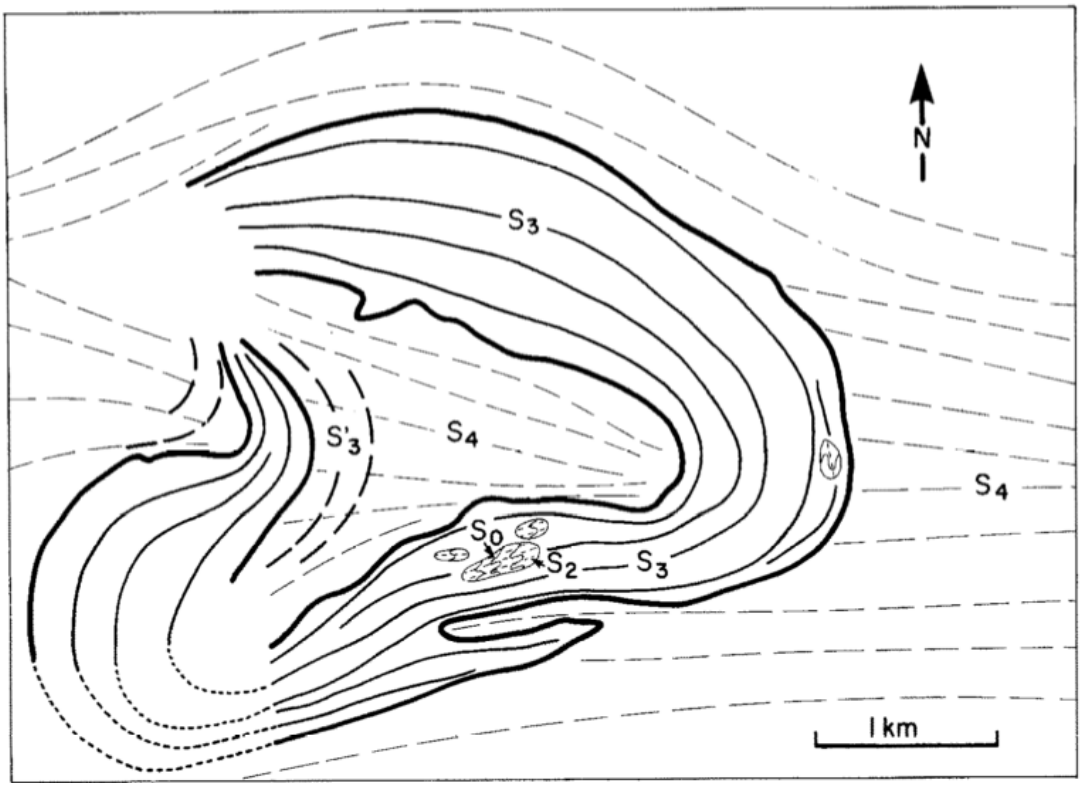

Figure 2.3: Interpretative structural map of the APM (Cordellier et al., 1981). The thick continuous lines represent foliations in the peridotite body and the dashed lines represent foliations in the surrounding gneisses. S_0 represents compositional layering in garnet peridotite, S_1 is parallel to S_0 and represents the isoclinal folding of S_0, S_2 represents the folding of garnet peridotite, S_3 represents the large scale foliation in the peridotite massif and S_4 represents the late stage deformation of the country rock gneisses.

2.2. Methods

In the summer of 2012, 15 garnet peridotite/garnet pyroxenite/eclogite samples were gathered by Herman van Roermund at the Gusdal Quarry locality within the APM (Fig. 2.2). The samples were taken from a new exploration blast in August, 2012. The 15 samples collected at Gusdal Quarry are numbered sample01 to sample15. Not all of the samples were equally suitable for electron microprobe analysis due to a strong retrograde metamorphic overprint. The 6 best samples were selected to be used in this study. The 6 selected samples are referred to as sample 2 (garnet, olivine-bearing websterite), sample 4 (garnet, olivine-bearing websterite), sample 7 (eclogite), sample 9 (epidote-eclogite), sample 11 (garnet websterite) and sample 12 (garnet websterite). Only these 6 samples are described in the sections for hand specimen analysis (section 3.1), thin section description (section 3.2) and mineral chemistry (section 3.4).

The 6 hand specimens collected for this study were studied for basic mineral identification and microstructural information (section 3.1).

From each sample thin sections were made to be used for optical microscopy (OM) and electron microprobe (EMP) analysis. The thin sections were studied under the optical microscope to look in more detail to the microstructure of the rocks and the various mineral assemblages. Flatbed scans of the thin sections in both plane-polarized light (ppl) and cross-polarized light (xpl) were made to gain an overview of each sample (Fig. 3.2A is an example of a ppl flatbed scan). Optical microscopy was also used to make selections of locations suitable for EMP analysis. To gather additional micro-structural information back-scattered electron (BSE) images were made using the EMP. The thin section description in terms of microstructure in relation to stable mineral assemblages can be found in section 3.2. An interpretation of the microstructure in relation to stable mineral assemblages (including paragenetic diagrams) is given in section 3.3.

The major element chemical composition of the selected samples was derived using a JEOL JXA8600 Electron Microprobe located at Utrecht University. The conditions of operation were 15kV, 20nA and a 30s counting time in WDS mode. The precision of major element analysis is ± 2.5%. For quick mineral identification EDS analyses were used.

To gain detailed data of the chemical variation throughout the minerals linescans were made. These linescans are made by selecting a start and end position under the electron microprobe and choosing a number of points in between. At each of the selected linescan points a WDS analysis was performed. For most linescans the starting location was set at the rim of a grain, with the end location at the opposite rim to make a chemical profile that goes straight through the core of the grain. In this way the chemical data can also easily be separated in core and rim data. The linescan data as well as the location within the thin section where the linescan was taken can be found in the appendix. In the images the

location of the linescan is indicated together with an arrow symbol indicating the start of the linescan.

The chemical data obtained from microprobe analysis was normalized using a free spreadsheet downloaded from http://serc.carleton.edu/research_education/equilibria/mineralformulaerecalculation.html This spreadsheet also allows the calculation of Fe^{3+} using stoichiometry and charge balance. End member plots for the different minerals were made using the triplot spreadsheet created by Graham and Midgley, (2000). The results of the chemical composition of minerals are presented in section 3.4.

The physical conditions in terms of pressure and temperature under which the various stable mineral assemblages in the rocks were formed were estimated using a method called 'geothermobarometry'. Geothermobarometric methodologies, reviewed by Krogh Ravna and Paquin (2003), were used. This method requires the EMP analyses of minerals from stable assemblages, which are assumed to be in equilibrium, as input data to derive pressure and temperature conditions. The geothermobarometric results are presented in chapter 4.

In the following sections the references to figures are such in the text: Figures in this MSc thesis are numbered by chapter and image number (example: Fig. 3.1. for thesis chapter 3 figure 1). Figures located in the appendix have an A in front of the image number (example: Fig. A1).

3. Results

3.1. Hand sample description

After selection the investigated rock samples are: Sample 2, 4, 7, 9 , 11 and 12. Macroscopic petrographic characteristics are described below.

Sample 2. Garnet olivine-bearing websterite

The sample contains a bimodal grain size distribution (Fig. 3.1A). The coarse grains are called porphyroclasts and are surrounded by a fine grained recrystallized matrix. The porphyroclast to matrix ratio is approximately 50% to 50%. The porphyroclast assemblage consists of a about 80% dark brown/yellow orthopyroxene crystals (up to 15 mm in size), about 15% dark ruby-red garnet crystals (with sizes up to 5 mm) and about 5% brightly green colored clinopyroxene crystals (with sizes up to 4 mm). The fine-grained recrystallized matrix has a grain size up to 1 mm and consists of about 70% yellow orthopyroxene, about 20% green olivine and about 10% bright green clinopyroxene. Around garnet porphyroclasts reaction rims with a secondary retrograde amphibole is present. *Note: Recrystallized M2 garnet was found in this sample by EMP analysis*.

Sample 4. Garnet olivine-bearing websterite

The sample contains a bimodal grain size distribution (Fig. 3.1B). Coarse grained porphyroclasts are surrounded by a fine grained recrystallized matrix. The porphyroclast to matrix ratio is approximately 30% to 70%. The porphyroclast assemblage in this sample contains about 70% large dark brown orthopyroxene crystals (up to 12 mm in size), about 20% bright green clinopyroxene (up to 5 mm in size) and 10% dark ruby-red garnet (up to 4 mm in size). The recrystallized matrix is up to 1 mm in grain size and consists of about 70% dark yellow orthopyroxene, 20% bright green clinopyroxene and 10% green olivine. In addition a retrograde assemblage can be recognized consisting of a dark kelyphitic rim around the garnet porphyroclasts and a grey chlorite group mineral in the matrix. *Note: No recrystallized M2 garnet was found in this sample by EMP analysis.*

Sample 7. Eclogite

The sample is characterized by a bimodal grain size distribution (Fig. 3.1C). Coarse grained porphyroclasts are surrounded by a fine graine recrystallized matrix. The porphyroclast to matrix ratio is about 50% to 50%. The porphyroclasts assemblage consists of red-brown garnet crystals (up to 10 mm in size). The garnet porphyroclasts are sometimes elongated (see also the thin section in Fig. 3.4). The matrix dominantly consists of fine-grained green

clinopyroxene up to 1 mm in size (about 95%), which is interpreted to have dynamically recrystallized. Near garnet porphyroclasts fine crystals of garnet up to 1 mm in size can be found in the matrix (about 5%), suggesting that garnet may also have recrystallized in this sample. The retrograde assemblage consists of a dark amphibole located around garnet porphyroclasts and/or as dark bands throughout the matrix. *Note: Recrystallized M2 garnet was found in this sample by EMP analysis.*

Sample 9. Allanite-bearing Eclogite

The sample is characterized by a bimodal grain size distribution (Fig. 3.1D). Coarse grained porphyroclasts are surrounded by a matrix of recrystallized minerals and secondary minerals. The porphyroclast to matrix ratio is approximately 40% to 60%. Large red/pink garnet crystals with a grain size up to 10 mm form the porphyroclast assemblage of this sample. The matrix consists of recrystallized green clinopyroxene with a grain size up to 1 mm. Secondary minerals in the matrix consist of a black amphibole and brown/yellow allanite. *Note: <u>No</u> recrystallized M2 garnet was found in this sample by EMP analysis.*

Sample 11. Garnet websterite

The sample contains a bimodal grain size distribution (Fig. 3.1E). Coarse grained porphyroclasts are surrounded by a fine grained recrystallized matrix. The porphyroclast to matrix ratio is approximately 40% to 60%. The porphyroclast assemblage consists of about 80% dark brown/yellow orthopyroxene crystals (up to 10 mm in size), about 10% green clinopyroxene (up to 5 mm in size) and about 10% dark ruby-red garnet (up to 4 mm in size). In the matrix a recrystallized assemblage consisting of about 85% yellow/brown orthopyroxene and 5% green clinopyroxene exists. No olivine was found in this sample. A retrograde phase is present as a dark kelyphitic rim around garnet porphyroclasts. *Note: Recrystallized M2 garnet was found in this sample by EMP analysis.*

Sample 12. Garnet websterite.

The sample is characterized by a bimodal grain size distribution (Fig. 3.1F). Coarse grained porphyroclasts are surrounded by a fine grained recrystallized matrix. The porphyroclast to matrix ratio is approximately 40% to 60%. The porphyroclast assemblage in this sample consist of about 70% dark brown/yellow orthopyroxene crystals (up to 10 mm in size), about 10% green clinopyroxene crystals (up to 5 mm in size) and 20% dark ruby-red garnet (up to 5 mm in size). The recrystallized matrix has a grain size up to 1 mm and consists of about 75% yellow/brown orthopyroxene, about 25% green clinopyroxene. The retrograde assemblage consists of a dark green amphibole in the matrix and a black kelyphitic rim around garnet. *Note: <u>No</u> recrystallized M2 garnet was found in this sample by EMP analysis.*

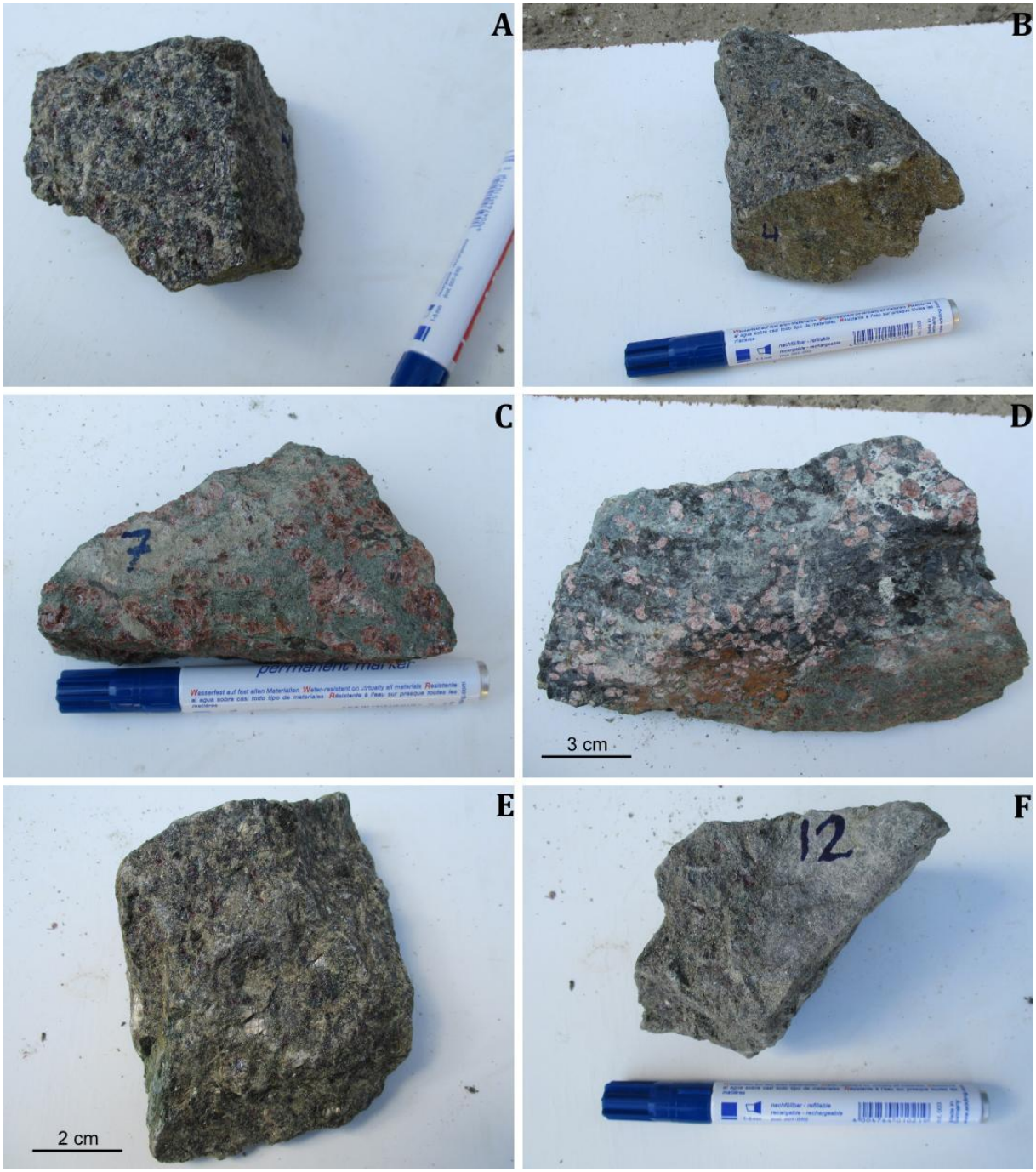

Figure 3.1: Investigated hand specimen from Gusdal Quarry within the Almklovdalen peridotite massif. The size of the marker is 12 cm. (A.) Sample 2. (B.) Sample 4. (C.) Sample 7. (D.) Sample 9. (E.) Sample 11. (F.) Sample 12.

3.2. Thin section description

In the hand specimen description section (section 3.1) a bimodal grainsize distribution has been recognized for all samples, consisting of coarse grained porphyroclasts and a fine grained recrystallized matrix. The porphyroclast assemblage will be called M1 and the recrystallized assemblage will be called M2. The retrograde mineral assemblage will be called M3. In this section the thin sections of sample 2, 4, 7, 9, 11 and 12 will be described in terms of stable mineral assemblages and microstructure. In the figures of this section, the abbreviations used to indicate minerals in figures are: gnt=garnet, opx=orthopyroxene, cpx=clinopyroxene, ol=olivine, spl=spinel, ilm=ilmenite, clch=clinochlore, kely=kelyphitic rim, pent=pentlandite and all=allanite. The numbers following the abbreviation refers to the assemblage in which the mineral is stable (example: opx2 refers to M2 opx).

Sample 2.

An overview of the thin section of this garnet olivine-bearing websterite can be found in Fig. 3.2A. From this image it can be seen that the M1 porphyroclastic mineral assemblage consists of garnet, orthopyroxene and clinopyroxene. The M1 porphyroclasts are randomly orientated. M1 Garnet is pink under PPL and may have a thick black M3 retrograde kelyphitic rim around the M1 porphyroclasts. Some M1 garnet porphyroclasts contain inclusions of orthopyroxene or clinopyroxene. M1 garnet porphyroclast domains are sometimes split into multiple segments with M2 matrix minerals or M3 retrograde minerals in between. M1 orthopyroxene is pale yellow to pale brown under PPL and contains exsolution lamellae of ilmenite. M1 clinopyroxene is light green under PPL, has a well-developed cleavage in 1 direction with a poorly developed cleavage at 90° to the first and has exsolution lamellae of spinel. A fine grained recrystallized matrix is present in between the porphyroclasts, consisting of M2 orthopyroxene, clinopyroxene, olivine and ilmenite. The crystals from the M2 microstructure are polygonal, strain free and have straight grain boundaries meeting in triple junctions at 120° angles (Fig 3.2B). In contrast, the M1 porphyroclasts are heavily strained since they contain cracks, kinks, subgrains, undulatory extinction and have an anhedral shape. This is taken as evidence for dynamic recrystallization through subgrain rotation. The abundance of M2 clinopyroxene and M2 orhopyroxene increases near M1 porphyroclasts of these minerals, while M2 olivine is more randomly distributed throughout the matrix. Locally, where the kelyphitic rim around M1 garnet is absent, small garnet crystals can be found within the M2 orthopyroxene polygonal microstructure that appear to be stable with M2 orthopyroxene and may therefore represent M2 recrystallized garnet (Fig. 3.2C). This M2 garnet appears to have grown together with fine grained M2 spinel. The retrograde assemblage consists of green pleochroic M3b amphibole replacing clinopyroxene and a M3a kelyphitic rim around M1 garnet composed of M3a amphibole and M3a spinel intergrowths. Additionally, a small amount of M3b clinochlore is present in this sample, which is a member of the chlorite-group of minerals.

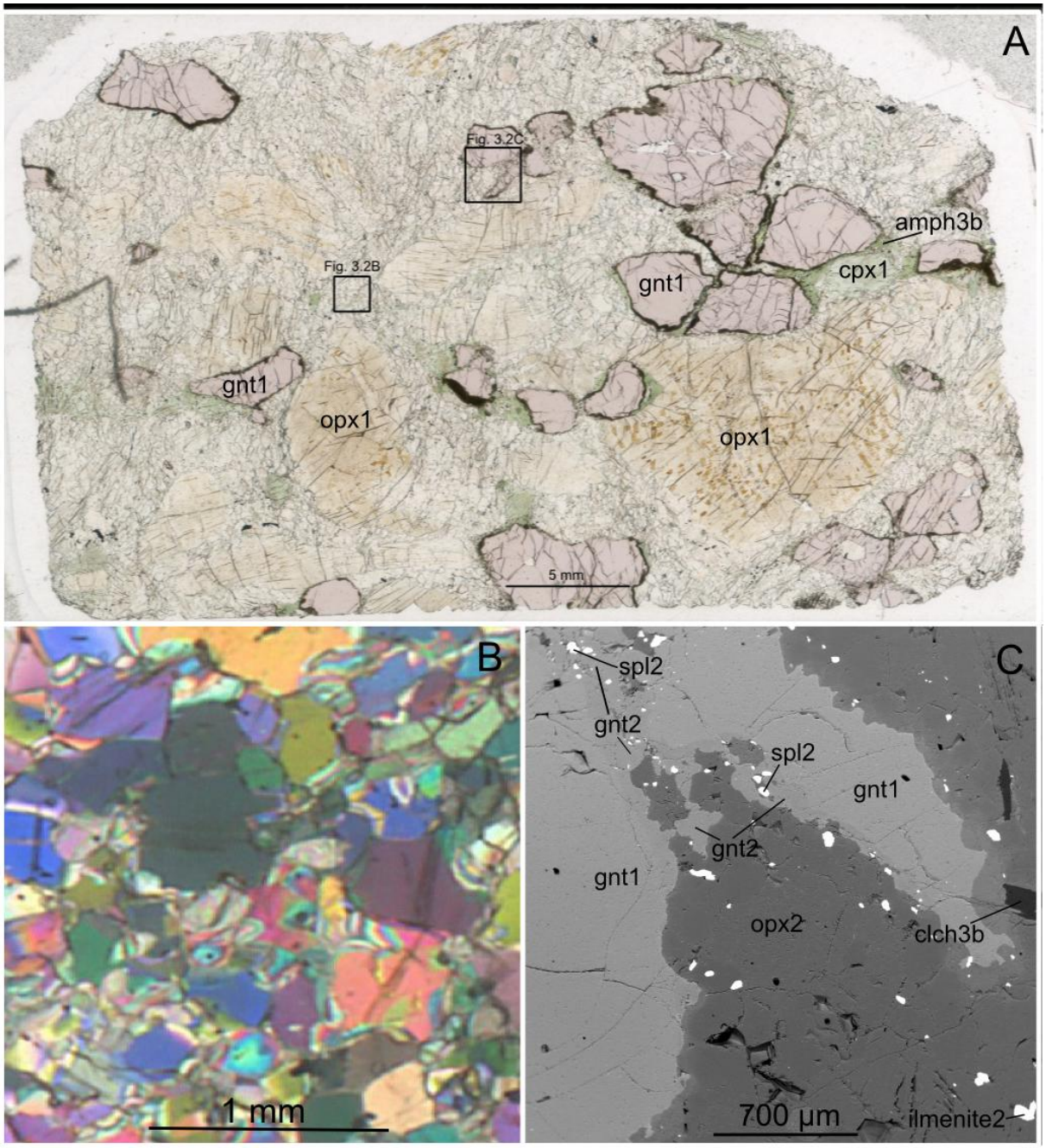

Figure 3.2: Sample 2. (A.) PPL overview of a thin section made from this garnet olivine-bearing websterite. The M1 porphyroclast assemblage of gnt-cpx-opx is surrounded by a matrix of the fine grained recrystallized M2 assemblage. The location of the images 3.2B and 3.2C are indicated. (B.) Cross-polarized light image of the polygonal microstructure in sample 2. (C.) BSE image of a locally recrystallized garnet porphyroclast. The small white minerals near M2 garnet are M2 spinel. A kelyphitic rim is absent around garnet in the middle of this image.

Sample 4.

An overview of the thin section of this garnet olivine-bearing websterite can be found in Fig. 3.3A. Randomly orientated porphyroclasts of orthopyroxene, clinopyroxene and garnet form the M1 mineral assemblage. Both M1 clino- and orthopyroxene contain exsolution lamellae. Some grains of M1 clino- and orthopyroxene domains are sometimes split into multiple segments with recrystallized M2 matrix minerals in between. M1 garnet has a black M3a kelyphitic rim around the crystals consisting of amphibole and spinel intergrowths. Retrogression of M1 garnet is inhomogeneous throughout the thin section, with some grains only affected by M3a kelyphitic retrograde overprinting, while other grains are also affected by infiltration of M3b chlorite. The M1 porphyroclasts are heavily strained since they contain cracks, kinks, subgrains, undulatory extinction and have an anhedral shape. The M2 recrystallized matrix assemblage in this section consists of orthopyroxene, clinopyroxene and olivine. The recrystallized M2 assemblage forms a polygonal microstructure defined by optically strain free grains with straight grain boundaries meeting at 120° triple point junctions. M2 clinopyroxene is mainly found in proximity to M1 clinopyroxene porphyroclasts, while M2 orthopyroxene is abundant throughout the entire section. The modal amount of M2 olivine increases towards the upper right part of the thin section. No recrystallized M2 garnet + M2 spinel have been observed in this sample, but may have been lost by retrograde overprinting. Coarse grained M1 olivine clasts have not been observed in the thin section, but are expected. Opaque minerals are relatively abundant in this sample and occur randomly distributed throughout matrix where they occur within triple junctions and M2 crystal grain boundaries. M3 retrograde minerals include clinochlore and the kelyphitic rim around garnet. M3b Clinochlore is found within the matrix together with opaque M3b FeNi-Sulfides (pentlandite) where they are interpreted to replace the M2 polygonal microstructure (Fig. 3.3B). M3b clinochlore is also present around strongly retrogressed M1 garnet porphyroclasts, where it occurs adjacent to the M3a kelyphitic rim around M1 garnet (Fig. 3.3C). Around the M1 garnet porphyroclast many small opaque minerals occur, interpreted to be M2 spinel that formed together with M2 garnet. M2 garnet was however completely replaced by M3a kelyphite. The larger opaque minerals are M3b pentlandite (Fig 3.3C). M3b FeNi-Sulfide always occurs near or adjacent to M3b clinochlore, suggesting that they formed after infiltration of a fluid phase.

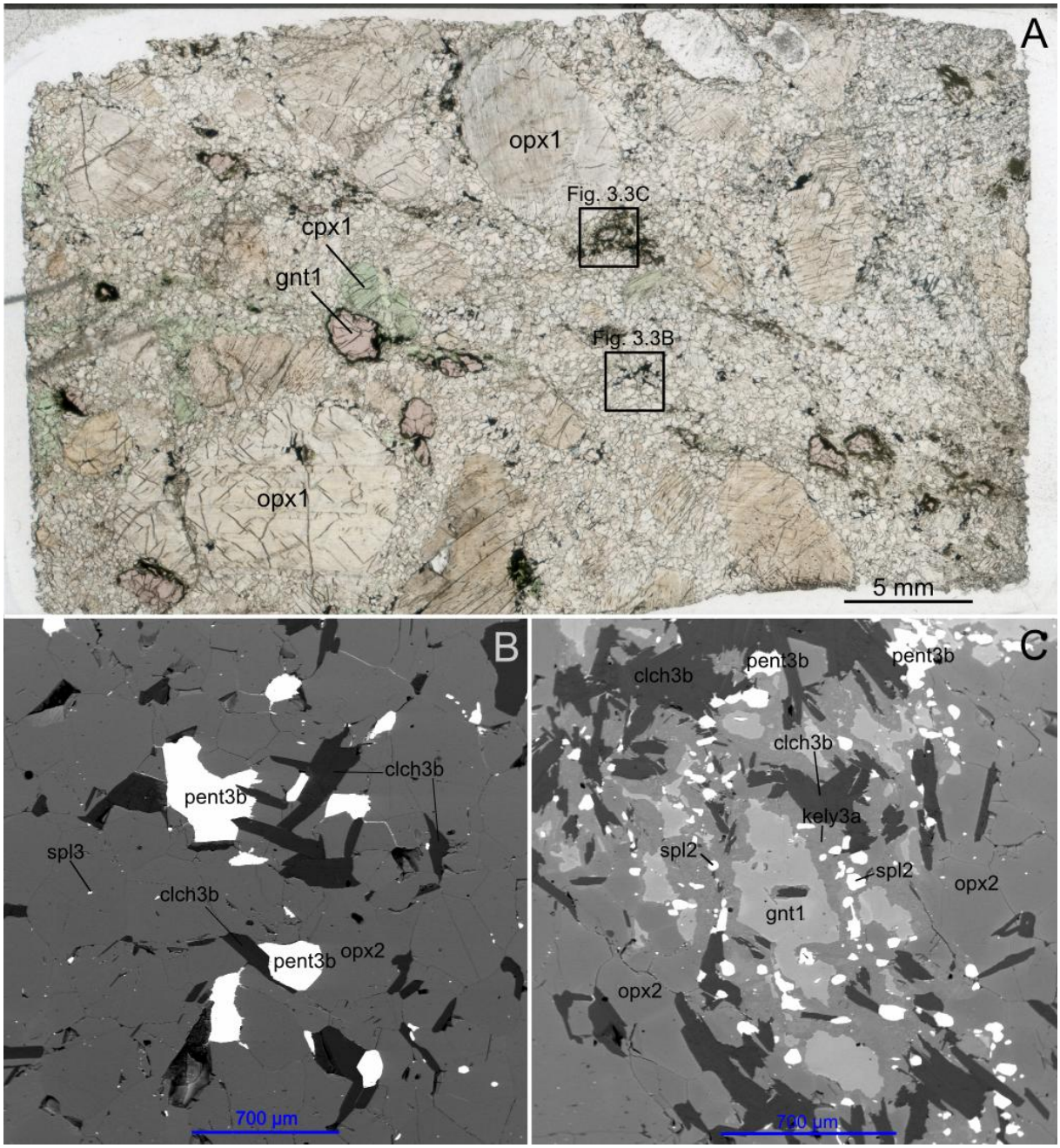

Figure 3.3: Sample 4. (A.) PPL overview of a thin section made from this garnet olivine-bearing websterite. The M1 porphyroclast assemblage of gnt-cpx-opx is surrounded by a matrix of the fine grained recrystallized M2 assemblage. The location of the images 3.3B and 3.3C are indicated. (B.) BSE image of the M2 opx matrix infiltrated with M3a clinochlore and M3a pentlandite (FeNi-Sulfide). Opaque minerals appear as white in the BSE image. The large opaques forming clusters with M3a clinochlore are M3a pentlandite, and the smaller opaques are M2 spinel (C.) BSE image showing retrograde alteration of an M1 garnet porphyroclast to M3a clinochlore and M3b kelyphitic intergrowth of amphibole and spinel. The large opaques forming clusters with M3a clinochlore are M3a pentlandite, and the smaller opaques are M3a spinel.

Sample 7.

An overview of the thin section made from this eclogite can be found in Fig. 3.4A. Pink M1 garnet porphyroclasts are surrounded by a recrystallized matrix of M2 clinopyroxene and randomly distributed M2 ilmenite. M1 garnet contains many cracks and appears to be locally elongated. M2 ilmenite in the matrix locally defines a foliation parallel to the elongation of M1 garnet. A single, 2 mm sized, porphyroclast of M1 clinopyroxene was found in the thin section. This clinopyroxene crystal is situated in between two M1 garnet crystals and was not entirely recrystallized (Fig. 3.4B). The crystals from the M2 microstructure are polygonal, strain free and have straight grain boundaries meeting in triple junctions at 120° angles (Fig. 3.4B). The M2 recrystallized assemblage is interpreted to have formed by dynamic recrystallization of M1 porphyroclasts through subgrain rotation. Garnet appears to have recrystallized together with clinopyroxene near some M1 garnet crystals, since small crystals of M2 garnet appear to be stable within the polygonal microstructure of the M2 clinopyroxene (Fig 3.4C). Along the rims of M1 garnet porphyroclasts, recrystallized M2 garnet can also be observed (Fig. 3.4C). An M3 retrograde mineral assemblage is present as dark green pleochroic amphibole replacing clinopyroxene. In contrast to garnet in the garnet (olivine-bearing) websterite samples (sample 2, 4, 11 and 12), the garnet in this eclogite does not have a retrograde kelyphitic rim.

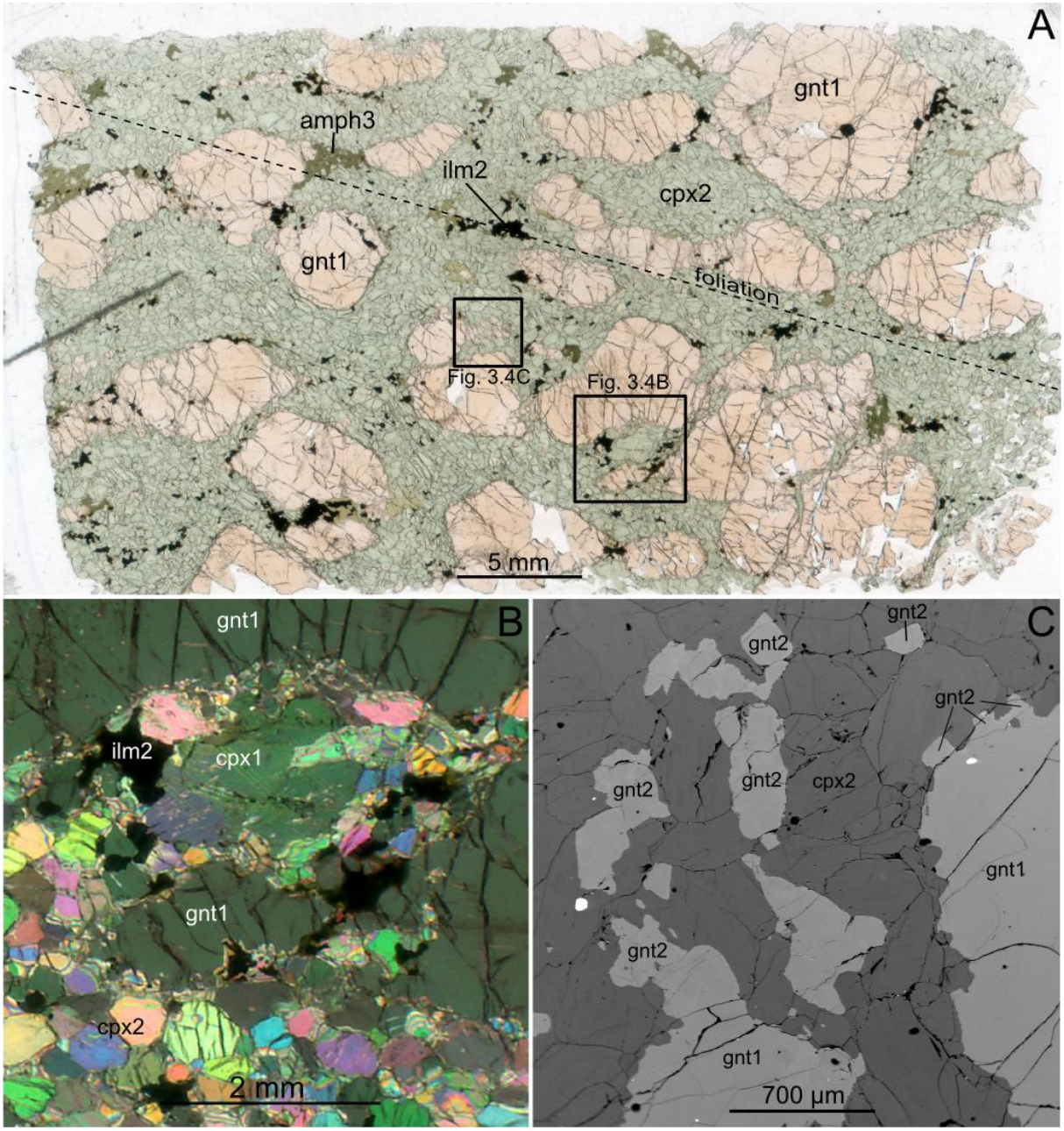

Figure 3.4: Sample 7. (A.) PPL flatbed scan of a thin section made from the eclogite sample. Coarse pink M1 garnet is surrounded by a recrystallized matrix of M2 green clinopyroxene and opaque M2 ilmenite. Opaque M2 ilmenite locally defines a foliation parallel to the elongation of M1 garnet. The dark green mineral is M3 amphibole replacing clinopyroxene. The locations of Fig. 3.4B and Fig. 3.4C are indicated (B.) XPL image of M1 garnet porphyroclasts and a M1 clinopyroxene porphyroclast surrounded by a recrystallized matrix of M2 clinopyroxene and opaque ilmenite. The M2 polygonal microstructure is well developed at the bottom and left of the image (C.) BSE image of M1 garnet porphyroclasts that recrystallized into M2 garnet, which is stable within the M2 clinopyroxene matrix.

Sample 9.

An overview of the thin section made from this allanite-bearing eclogite can be found in Fig. 3.5A. The thin section made from sample 9 is unique compared to the other samples used in this study. Coarse pink garnet and green clinopyroxene porphyroclasts form the M1 assemblage together with a brightly yellow colored epidote-group mineral which was determined to be allanite by electron microprobe analysis. Allanite contains rare earth elements as well as the radioactive element thorium. The M1 assemblage is highly strained, since numerous cracks are present in M1 garnet porphyroclasts and M1 crystals have an anhedral shape. The matrix consists of optically strain free, dark brown M2 allanite, which is interpreted to have formed by complete dynamic recrystallization of M1 allanite, which is no longer present (Fig. 3.5A). Within the M2 recrystallized allanite many multiphase solid inclusions occur (Fig. 3.5B). The multiphase solid inclusions vary strongly in mineral compositions including very dense monazites and zircons in addition to low density carbonates (Fig. 3.5C). A mineral composed of a high amount of Thorium and Silica (probably thorite) was also found as a solid inclusion. The retrograde assemblage is composed of M3 amphibole replacing M1 garnet (3.5B).

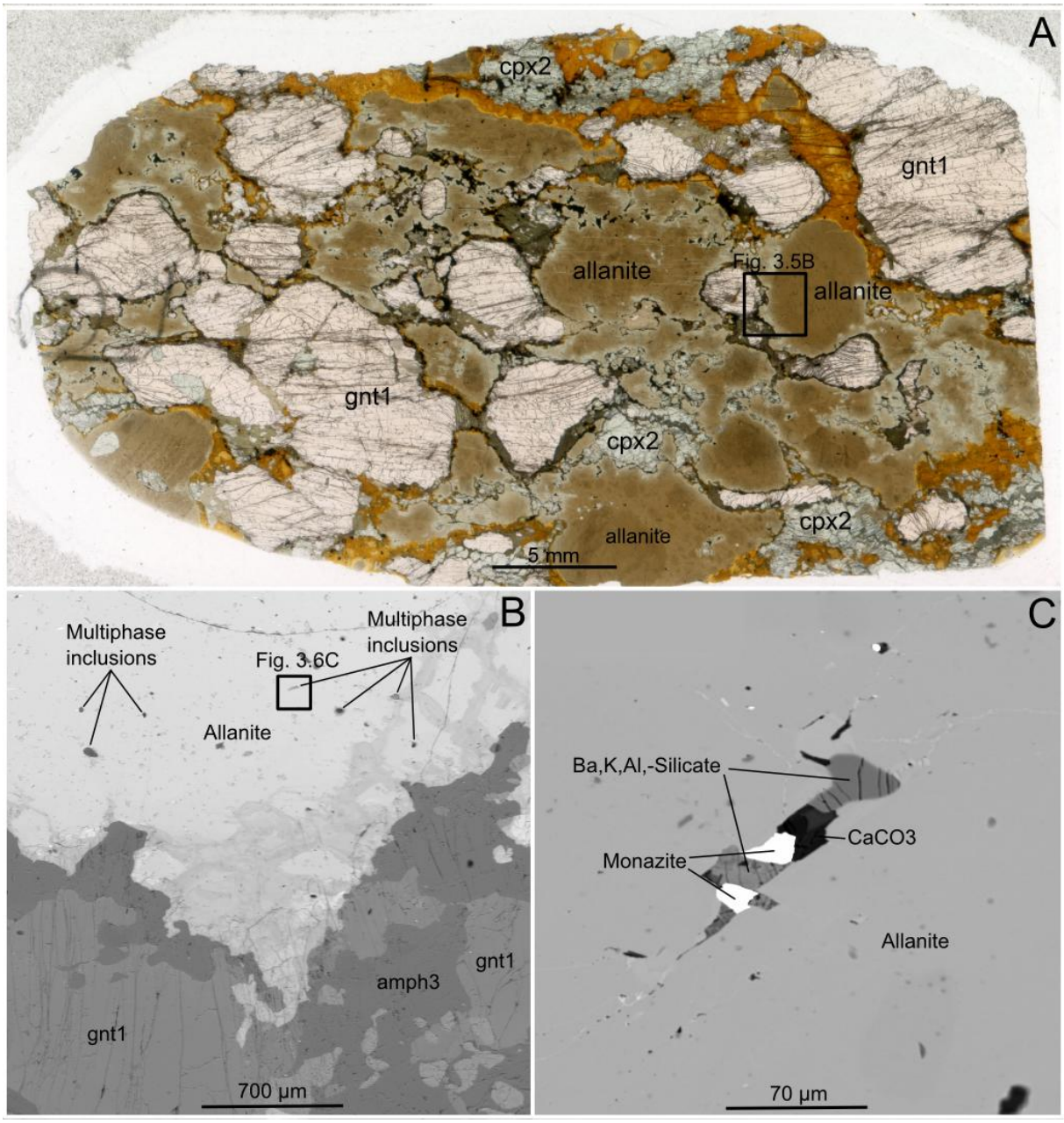

Figure 3.5: (A.) A flatbed scan of sample 9 under PPL, showing large porphyroclasts of M1 garnet with a matrix of pale green M2 clinopyroxene (top and bottom), dark brown allanite and a dark yellow mineral with a similar composition. (B.) BSE image of partly retrogressed M1 garnet with M3 amphibole surrounded by allanite. The black spots within allanite are multiphase inclusions. (C.) BSE image of a multiphase inclusion within allanite.

Sample 11.

An overview of the thin section of this garnet websterite can be found in Fig. 3.6A. From this image it can be seen that the M1 mineral assemblage consists of apparently randomly orientated garnet, orthopyroxene and clinopyroxene porphyroclasts. All porphyroclasts may be 'split' into segments with recrystallized M2 matrix minerals or M3 retrograde minerals in between. M1 orthopyroxene is dark brown/yellow and has exsolution lamellae of a dark brown ilmenite. M1 clinopyroxene has a green color and has orthopyroxene exsolution lamellae. A dark M3b kelyphitic rim around M1 garnet porphyroclasts is locally present and some M1 garnet porphyroclasts contain inclusions of clinopyroxene (Fig. 3.6A). The M1 porphyroclasts are heavily strained since they contain cracks, kinks, subgrains, undulatory extinction and have an anhedral shape. The M2 recrystallized assemblage in this sample consists of predominantly M2 orthopyroxene, M2 clinopyroxene and subordinate M2 garnet. No olivine was found in this sample. The crystals that form the M2 microstructure are polygonal, optically strain free and have straight grain boundaries meeting in triple junctions at 120° angles (Fig 3.6B). The M2 assemblage is interpreted to have formed by dynamic recrystallization of M1 porphyroclasts through subgrain rotation. Locally, where the kelyphitic rim around M1 garnet porphyroclasts is thin or absent, fine M2 garnet grains can be found occurring together with M2 spinel (Fig. 3.6C). These small garnet grains are interpreted to be remnants of M2 recrystallized garnet that formed together with M2 spinel and were stable in the M2 recrystallized microstructure. Retrograde minerals include a M3b green pleochroic amphibole replacing clinopyroxene (Fig 3.6A) and the M3a kelyphitic rims around garnet. A single cluster of opaque M2 ilmenites occur within the thin section (Fig. 3.6A).

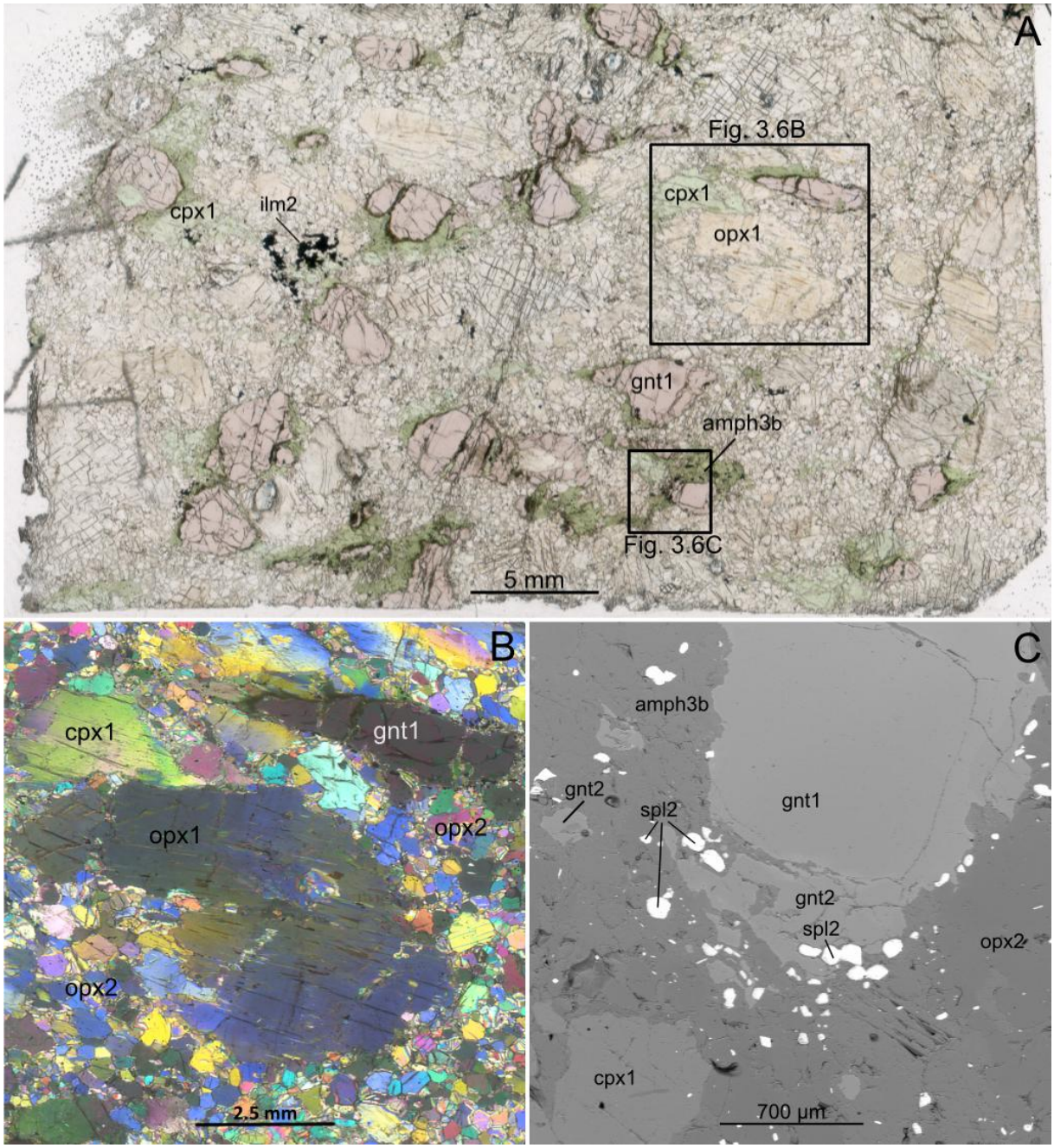

Figure 3.6: Sample 11. (A.) PPL overview of a thin section made from this garnet websterite. The M1 porphyroclast assemblage of gnt-cpx-opx is surrounded by a matrix of the fine grained recrystallized M2 assemblage. The location of the images 3.6B and 3.6C are indicated. (B.) XPL image of M1 garnet (top right), M1 clinopyroxene (top left) and large M1 orthopyroxene (center) porphyroclasts surrounded by a matrix of recrystallized M2 orthopyroxene. (C.) BSE image of M1 garnet recrystallizing into M2 garnet + M2 spinel. The surrounding matrix consists of M3b amphibole and M2 orthopyroxene.

Sample 12.

An overview of the thin section of this garnet websterite can be found in Fig. 3.7A. From this image it can be seen that the M1 mineral assemblage consists of apparently randomly orientated garnet, orthopyroxene and clinopyroxene porphyroclasts. M1 orthopyroxene contains many cracks, kinks and has exsolution lamellae of brown ilmenite. M1 garnet is affected by retrogression expressed by the presence of thick M3a kelyphitic rim around the crystal or the infiltration with M3b clinochlore and M3b Fe,Ni,-Sulfide (pentlandite) (Fig. 3.7B). The matrix consists of a recrystallized M2 assemblage consisting of colorless orthopyroxene and green clinopyroxene. No olivine was found in this sample. The M2 grains are polygonal, optically strain-free and have straight grain boundaries that join in 120° angle triple junctions (Fig. 3.7B). The M2 assemblage is interpreted to have formed by dynamic recrystallization of M1 porphyroclasts through subgrain rotation. No recrystallized M2 garnet was found in this sample, but may have been lost by retrograde overprinting. This sample is strongly affected by late stage retrogression forming a M3b mineral assemblage composed of clinochlore and pentlandite. M3b clinochlore occurs within the recrystallized matrix (Fig. 3.7C) as well as in some M1 garnet crystals where it appears to partly replace the garnet porphyroclasts (Fig. 3.7B). The opaque M3b pentlantdite (Fe,Ni, -sulfide) forms clusters with M3b clinochlore and/or is present near M3b clinochlore (Fig. 3.7B), suggesting that they are introduced in the rock during the same stage. M3b clinochlore also locally replaces the M2 recrystallized microstructure (Fig 3.7C). M3b amphibole is found in the matrix where it replaces M2 clinopyroxene (Fig 3.7C). A late stage M3c vein composed of green pleochroic M3c amphibole crosscuts the middle of the thin section (Fig 3.7A).

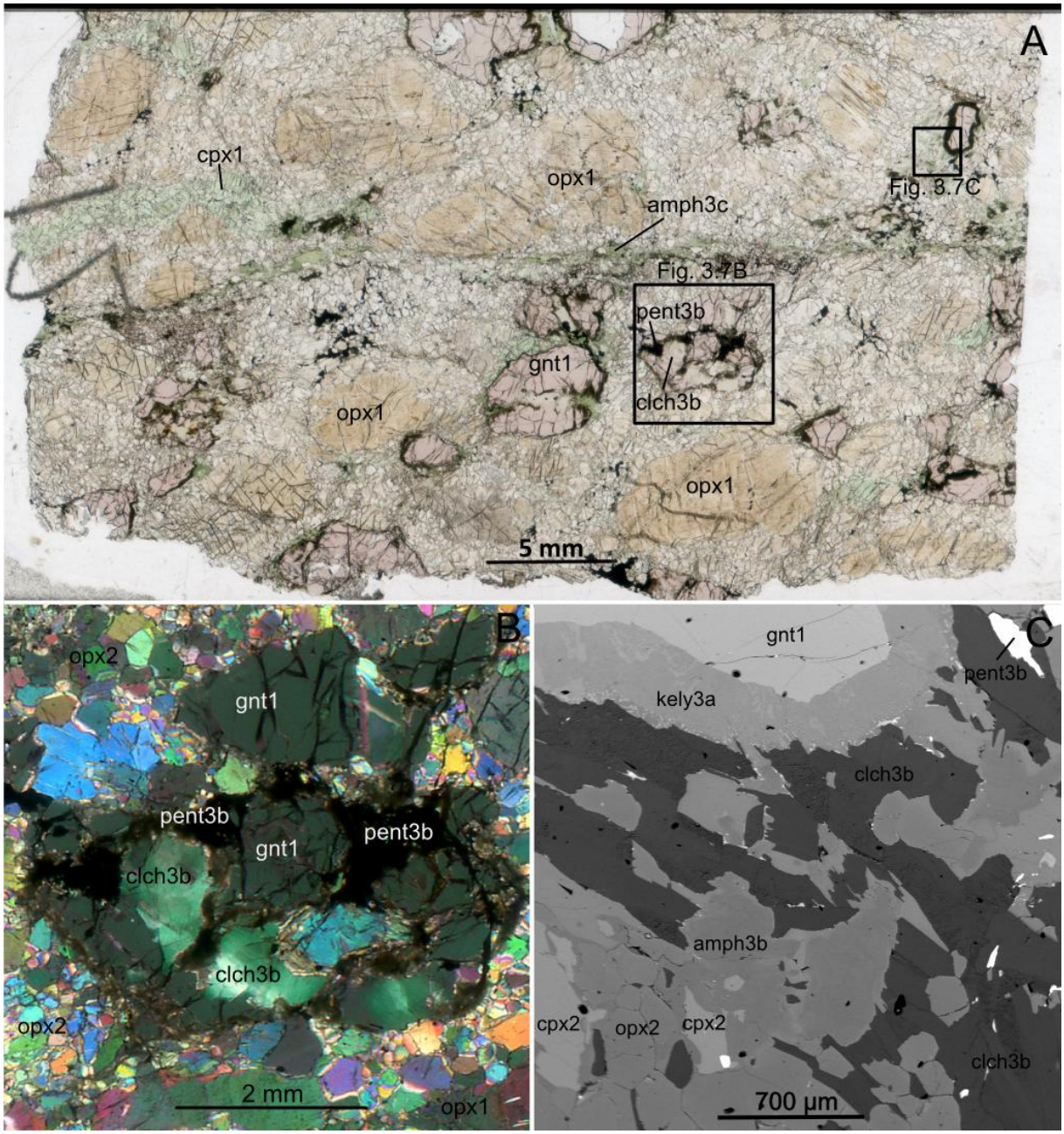

Figure 3.7: Sample 12 (A.) PPL overview of a thin section made from this garnet websterite. The M1 porphyroclast assemblage of gnt-cpx-opx is surrounded by a matrix of the fine grained recrystallized M2 assemblage and the M3a retrograde assemblage. The location of the images 3.7B is indicated. A vein consisting of green M3c amphibole cuts through the middle of the thin section. (B.) XPL image of an M1 garnet porphyroclast partly replaced with M3a clinochlore and M3a opaque pentlandite, surrounded by a polygonal matrix of recrystallized M2 orthopyroxene. Some M1 orthopyroxene porphyroclasts are also present. (C.) BSE image of an M1 garnet porphyroclast (top) with an undisturbed M3b kelyphitic rim surrounded by an M2 matrix with orthopyroxene and clinopyroxene that is replaced with late stage M3a clinochlore and M3a amphibole. Some M3a pentlandite is also visible at the top right of the image.

3.3. Interpretation of the microstructure and paragenetic diagram

Garnet websterite (sample 11 and 12) and garnet olivine-bearing websterite (sample 2 and 4)

M1 is represented by a porphyroclast assemblage of garnet, orthopyroxene and clinopyroxene in all the (olivine-bearing) websterite samples. M1 olivine was initially also present in the olivine-bearing samples (sample 2 and 4), but the M1 porphyroclasts have completely recrystallized into optically strain free M2 olivine. The M1 porphyroclast assemblage was formed after infiltration and crystalization of fertile ultramafic mantle-derived melts forming compositional layering (S_0) within the depleted dunite of the sub-Laurentian mantle during the proterozoic as described by Brueckner et al., (2010). Deformation of these ultramafic layers led to a S_1 compositional layering parallel to S_0 defined by the crystallographic orientation of M1 porphyroclasts. These ultramafic layers are slightly different in bulk rock composition, since not all samples contain olivine. The M2 recrystallized assemblage consists of orthopyroxene and clinopyroxene in the garnet websterite and garnet olivine-bearing websterite samples. M2 Olivine was found in the garnet olivine-bearing websterites (sample 2 and 4). Recrystallized M2 garnet + M2 spinel was found in samples with the least retrograde alteration (sample 2 and 11). However, one can only really determine the difference between M1 and M2 garnet components when the bulk rock composition has high Cr-content (see mineral chemistry section where M1 garnet in garnet websterite has Cr-contents of >2.5%, M1 garnet in eclogite has <0.1% Cr-content). The M2 assemblage was formed by dynamic recrystallization of the M1 porphyroclasts through subgrain rotation, which occurred during the emplacement of the Almklovdalen peridotite massif into continental crust during the Caledonian orogeny. The presence of recrystallized M2 garnet in sample 2 and sample 11 indicates that the emplacement of the peridotite body into the gneisses occurred within the garnet-olivine-pyroxene stability field for this rock type. Ilmenite was found in the matrix of sample 2 and 11, meaning that they probably belong to the M2 assemblage, since at least no primary M1 ilmenite was found. The M3 retrograde mineral assemblage consists of amphibole and spinel in the chlorite-poor or -absent samples (sample 2 and 11). The chlorite-rich samples (sample 4 and 12), have an M3a assemblage consisting of clinochlore, amphibole, spinel and pentlandite. All garnet (olivine-bearing) websterite samples have M1 garnet with M3b kelyphitic rims around at least some of the garnet crystals. The formation of the M3 assemblage occurred during exhumation of the Almklovdalen peridotite massif towards the surface during the late-Scandian phase of the Caledonian orogeny under HP granulite, amphibolite and greenschist facies conditions. The presence of clinochlore and pentlandite in sample 4 and 12 means that these samples experienced infiltration of a fluid phase that led to the crystallization of these minerals sometime during exhumation. The absence of these phases in sample 2 and 11, suggests that fluid infiltration occurred in an irregular distribution within the APM, consistent with Kostenko et al., 2002.

Eclogite (sample 7 and 9)

In sample 7 the M1 assemblage consists of large garnet crystals with a single remnant of an M1 clinopyroxene crystal. Since M1 garnet lacks poikiloblasts of feldspar or quartz and only has inclusions of clinopyroxene, one can assume that this eclogite formed within the mantle after the infiltration and crystallization of a mafic melt during the Proterozoic under HP/UHP conditions (similar to the websterites above) instead of representing prograde Scandian metamorphism of lower pressure mafic complexes present within the Baltica basement. This interpretation makes it an 'internal' eclogite and may be further confirmed or denied by the chemical analyisis of this eclogite sample. The M2 assemblage can be found within the matrix of sample 7 and consists of a recrystallized microstructure with mainly clinopyroxene and some small dynamically recrystallized M2 garnets in the matrix surrounding M1 garnet porphyroclasts. The formation of the M2 assemblage occurred after almost complete recrystallization of M1 clinopyroxene and partial recrystallization of the more resistant M1 garnet during the UHP crustal emplacement of the APM. The random occurrence of ilmenite spread throughout the fine grained M2 matrix, suggests that this phase belongs to the M2 assemblage. The M3 retrograde assemblage in sample 7 consists only of green amphibole, indicating that this eclogite was not significantly hydrated.

Sample 9 has an M1 assemblage of large garnets with a lot of parallel cracks that appear to form a horizontal foliation parallel to the thin section. The M1 garnets also have clinopyroxene inclusions, suggesting the same origin of formation as the eclogite in sample 7. The porphyroclast assemblage in sample 9 is however different from sample 7, since it contains allanite in addition to clinopyroxene and garnet. This makes it an allanite-bearing eclogite. The allanite appears to have crystallized from a melt together with garnet and clinopyroxene, forming the porphyroclast assemblage. The high amount of incompatible elements present in the allanite-bearing eclogite suggest that the melt from which it crystallized was enriched in these incompatible elements. During the crustal emplacement of the APM, the yellow allanite in sample 9 dynamically recrystallized into optically strain-free brown M2 allanite with many multiphase solid inclusions introduced during the recrystallization of M2 allanite (Fig. 3.5A). These multiphase solid inclustions may contain rare earth elements and elements like Ca, P, Th, K, Ba.

Paragenetic Diagram

The interpretation of the microstructural relations between minerals in the garnet (olivine-bearing) websterite and eclogite samples from the APM has led to the integrated paragenetic diagram illustrated in Fig. 3.8.

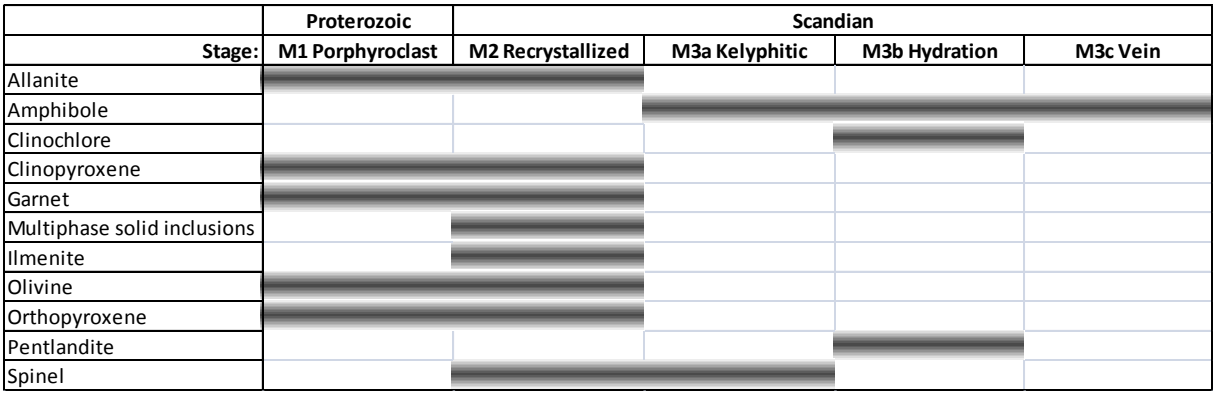

Figure 3.8: Integrated Paragenetic diagram for garnet (olvine-bearing) websterite and eclogite from the APM.

3.4. Mineral Chemistry

In this section the mineral chemistry is presented for the minerals found in the garnet websterite and eclogite samples described in the previous section. In this section: (1) each mineral is expressed by end member compositions, (2) the chemical variation throughout grains of each mineral is presented as linescan profiles and (3) representative mineral-chemical EMP analyses of core and rim are summarized for each mineral. The representative mineral-chemical EMP analyses are presented, but many more EMP analyses were done on the samples. For the additional EMP analyses performed on individual samples the reader is referred to the appendix where tables and locations of the EMP analyses can be found.

Orthopyroxene

Orthopyroxene mineral composition can be expressed by the end members wollastonite ($Ca_2Si_2O_6$), enstatite ($Mg_2Si_2O_6$) and ferrosilite ($Fe_2Si_2O_6$). The orthopyroxene end member diagram is illustrated in Fig. 3.9, in which both the core and rim analyses for all garnet websterite samples are plotted without distinguishing between M1 and M2 minerals since the chemical variation in Ca, Mg and Fe is small (Table 3.1). The orthopyroxene from garnet websterite samples vary from about 83% to 89% in the enstatite component, 11% to 17% in the ferrosilite component and the wollastonite component is under 1%.

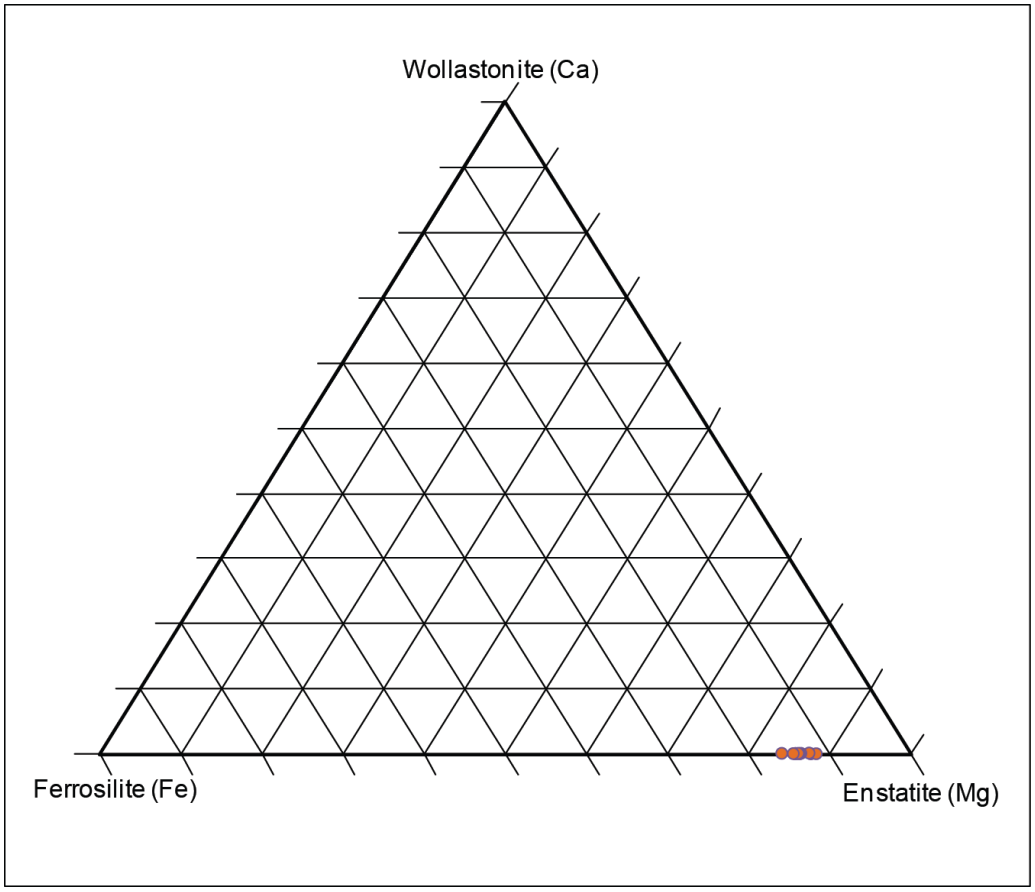

Figure 3.9: Representative orthopyroxene mineral compositions (from garnet websterite samples) plotted in a triangular end-member diagram. In this diagram the orthopyroxene composition is expressed in terms of the end members wollastonite ($Ca_2Si_2O_6$), enstatite ($Mg_2Si_2O_6$) and ferrosilite ($Fe_2Si_2O_6$).

Linescans through M1 orthopyroxene grains show a flat chemical profile interrupted by some peaks/valleys (Fig. 3.10). These peaks/valleys are caused by the cracks in the porphyroclasts or exsolved phases in the porphyroclast. Apart from the cracks the chemical profile is homogenous. The flat chemical profile means that mineral growth occurred under the same PT conditions and/or that the chemical composition is reset by intragranular diffusion in the case of an originally chemically zoned crystal. In the detailed Al_2O_3 profile (Fig. 3.10) the Al_2O_3 content is about 0.55% and the profile is homogeneous apart from the peaks in Al_2O_3, which represent cracks in the M1 orthopyroxene porphyroclast.

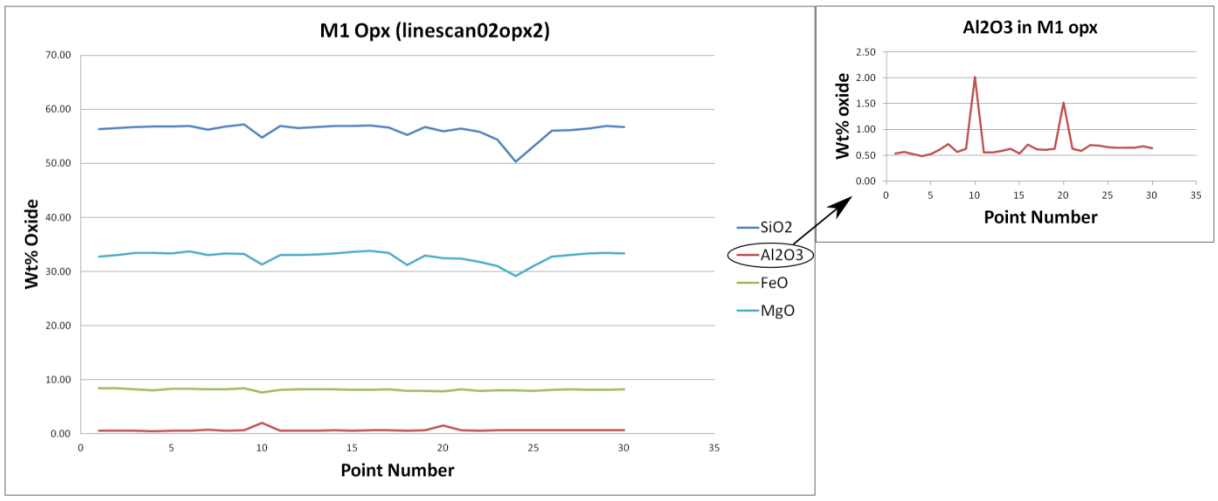

Figure 3.10: Representative example of a linescan through a M1 orthopyroxene grain (see appendix: Fig. A13 for location). The peaks/valleys in the data are due to local cracks in the porphyroclast or the effect of exsolution compounds. Al_2O_3 is shown in more detail, the peaks represent cracks in the orthopyroxene porphyroclast.

Linescans through M2 orthopyroxene grains show homogeneous, uninterrupted chemical profile for FeO, MgO and SiO (Fig. 3.11). No peaks or valleys are present in the linescans for M2 orthopyroxene, since the grains are recrystallized, strain free and therefore do not contain exsolved phases or cracks like M1 orthopyroxene. The homogeneous chemical profile means that mineral growth occurred under the same PT conditions and/or that the chemical composition is reset by intragranular diffusion in the case of an originally chemically zoned crystal. The detailed linescan profile for Al_2O_3 in M2 orthopyroxene (Fig. 3.11) appears to be different from the detailed Al_2O_3 profile in M1 orthopyroxene (Fig. 3.10). The Al_2O_3 core content in M2 orthopyroxene is about 0.35% and therefore lower than the 0.55% Al_2O_3 core content in M1 orthopyroxene. Another difference in the detailed profile for Al_2O_3 in M2 orthopyroxene is that a zonation can be observed. The Al_2O_3 content of 0.35% in the core increases to 0.85% in the rim. Since Al_2O_3 in orthopyroxene defines pressure, the increase in Al_2O_3 at the rim represents retrograde zoning as a result of diffusion during decompression.

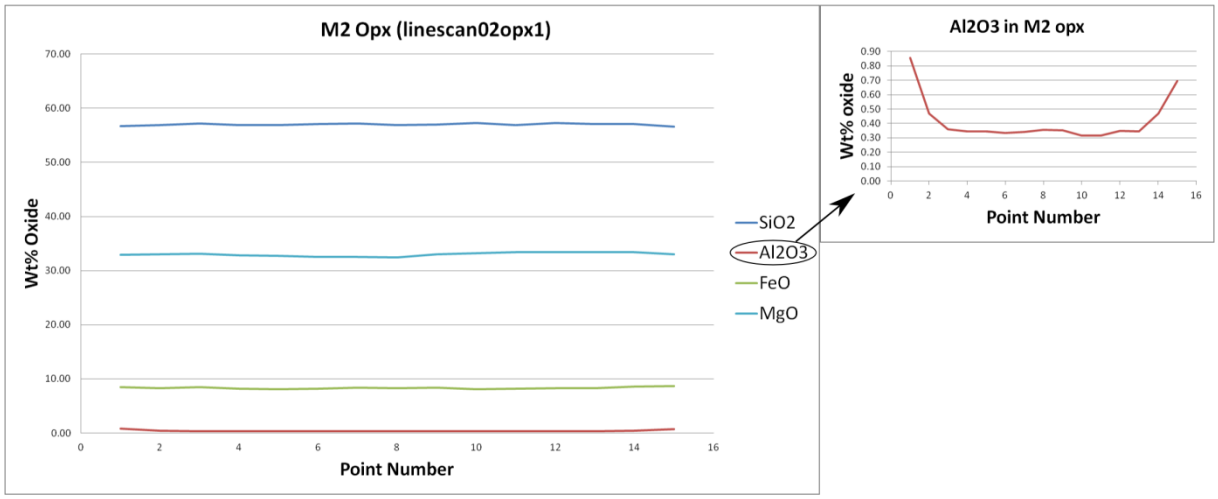

Figure 3.11: Representative example of a linescan through a M2 orthopyroxene grain (see appendix: Fig. A12 for location) showing a clear flat chemical profile. Al_2O_3 is chemically zoned and shown in more detail.

Representative mineral-chemical EMP analyses of core and rim for orthopyroxene (derived from linescans) are summarized in Table 3.1. The orthopyroxene found in garnet websterites is rich in magnesium and has a Mg# ranging from 0.84 to 0.88. The other major oxide (apart from SiO_2) in orthopyroxene is FeO with a mass fraction ranging from 8.2 to 10.2%. There is no notable variation in the major oxides core composition between M1 and M2 grains: M1 orthopyroxene has an MgO content ranging from 31.95 to 33.42% and M2 orthopyroxene has an MgO content ranging from 32.30 and 32.69%. For a single analysis significant variation between core and rim MgO composition was found, while no significant variation from the 2% error range is present in the other analyses. The analysis with a variation between core and rim MgO composition is an M1 orthopyroxene grain in sample 4 where the core composition is 32.58% and rim composition 29.80% (Table 3.1). For FeO the difference between core and rim composition is under 2% in all measurements.

	Sample 2				Sample 4				Sample 11				Sample 12			
	02opx2 (M1)		02opx1 (M2)		04opx2 (M1)		04opx3 (M2)		11opx1 (M1)		11opx2 (M2)		12opx1 (M1)		12opx2 (M2)	
Appendix:	Fig. A13		Fig. A12		Fig. A25		Fig. A26		Fig. A55		Fig. A56		Fig. A68		Fig. A69	
	Core	Rim	Core	Rim	Core	Rim	Core	Rim	Core	Rim	Core	Rim	Core	Rim	Core	Rim
SiO2	56.87	56.29	57.18	56.64	56.54	56.20	56.52	55.94	57.01	56.91	57.26	57.16	55.47	57.04	57.09	56.81
TiO2	0.03	0.05	0.02	0.03	0.04	0.03	0.04	0.00	0.02	0.03	0.03	0.04	0.03	0.04	0.01	0.03
Al2O3	0.67	0.53	0.34	0.86	0.45	0.50	0.35	0.41	0.78	0.43	0.33	0.60	1.52	0.71	0.44	0.76
Cr2O3	0.12	0.09	0.04	0.10	0.06	0.06	0.05	0.07	0.12	0.07	0.10	0.09	0.16	0.08	0.09	0.08
FeO	8.17	8.44	8.35	8.52	9.69	9.88	9.87	10.15	9.48	9.44	9.49	10.02	9.51	9.68	9.61	9.62
MnO	0.09	0.06	0.10	0.10	0.15	0.15	0.14	0.11	0.12	0.12	0.12	0.15	0.14	0.13	0.12	0.13
MgO	33.42	32.80	32.57	32.94	32.58	29.80	32.30	31.97	32.60	32.58	32.53	32.55	31.95	32.06	32.69	31.64
CaO	0.11	0.12	0.13	0.12	0.14	0.12	0.13	0.12	0.12	0.14	0.11	0.12	0.17	0.14	0.11	0.14
Na2O	0.00	0.00	0.00	0.00	0.01	0.00	0.01	0.00	0.00	0.01	0.00	0.01	0.02	0.00	0.00	0.00
NiO	0.17	0.13	0.16	0.13	0.03	0.07	0.09	0.10	0.05	0.09	0.10	0.09	0.10	0.10	0.08	0.09
Sum	99.67	98.52	98.88	99.42	99.70	96.80	99.50	98.87	100.29	99.82	100.07	100.83	99.07	99.99	100.23	99.31
	Cations p.f.u.															
Si	1.98	1.99	2.02	1.98	1.98	2.05	1.99	1.98	1.99	1.99	2.00	1.99	1.96	2.00	1.99	2.01
Ti	0.00	0.00	0.00	0.00	0.00	0.00	0.00	0.00	0.00	0.00	0.00	0.00	0.00	0.00	0.00	0.00
Al	0.03	0.02	0.01	0.04	0.02	0.02	0.01	0.02	0.03	0.02	0.01	0.02	0.06	0.03	0.02	0.03
Cr	0.00	0.00	0.00	0.00	0.00	0.00	0.00	0.00	0.00	0.00	0.00	0.00	0.00	0.00	0.00	0.00
Fe3	0.00	0.00	0.00	0.00	0.01	0.00	0.01	0.02	0.00	0.00	0.00	0.00	0.02	0.00	0.00	0.00
Fe2	0.24	0.25	0.25	0.25	0.27	0.30	0.28	0.29	0.28	0.28	0.28	0.29	0.26	0.28	0.28	0.28
Mn	0.00	0.00	0.00	0.00	0.00	0.00	0.00	0.00	0.00	0.00	0.00	0.00	0.00	0.00	0.00	0.00
Mg	1.74	1.73	1.71	1.72	1.70	1.62	1.69	1.69	1.69	1.70	1.70	1.69	1.68	1.68	1.70	1.67
Ca	0.00	0.00	0.00	0.00	0.01	0.00	0.00	0.00	0.00	0.01	0.00	0.00	0.01	0.01	0.00	0.01
Na	0.00	0.00	0.00	0.00	0.00	0.00	0.00	0.00	0.00	0.00	0.00	0.00	0.00	0.00	0.00	0.00
Mg#	0.88	0.87	0.87	0.87	0.86	0.84	0.85	0.85	0.88	0.86	0.86	0.85	0.86	0.86	0.86	0.85

Table 3.1: Representative EMP analyses of core and rim compositions of M1 and M2 orthopyroxene in garnet websterite. Top columns: Element oxides in wt% oxide. Middle columns: Elements in cations p.f.u. Lower row: Mg# of the analyses.

The Al_2O_3 content varies in the representative analyses of orthopyroxene, to illustrate this the average Al_2O_3 contents of core and rim for M1 and M2 orthopyroxene were calculated (Table 3.2). In M1 orthopyroxene the average Al_2O_3 content decreases from 0.86% in the core to 0.54% in the rim. In M2 orthopyroxene the Al_2O_3 content increases from 0.36% in the core to 0.66% in the rim. Another important observation is that the average Al_2O_3 core content is lower in M2 grains. The average Al_2O_3 content is 0.36% in M2 orthopyroxene cores compared to 0.86% in M1 cores. This is important since Al- in opx barometry defines pressure (see chapter. 4).

	M1 core	M1 rim	M2 core	M2 rim
Al2O3 (wt% oxide)	0.86	0.54	0.36	0.66

Table 3.2: Average Al_2O_3 content of orthopyroxene in garnet websterite calculated for the representative analyses (Table 3.1).

Clinopyroxene

Clinopyroxene mineral composition can be expressed in terms of the end members diopside $(CaMg)_2Si_2O_6$, aegerine $(NaFe)_2Si_2O_6$ and jadeite $(NaAl)_2Si_2O_6$. The clinopyroxene composition for both the garnet websterites and eclogites are plotted (Fig. 3.12). Clinopyroxene in garnet websterite plots high in the diopside field close to pure diopside and clinopyroxene in eclogite plots in the omphacite field. The chemical composition of clinopyroxene from sample 7 (eclogite) is represented by the cluster of blue dots that plot in the omphacite field, while the single isolated blue dot below the cluster represents a clinopyroxene grain from sample 9 (allanite-eclogite), which has a different bulk rock composition (Fig. 3.12).

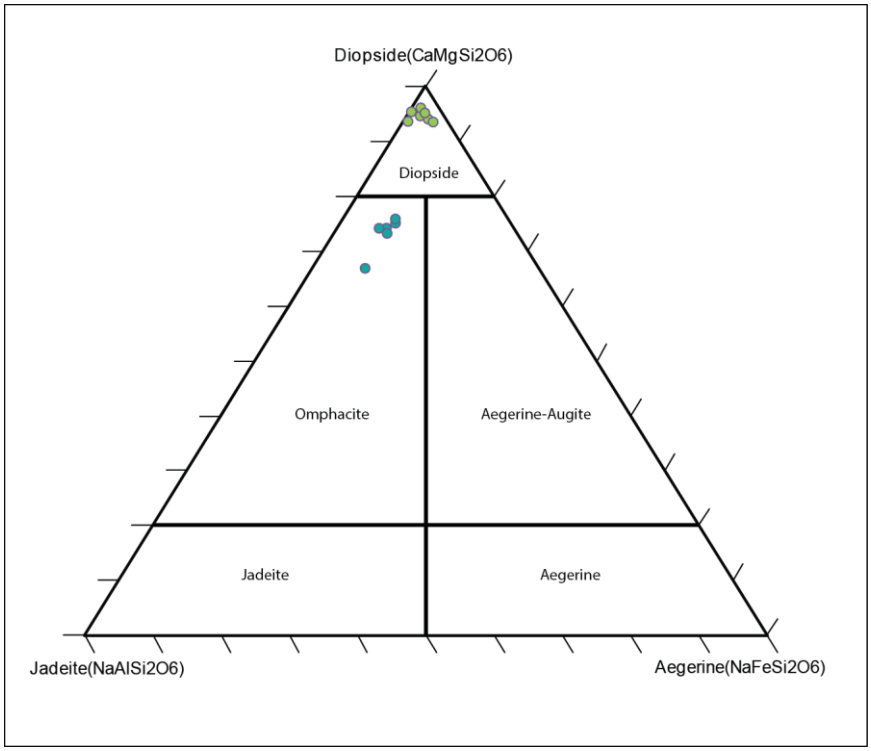

Figure 3.12: Triangular end member diagram of clinopyroxene from garnet websterite (green dots) and eclogite samples (blue dots). In this diagram the clinopyroxene composition is expressed in terms of the end members diopside $(CaMg)_2Si_2O_6$, aegerine $(NaFe)_2Si_2O_6$ and jadeite $(NaAl)_2Si_2O_6$.

Linescans through M1 clinopyroxene grains from garnet websterite show a flat chemical profile interrupted by some peaks/valleys (Fig. 3.13). These peaks/valleys are caused by the exsolved phases or cracks in the porphyroclasts. Apart from the cracks the chemical profile is homogenous. The flat chemical profile means that mineral growth occurred under the same PT conditions and/or that the chemical composition is reset by intragranular diffusion in the case of an originally chemically zoned crystal. In the detailed Cr_2O_3 profile (Fig. 3.13) the Cr_2O_3 content is about 0.95% in the core of the crystal. The Cr_2O_3 appears to be zoned and decreases to 0.70% and 0.30% at the rim of the crystal.

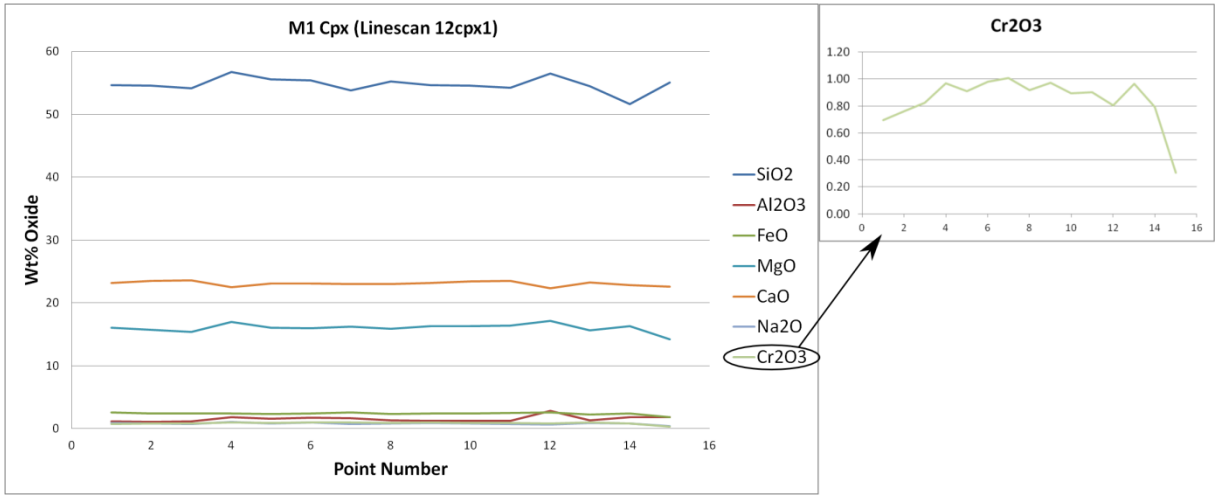

Figure 3.13: : Representative example of a linescan through a M1 clinopyroxene grain in garnet websterite (see appendix: Fig. A64 for location) showing a clear homogeneous chemical profile with a minor variation caused by cracks or exsolution compounds in the porphyroclast. Cr_2O_3 is shown in more detail.

Linescans through M2 clinopyroxene grains from garnet websterite samples show homogeneous chemical profile (Fig. 3.14). No major peaks or valleys are present in the linescans for M2 clinopyroxene, since the grains are recrystallized, strain free and therefore do not contain exsolved phases or cracks like M1 clinopyroxene. In the more detailed chemical profile for Cr_2O_3 in M2 clinopyroxene (Fig. 3.14), the amount of Cr_2O_3 appears to be lower than in M1 clinopyroxene. The Cr_2O_3 content of M2 clinopyroxene is between 0.30% and 0.38% throughout crystal and is therefore lower than the 0.95% core content in M1 clinopyroxene. The detailed chemical profile of Cr_2O_3 in M2 clinopyroxene is also homogeneous and lacks clear compositional zoning.

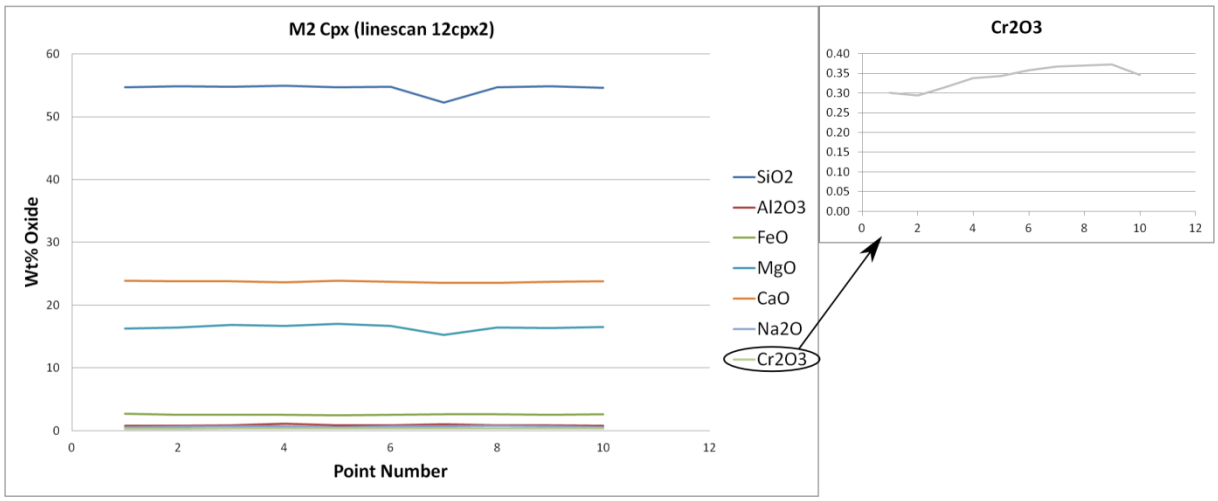

Figure 3.14: : Representative example of a linescan through a M2 clinopyroxene grain in garnet websterite (see appendix Fig. A65 for location) showing a clear homogeneous chemical profile. Cr_2O_3 is shown in more detail.

Linescans through M1 clinopyroxene grains from eclogite samples show a flat chemical profile interrupted by some minor peaks/valleys (Fig. 3.15). These peaks/valleys are due to cracks in the porphyroclasts. Apart from the cracks the chemical profile is homogenous. The flat chemical profile means that mineral growth occurred under the same PT conditions and/or that the chemical composition is reset by intragranular diffusion in the case of an originally chemically zoned crystal.

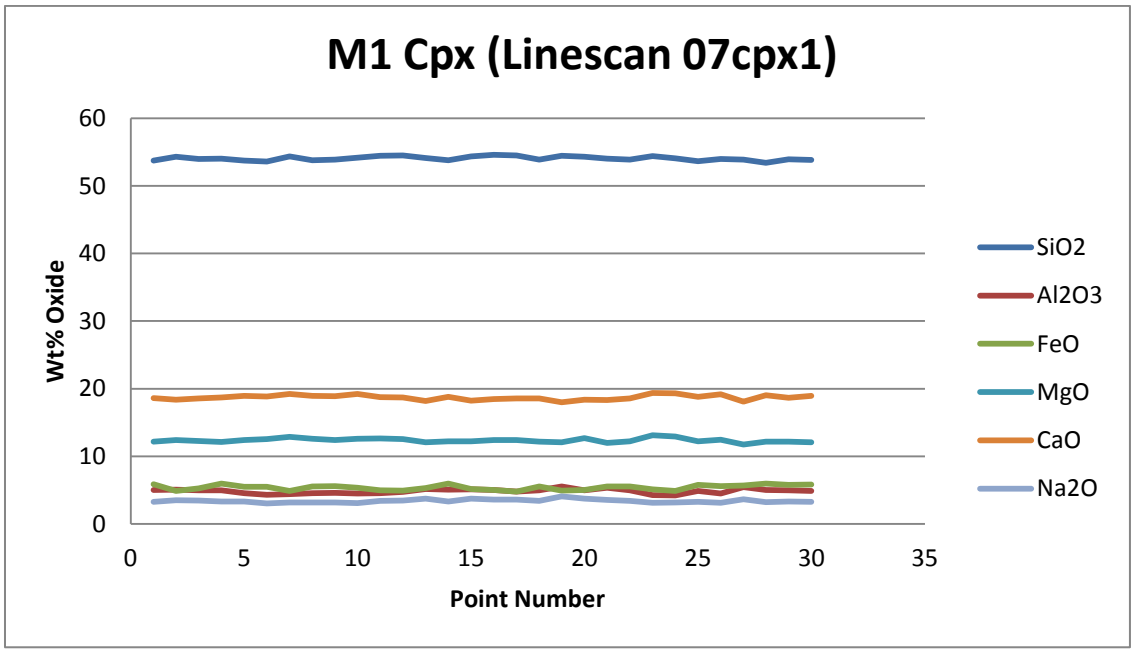

Figure 3.15: Representative example of a linescan through a M1 clinopyroxene grain in eclogite (see appendix Fig. A31 for location) showing a clear homogeneous chemical profile with a minor variation due to cracks in the porphyroclast. Cr_2O_3 was not plotted because it is <0.05%.

Linescans through M2 clinopyroxene from eclogite samples show a homogeneous, uninterrupted chemical profile (Fig. 3.16). No compositional zoning can be observed in linescans of M2 clinopyroxene from eclogite. The flat chemical profile means that mineral growth occurred under the same PT conditions and/or that the chemical composition is reset by intragranular diffusion in the case of an originally chemically zoned crystal.

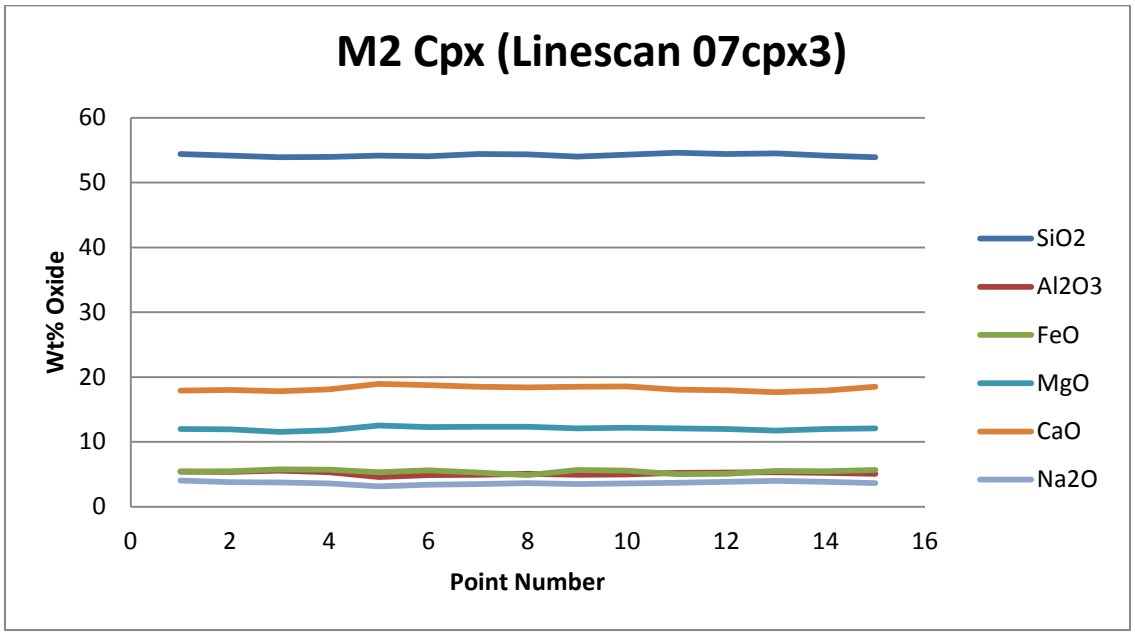

Figure 3.16: Representative example of a linescan through a M2 clinopyroxene grain in eclogite (see appendix Fig. A33 for location) showing a clear homogeneous and uninterrupted chemical profile. Cr_2O_3 was not plotted because it is <0.05%.

Representative mineral-chemical EMP analyses of core and rim for clinopyroxene from garnet websterite samples (derived from linescans) are summarized in Table 3.3. Clinopyroxene in garnet websterite is rich in CaO and MgO with mass fractions ranging from 23.1 to 24.3% in CaO and 15.8 to 16.7% in MgO. The FeO content is 2.15 to 2.68% and the Na_2O content is 0.31 to 1.00%. The Mg# ranges from 0.92 to 0.93. No difference in these major oxide composition can be observed between M1 and M2 grains outside the 2% error range for the analyses. The same is applicable when comparing core and rim compositions.

	Sample 2				Sample 4				Sample 11				Sample 12			
	02cpx1 (M1)		02cpx3 (M2)		04cpx1 (M1)		04cpx2 (M2)		11cpx1 (M1)		11cpx2 (M2)		12cpx1 (M1)		12cpx2 (M2)	
Appendix:	Fig. A6		Fig. A8		Fig. A20		Fig. A21		Fig. A50		Fig. A51		Fig. A64		Fig. A65	
	Core	Rim	Core	Rim	Core	Rim	Core	Rim	Core	Rim	Core	Rim	Core	Rim	Core	Rim
SiO2	53.86	54.02	53.89	53.95	54.17	53.69	53.91	53.82	54.98	54.40	54.62	54.88	55.21	54.61	54.80	54.65
TiO2	0.03	0.05	0.07	0.04	0.02	0.02	0.05	0.06	0.05	0.03	0.05	0.04	0.06	0.04	0.04	0.01
Al2O3	1.05	0.89	1.07	1.15	0.98	0.65	0.73	0.67	1.50	0.86	1.14	1.06	1.35	1.16	0.84	0.78
Cr2O3	0.68	0.55	0.43	0.66	0.70	0.42	0.32	0.27	0.88	0.78	0.67	0.53	0.92	0.69	0.36	0.30
FeO	2.15	2.23	2.22	2.17	2.40	2.50	2.41	2.48	2.39	2.58	2.58	2.56	2.30	2.59	2.57	2.68
MnO	0.05	0.06	0.04	0.05	0.05	0.10	0.06	0.07	0.07	0.03	0.03	0.06	0.07	0.05	0.06	0.06
MgO	16.30	16.65	16.63	16.43	16.42	16.81	16.24	17.07	16.51	16.54	16.27	16.26	15.88	16.06	16.65	16.25
CaO	23.60	23.90	23.69	23.03	23.36	24.14	23.88	24.28	23.05	23.55	23.04	23.12	23.02	23.12	23.73	23.86
Na2O	0.73	0.51	0.52	0.97	0.76	0.31	0.57	0.35	1.00	0.65	0.82	0.87	0.83	0.88	0.67	0.55
NiO	0.06	0.07	0.10	0.04	0.04	0.04	0.04	0.05	0.04	0.06	0.05	0.04	0.03	0.06	0.05	0.05
Sum	98.50	98.93	98.65	98.50	98.91	98.67	98.21	99.12	100.48	99.50	99.27	99.43	100.73	100.30	100.81	101.66
	Cations p.f.u.															
Si	1.99	1.98	1.98	1.98	1.99	1.98	2.00	1.97	1.99	1.99	2.00	2.01	2.02	2.00	2.00	2.01
Ti	0.00	0.00	0.00	0.00	0.00	0.00	0.00	0.00	0.00	0.00	0.00	0.00	0.00	0.00	0.00	0.00
Al	0.05	0.04	0.05	0.05	0.04	0.03	0.03	0.03	0.06	0.04	0.05	0.05	0.06	0.05	0.04	0.03
Cr	0.02	0.02	0.01	0.02	0.02	0.01	0.01	0.01	0.03	0.02	0.02	0.02	0.03	0.02	0.01	0.01
Fe3	0.01	0.01	0.00	0.03	0.01	0.02	0.01	0.04	0.01	0.01	0.00	0.00	0.00	0.00	0.01	0.00
Fe2	0.05	0.06	0.06	0.04	0.06	0.05	0.07	0.04	0.06	0.07	0.08	0.08	0.07	0.08	0.07	0.08
Mn	0.00	0.00	0.00	0.00	0.00	0.00	0.00	0.00	0.00	0.00	0.00	0.00	0.00	0.00	0.00	0.00
Mg	0.90	0.91	0.91	0.90	0.90	0.92	0.90	0.93	0.89	0.90	0.89	0.89	0.86	0.88	0.90	0.89
Ca	0.93	0.94	0.93	0.91	0.92	0.95	0.95	0.95	0.89	0.92	0.90	0.91	0.90	0.91	0.93	0.94
Na	0.05	0.04	0.04	0.07	0.05	0.02	0.04	0.02	0.07	0.05	0.06	0.06	0.06	0.06	0.05	0.04
Mg#	0.93	0.93	0.93	0.93	0.92	0.92	0.92	0.92	0.92	0.92	0.92	0.92	0.92	0.92	0.92	0.92

Table 3.3: Representative EMP analyses of core and rim composition for M1 and M2 clinopyroxene in the garnet websterite samples. Top columns: Element oxides in wt% oxide. Middle columns: Elements in cations p.f.u. Lower row: Mg# of the analyses.

A difference in the Cr_2O_3 content of clinopyroxene in garnet websterite can be observed between M1 and M2 grains, to illustrate this the average values of Cr_2O_3 in the cores and rims of M1 and M2 clinopyroxene were calculated (Table 3.4). The core of M1 clinopyroxene contains an average Cr_2O_3 content of 0.79%, compared to a Cr_2O_3 content of 0.45% for M2 clinopyroxene. For M1 clinopyroxene there is also a difference between core and rim Cr_2O_3 content: M1 cores contain 0.79% Cr_2O_3 versus 0.61% Cr_2O_3 in the rim.

	M1 core	M1 rim	M2 core	M2 rim
Cr2O3 (wt% oxide)	0.79	0.61	0.45	0.44

Table 3.4: Average Cr_2O_3 content of clinopyroxene in garnet websterite calculated for the representative analyses in Table 3.3.

Representative mineral-chemical EMP analyses of core and rim for clinopyroxene from eclogite samples (derived from linescans) are summarized in Table 3.5. The clinopyroxene in eclogite is most abundant in CaO and MgO: The CaO content ranges from 16.52 to 17.21% and the MgO content ranges from 10.70 to 12.43%. FeO in eclogite ranges from 4.82 to 5.67%, Al_2O_3 ranges from 4.95 to 6.94% and Na_2O ranges from 3.25 to 4.74%. No differences outside the 2% error range for EMP analyses can be observed between the composition of M1 and M2 grains in eclogite or between the composition of cores and rims. There is a slight compositional difference in clinopyroxene between the eclogites of sample 7 and sample 9: In sample 7 the average CaO, MgO, FeO, Al_2O_3 and Na_2O core contents are 18.44%, 12.41%, 4.91%, 5.00% and 3.61%, respectively. In sample 9 the core contents for CaO, MgO, FeO, Al_2O_3 and Na_2O are 17.21%, 10.94%, 5.67%, 6.37% and 4.51%, respectively.

	Sample 7				Sample 9	
	07cpx1 (M1)		07cpx2 (M2)		09cpx1 (M2)	
Appendix:	Fig. A31		Fig. A32		Fig. A44	
	Core	Rim	Core	Rim	Core	Rim
SiO2	54.59	53.74	54.51	53.64	54.82	54.36
TiO2	0.08	0.13	0.09	0.17	0.12	0.13
Al2O3	5.04	5.04	4.95	5.10	6.37	6.94
Cr2O3	0.04	0.05	0.03	0.05	0.04	0.04
FeO	5.00	5.86	4.82	5.35	5.67	5.46
MnO	0.01	0.02	0.01	0.02	0.03	0.00
MgO	12.43	12.15	12.38	12.15	10.94	10.70
CaO	18.45	18.60	18.43	18.33	17.21	16.52
Na2O	3.60	3.25	3.62	3.58	4.51	4.74
NiO	0.01	0.02	0.02	0.04	0.00	0.00
Sum	99.26	98.85	98.86	98.43	99.72	98.91
Si	1.98	1.97	1.99	1.97	1.98	1.98
Ti	0.00	0.00	0.00	0.00	0.00	0.00
Al	0.22	0.22	0.21	0.22	0.27	0.30
Cr	0.00	0.00	0.00	0.00	0.00	0.00
Fe3	0.07	0.06	0.06	0.09	0.08	0.08
Fe2	0.09	0.12	0.08	0.08	0.10	0.09
Mn	0.00	0.00	0.00	0.00	0.00	0.00
Mg	0.67	0.66	0.67	0.66	0.59	0.58
Ca	0.72	0.73	0.72	0.72	0.67	0.64
Na	0.25	0.23	0.26	0.26	0.32	0.33
Mg#	0.82	0.79	0.82	0.80	0.77	0.78

Table 3.5: Representative EMP analyses of core and rim composition for M1 and M2 clinopyroxene in the two eclogite samples. Top columns: Element oxides in wt% oxide. Middle columns: Elements in cations p.f.u. Lower row: Mg# of the analyses.

Garnet

Garnet mineral composition can be expressed as the end members almandine ($Fe_3Al_2Si_3O_{12}$) + spessartine ($Mn_3Al_2Si_3O_{12}$), pyrope ($Mg_3Al_2Si_3O_{12}$) and grossular ($Ca_3Al_2Si_3O_{12}$) (Fig. 3.16). Garnet from garnet websterite samples (red in Fig. 3.16) ranges in end member composition from almandine + spessartine 27.39% to 38.91%, pyrope 46% to 58.01% and grossular 13.38% to 15.06%. The garnet in eclogite ranges in end member composition from almandine + spessartine 42.98% to 46.17%, pyrope 27.24% to 32.19% and grossular 24.06% to 26.88%. The single isolated red circle plotted in Fig 3.16 represents a strongly retrogressed M1 garnet porphyroclast in sample 4 that has a slightly different composition than other garnet porphyroclasts from garnet websterite (see Appendix: Fig. A23 for location). This means that sample 4 is of heterogeneous bulk rock composition and perhaps consists of 2 layers of slightly different bulk rock compositions.

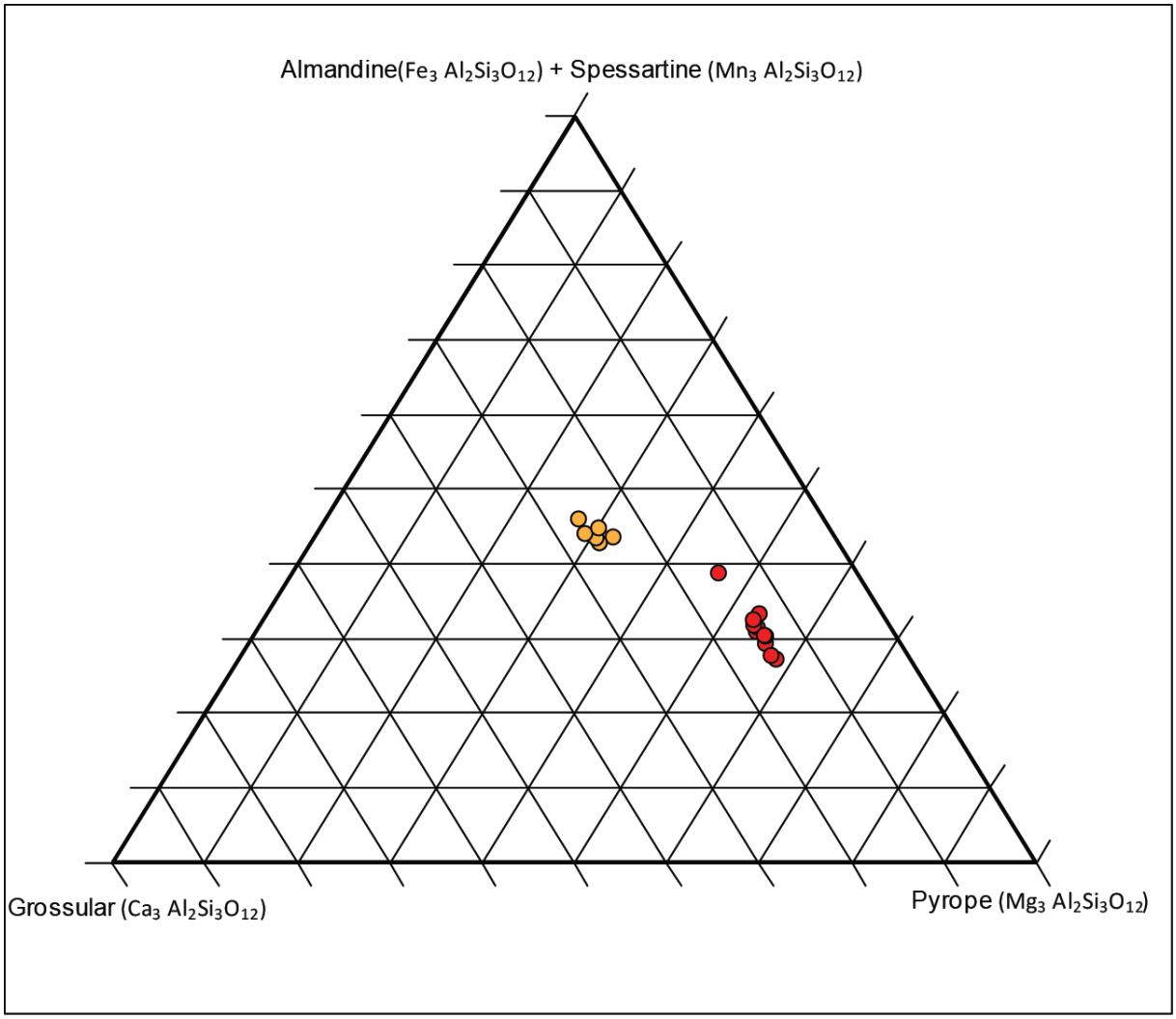

Figure 3.16: Triangular end member diagram of garnet from garnet websterite (red dots) and eclogite (yellow dots) samples. In this diagram the garnet composition is expressed in terms of the end members almandine ($Fe_3Al_2Si_3O_{12}$) + spessartine ($Mn_3Al_2Si_3O_{12}$), pyrope ($Mg_3Al_2Si_3O_{12}$) and grossular ($Ca_3Al_2Si_3O_{12}$).

Linescans through M1 garnet porphyroclasts in garnet websterite show homogenous chemical profiles with a slight increase in FeO and a decrease in MgO towards the rim (Fig 3.17. The homogeneous chemical profile means that mineral growth occurred under the same PT conditions and/or that the chemical composition is reset by intragranular diffusion in the case of an originally chemically zoned crystal. Slight retrograde zoning is present in one rim side of the crystal, illustrated by an increase in FeO of 13% to 15% from core to rim and a decrease in MgO of 16% to 15% from core to rim.

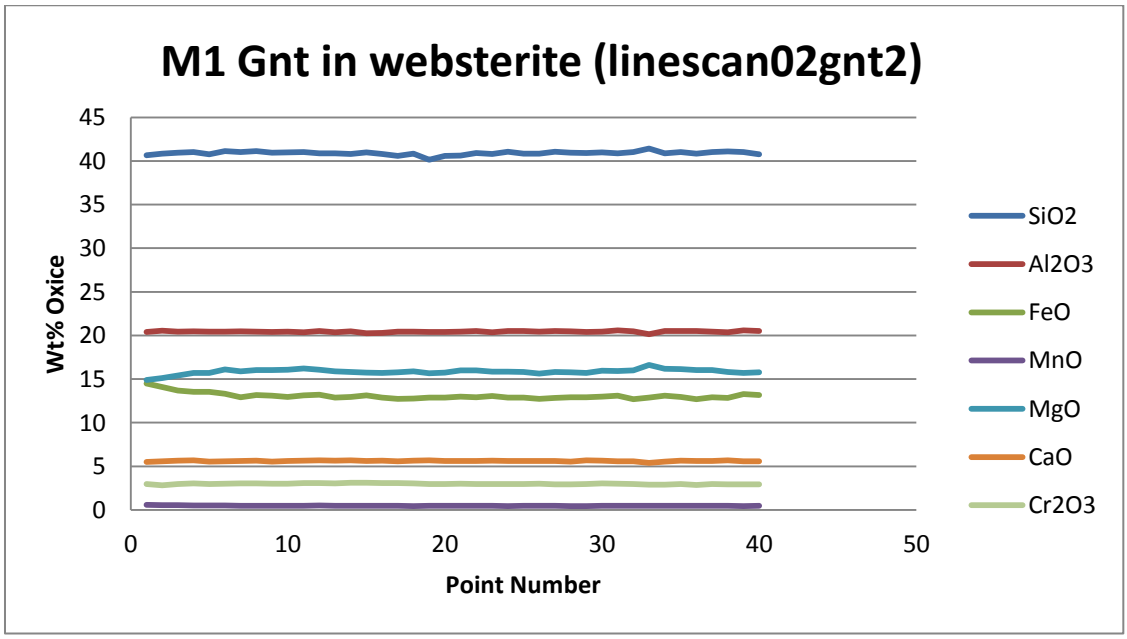

Figure 3.17: Representative example of a linescan through a M1 garnet porphyroclast in garnet websterite (see appendix: Fig. A10 for location) showing a homogenous chemical profile.

Linescans through M1 garnet porphyroclasts in eclogite samples also show a homogenous chemical profile (Fig. 3.18). The homogeneous chemical profile suggests that mineral growth occurred under the same PT conditions and/or that the chemical composition is reset by intragranular diffusion in the case of an originally chemically zoned crystal. Retrograde zoning can be observed at the rim of the crystal (start of the profile), illustrated by an increase in FeO of 20% to 22% from core to rim and a decrease in MgO of 8% to 7% from core to rim.

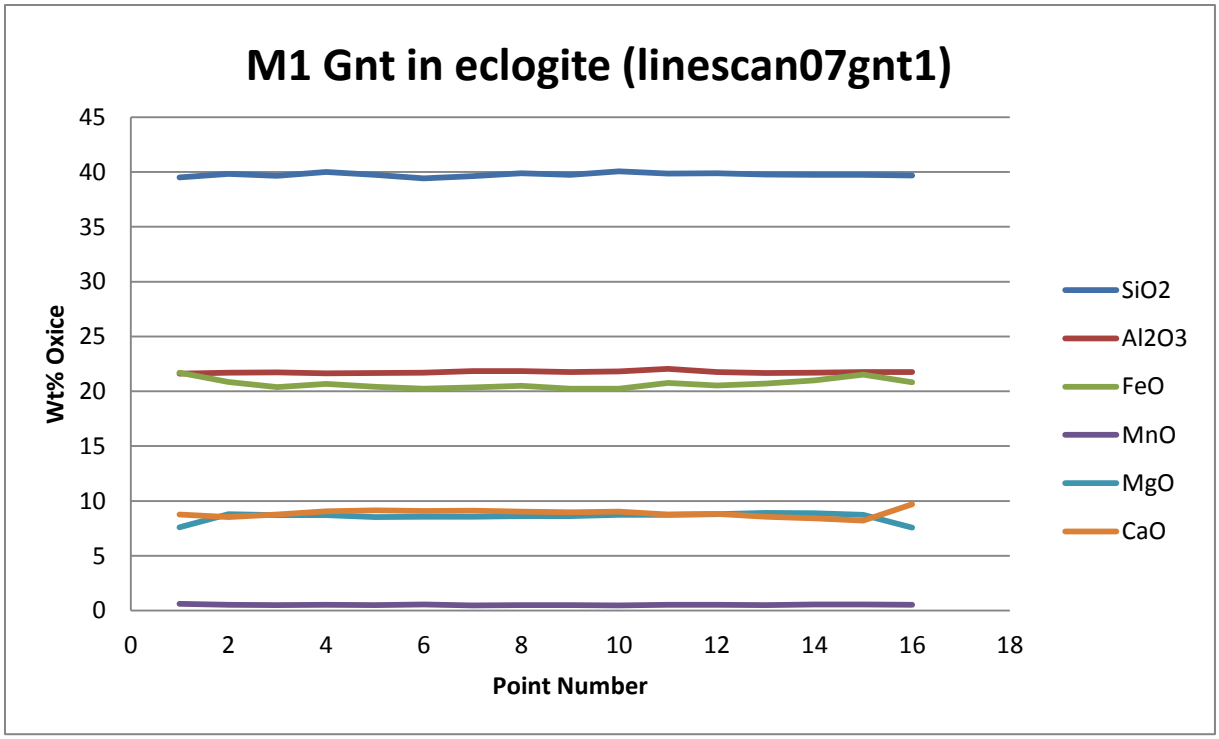

Figure 3.18: Representative example of a linescan through a M1 garnet porphyroclast in eclogite (see appendix Fig. A31 for location) showing a homogenous chemical profile.

When the M1 and M2 garnet chemical compositions are compared, not many differences can be observed in their major element oxide composition. However, when an element like Chromium is considered, some differences can be observed between the chemical profiles across M1 and M2 garnet in websterite (Fig. 3.19a). A linescan was made starting in an M2 garnet crystal within the matrix and ending in the core of an M1 garnet porphyroclast (Fig. 3.19). The Cr_2O_3 content increases from about 1% to 3% towards the core of the M1 garnet with a corresponding decrease in Al_2O_3 from about 22.5% to 20.5%. The occurrence of M2 spinel adjacent to M2 garnet suggests that, in addition to other elements, Cr was used to form M2 spinel during the recrystallization of high-Cr M1 garnet to low-Cr M2 garnet.

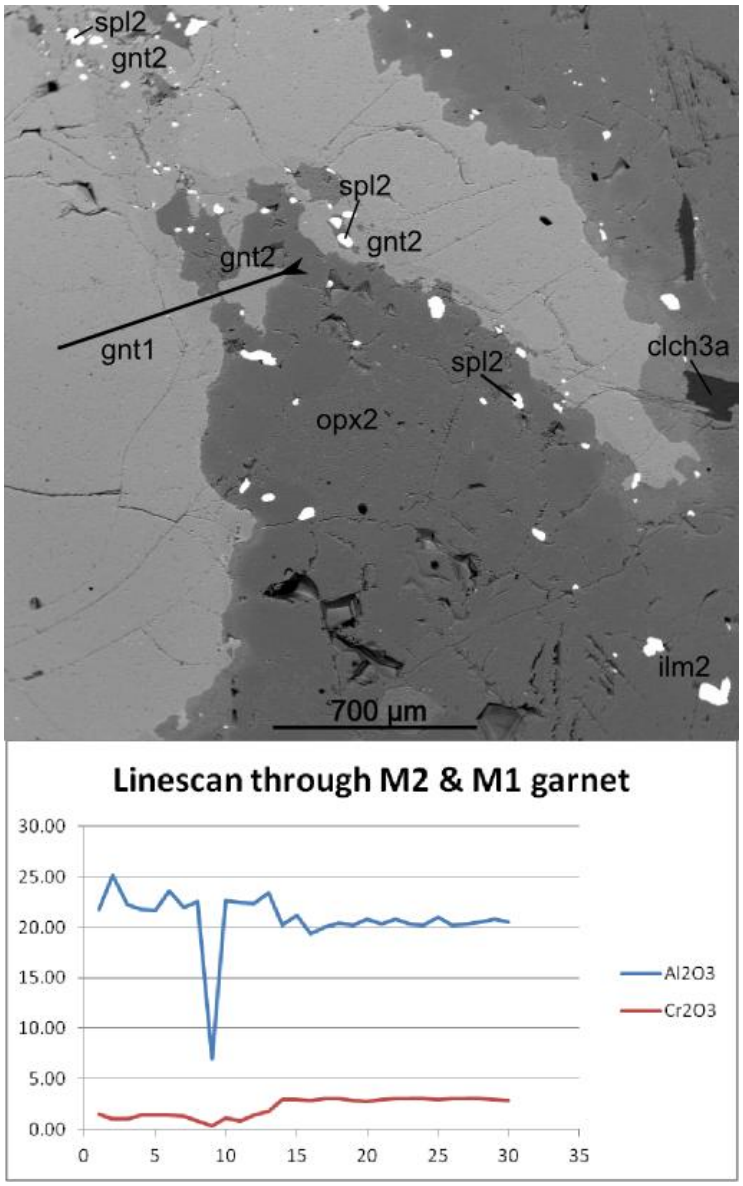

Figure 3.19: A linescan starting at M2 garnet in the recrystallized matrix and ending in the core of an M1 garnet porphyroclast (arrow in the top image indicates the start of the linescan). An increase in Cr is present from M2 towards M1, which is compensated by a decrease in Al content. The sharp valley at point 9 is due to orthopyroxene situated in between garnet grains. See appendix Fig. A9 for the chemical composition of the other elements.

To further illustrate the difference in Cr_2O_3 content between M1 and M2 garnet in garnet websterite and M1 garnet in eclogite a Cr_2O_3 vs. CaO plot was made (Fig. 3.20). The CaO content of M1 and M2 garnet in websterite are roughly the same with values between 5.10% and 5.72% (Fig. 3.20). The Cr_2O_3 content of M1 garnet in websterite is between 2.42% and 3.03% and therefore higher than the Cr_2O_3 content of M2 garnet in websterite, which is between 1.36% and 1.70% (Fig. 3.20). The lower Cr_2O_3 content of M2 garnet in websterite suggests that some Cr_2O_3 was lost to form M2 Cr-spinel when M1 garnet dynamically recrystallized into M2 garnet (Fig. 3.19). M1 garnet in eclogite has a Cr_2O_3 content of <0.1%.

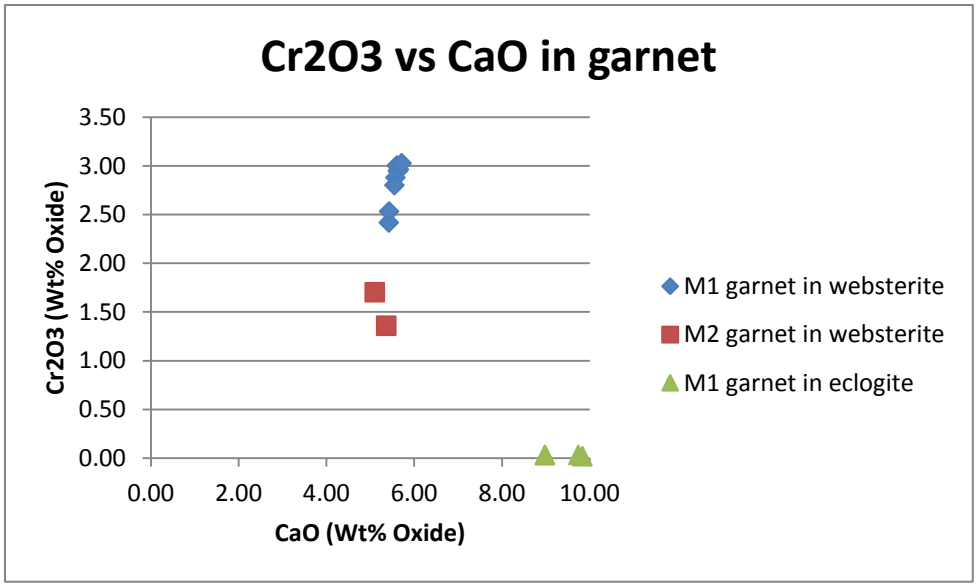

Figure 3.20: Cr_2O_3 vs. CaO plot. The Cr_2O_3 content of M1 garnet is higher than that of M2 garnet in garnet websterite.

Representative mineral-chemical EMP analyses of core and rim composition for M1 and M2 garnet in garnet websterite are summarized in table 3.6. The garnet has a core MgO content of 12.48% to 15.39% and a rim MgO content of 11.58% to 15.5%. There is a variation between core and rim MgO content, but it appears to be insignificant. For some analyses the MgO content of core and rim varies less than the 2% error range, while for other analyses there is a decrease in MgO in the rim. The FeO ranges from 13.6% to 17,7% for the core data and from 14.0% to 17.9% for the rim data. Some samples show an increase in Fe from core to rim compensated by a drop in Mg, but others vary less than the 2% error range. The highest Cr_2O_3 content is found in M1 garnets with core compositions near 3.0%, while the M2 garnets within the same sample have core Cr_2O_3 contents of 1.4 to 1.7 wt% oxide.

	Sample 2				Sample 4		Sample 11				Sample 12	
	02gnt1a (M2)		02gnt1b (M1)		04gnt1 (M1)		11gnt2 (M1)		11gnt3 (M2)		12gnt2 (M1)	
Appendix:	Fig. A9		Fig. A9		Fig. A22		Fig. A53		Fig. A54		Fig. A67	
	Core	Rim	Core	Rim	Core	Rim	Core	Rim	Core	Rim	Core	Rim
SiO2	41.15	40.96	40.76	39.85	40.70	40.50	40.24	39.43	40.18	39.45	41.39	42.83
TiO2	0.01	0.03	0.07	0.05	0.08	0.05	0.06	0.02	0.03	0.03	0.04	0.06
Al2O3	21.73	21.81	20.81	22.69	20.24	20.32	20.53	20.21	21.27	20.63	20.99	20.48
Cr2O3	1.36	1.47	2.96	1.07	3.03	3.09	2.80	2.60	1.70	1.87	2.53	2.40
FeO	14.18	14.59	13.65	14.61	14.67	15.36	14.48	17.90	15.61	17.59	14.41	14.64
MnO	0.57	0.57	0.53	0.60	0.61	0.59	0.58	1.14	0.63	0.89	0.58	0.58
MgO	15.04	15.15	15.26	16.41	14.91	14.30	14.84	11.58	14.51	12.65	15.39	15.62
CaO	5.36	4.87	5.65	4.73	5.71	5.77	5.55	5.87	5.10	5.18	5.43	5.04
Na2O	0.00	0.00	0.00	0.00	0.03	0.00	0.00	0.01	0.04	0.01	0.02	0.02
NiO	0.00	0.00	0.00	0.00	0.00	0.01	0.00	0.00	0.01	0.00	0.03	0.00
Sum	99.41	99.46	99.70	100.02	99.98	100.00	99.06	98.75	99.09	98.30	99.76	99.19
	Cations p.f.u.											
Si	3.04	3.02	3.01	2.91	3.01	3.00	3.00	3.01	3.00	3.00	3.03	3.11
Ti	0.00	0.00	0.00	0.00	0.00	0.00	0.00	0.00	0.00	0.00	0.00	0.00
Al	1.89	1.90	1.81	1.95	1.88	1.90	1.80	1.82	1.87	1.85	1.81	1.75
Cr	0.08	0.09	0.17	0.06	0.08	0.07	0.17	0.16	0.10	0.11	0.15	0.14
Fe3	0.00	0.00	0.00	0.17	0.02	0.03	0.03	0.00	0.04	0.03	0.00	0.00
Fe2	0.88	0.90	0.84	0.72	1.09	1.02	0.87	1.14	0.94	1.09	0.88	0.89
Mn	0.04	0.04	0.03	0.04	0.07	0.05	0.04	0.07	0.04	0.06	0.04	0.04
Mg	1.66	1.67	1.68	1.78	1.39	1.51	1.65	1.32	1.61	1.44	1.68	1.69
Ca	0.42	0.39	0.45	0.37	0.46	0.41	0.44	0.48	0.41	0.42	0.42	0.39
Mg#	0.65	0.65	0.67	0.67	0.56	0.59	0.65	0.54	0.62	0.56	0.66	0.66

Tabel 3.6: Representative EMP analyses of core and rim composition for M1 and M2 garnet in garnet websterite samples. Top columns: Element oxides in wt% oxide. Middle columns: Elements in cations p.f.u. Lower row: Mg# of the analyses.

Representative mineral-chemical EMP analyses of core and rim composition for M1 and M2 garnet in eclogite are summarized in table 3.7. The FeO content of garnet in eclogite is higher in the rim of the crystal than in the core with a FeO content ranging from 20.0% to 20.3% in the core and 21.6% to 23.6% in the rim. The MgO and CaO contents are lower in the rim of garnet crystals than in the core with a MgO content ranging from 7.24% to 8.25% in the core and 7.07% to 7.82% in the rim and a CaO content of 9.83% to 11.05% in the core and 7.52% to 8.72% in the rim.

	Sample 7				Sample 9	
	07gnt2 (M1)		07gnt3 (M2)		09gnt2 (M1)	
Appendix:	Fig. A37		Fig. A38		Fig. A46	
	Core	Rim	Core	Rim	Core	Rim
SiO2	39.60	39.65	39.56	39.46	39.63	39.09
TiO2	0.14	0.04	0.04	0.06	0.04	0.03
Al2O3	21.68	21.91	21.87	21.77	21.90	21.60
Cr2O3	0.02	0.04	0.04	0.03	0.03	0.03
FeO	19.97	21.66	20.34	22.15	20.09	23.61
MnO	0.48	0.59	0.53	0.59	0.51	0.77
MgO	8.25	7.82	8.19	7.65	7.24	7.07
CaO	9.83	8.72	9.92	8.07	11.05	7.52
Na2O	0.02	0.01	0.01	0.02	0.00	0.01
NiO	0.03	0.01	0.00	0.00	0.00	0.00
Sum	100.03	100.45	100.49	99.80	100.49	99.73
Si	3.01	3.02	2.99	3.03	3.01	3.02
Ti	0.01	0.00	0.00	0.00	0.00	0.00
Al	1.94	1.96	1.95	1.97	1.96	1.97
Cr	0.00	0.00	0.00	0.00	0.00	0.00
Fe3	0.02	0.00	0.05	0.00	0.02	0.00
Fe2	1.25	1.38	1.23	1.42	1.26	1.52
Mn	0.03	0.04	0.03	0.04	0.03	0.05
Mg	0.94	0.89	0.92	0.88	0.82	0.81
Ca	0.80	0.71	0.80	0.66	0.90	0.62
Mg#	0.42	0.39	0.42	0.38	0.39	0.35

Tabel 3.7: Core and rim data for M1 and M2 garnet in the eclogite samples. Top columns: Element oxides in wt% oxide. Middle columns: Elements in cations p.f.u. Lower row: Mg# of the analyses.

Spinel

Linescans through M2 spinel crystals in garnet websterite show zoned chemical profiles (Fig 3.21. M2 spinel is of the Cr-spinel type and has a core Cr content of 45% and a rim Cr content of about 37%. M2 spinel crystallized together with low Cr M2 garnet (Fig. A48).

The Composition of M3a kelyphitic spinel can be derived from the appendix: figure A67point#9. M3a spinel consist of 56% Al_2O_3, 17% FeO, 4% SiO_2, 16% MgO, 3% Cr_2O_3 and 1.5% CaO.

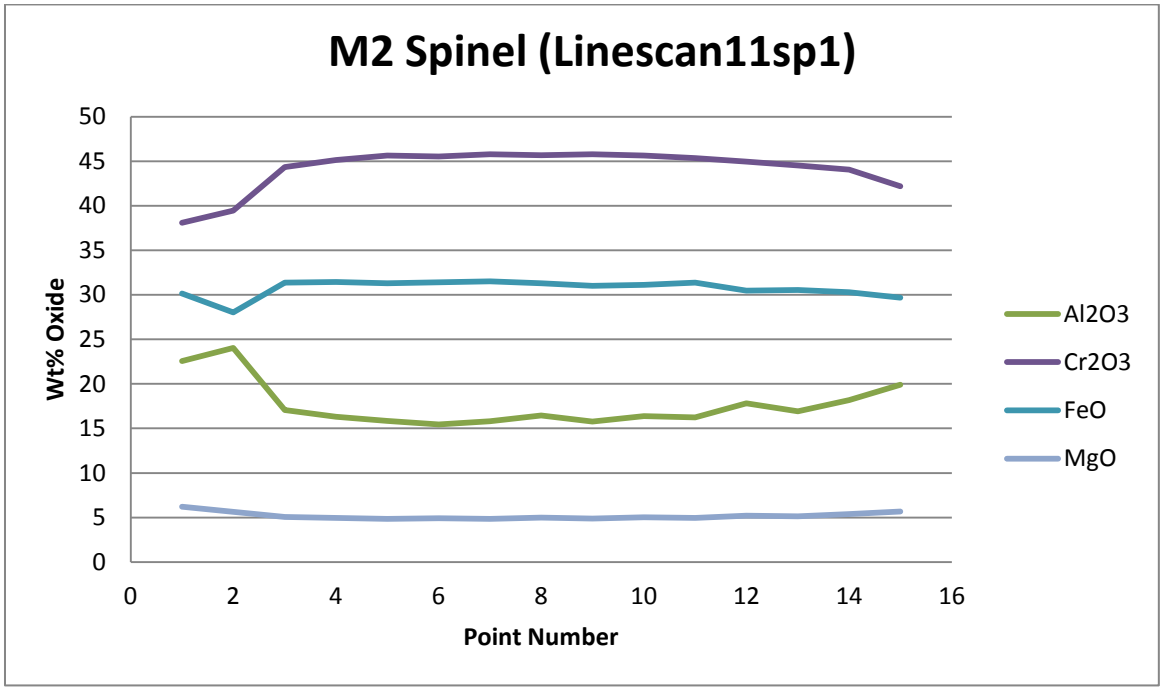

Figure 3.21: Representative example of a linescan through a M2 spinel crystal in garnet websterite (see appendix Fig. A57 for location) showing a homogenous chemical profile.

	Sample 11	
	11sp1 (M2)	
	Fig. A57	
Appendix:	Core	Rim
SiO2	0.19	0.07
TiO2	0.23	0.14
Al2O3	16.45	22.57
Cr2O3	45.69	38.10
FeO	31.29	30.14
MnO	0.84	0.71
MgO	4.98	6.21
CaO		
Na2O		
NiO		
Sum	99.65	97.95
Si	0.01	0.00
Ti	0.01	0.00
Al	0.64	0.87
Cr	1.20	0.98
Fe3	0.13	0.14
Fe2	0.74	0.68
Mn	0.02	0.02
Mg	0.25	0.30
Ca		
Na		

Table 3.8: Tabel 3.7: Core and rim data for M2 spinel in a garnet websterite sample. Top columns: Element oxides in wt% oxide. Middle columns: Elements in cations p.f.u. Lower row: Mg# of the analyses.

Amphibole and Clinochlore

M3b Amphibole and M3b clinochlore were captured in a linescan through multiple crystals found in figure 3.22. Clinochlore was measured in point 1-4 and amphibole was measured in point 5-14.

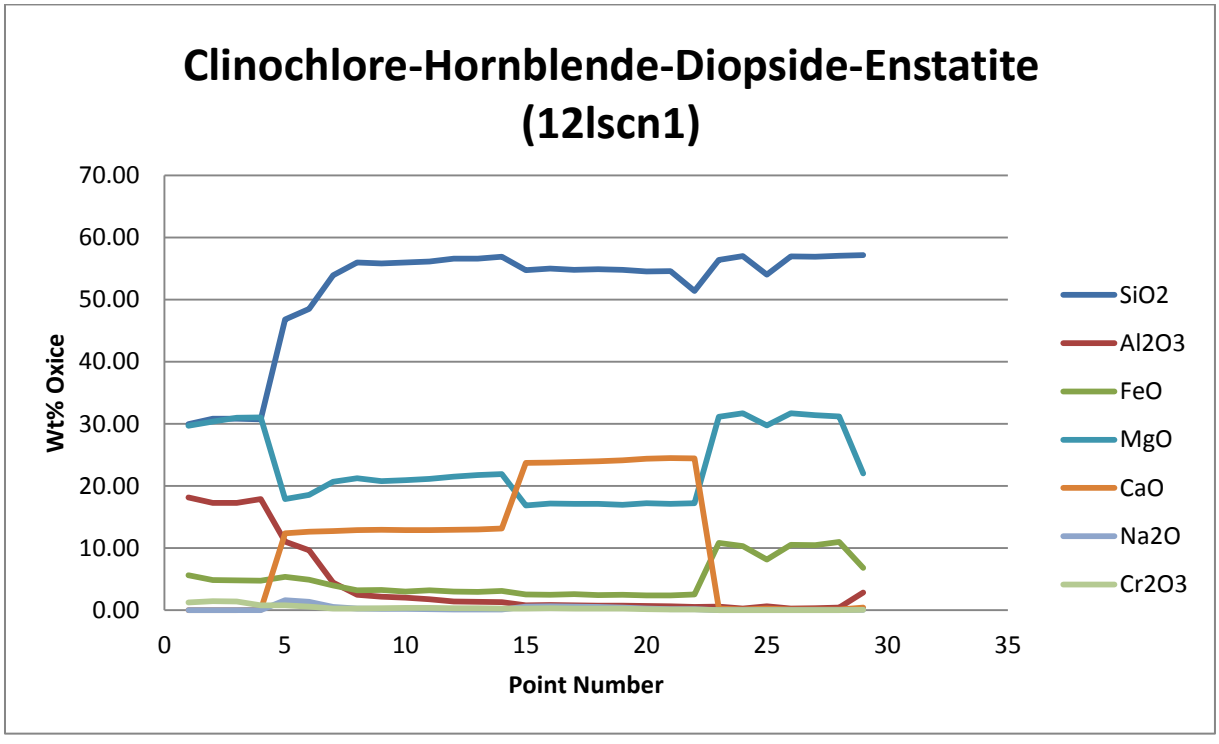

Figure 3.22: Representative example of a linescan through a M3b clinochlore and M3b amphibole in garnet websterite (see appendix Fig. A71 for location).

4. Geothermobarometry

In this section the geothermobarometric results will be presented. Geothermobarometry is a method to estimate the pressure and temperature conditions of a metamorphic rock using the chemical composition of stable mineral assemblages assumed to be in equilibrium. Geothermometers and geobarometers are based on the exchange of elements in temperature or pressure sensitive reactions between minerals. The minerals used for geothermobarometry are assumed to have grown in equilibrium. Geothermometers are based on temperature dependant exchange reactions of elements between two adjacent minerals. These reactions have a low volume change combined with high entropy and enthalpy resulting in steep slopes of reaction lines in PT diagrams (Krogh Ravna & Paquin, 2003). Geobarometers are based on reactions with a high volume change combined with low changes in entropy and enthalpy and are therefore strongly pressure dependant resulting in flat slopes of reaction lines in PT diagrams (Krogh Ravna & Paquin, 2003). Combining thermometers and barometers applied to the same mineral assemblage creates intersecting lines in a PT diagram. The point of intersection between the two lines yields a pressure and temperature estimate for the mineral assemblage within the investigated sample.

The thermobarometric methodologies are described by Krogh Ravna & Paquin (2003). A summary of available thermometers and barometers is given in the spreadsheet PTEXL, created by Thomas Keuhler and modified by Andrei Girnis in 2000. PTEXL allows the calculation of pressure and temperature for many commonly used thermometric and barometric reactions, using the element oxide wt% obtained from EMP mineral analysis. Each symbol for a thermometer or barometer also includes a reference to the original author(s) i.e: T[EG79]: Ellis, D.J. & Green, D.H. (1979), p[NG85]: Nickel, K.G. & Green, D.H. (1985), T[Powell85]: Powell, R. (1985), T[BKN90]: Brey, G.P. & Koehler, T. (1990), T[OpxBK90]: Brey, G.P. & Koehler, T. (1990), p[NimisTaylor00]: Nimis, P. & Taylor, W.R. (2000). PTEXL was used in this section to estimate the PT conditions during the formation of the Scandian M2 mineral assemblage. However, the meaning of the resulting PT conditions will be discussed later, since intragranular diffusion may continue after the maximum PT conditions are reached if these conditions are above the blocking temperature of intragranular diffusion. This means that the resulting PT conditions may reflect the blocking temperature of intragranular diffusion for the elements used in the calculations, rather than the maximum temperature reached during Scandian peak metamorphism. The results of geothermobarometry applied to the M2 assemblage can also be tested by applying the same methods to the M1 assemblage, assuming that a full compositional reset of the M1 assemblage took place during the Scandian. The M1 assemblage must therefore yield similar PT results.

First however, a suitable geothermobarometric method must be selected. The geothermobarometric methods described by Krogh Ravna & Paquin (2003) have been developed over the years by different laboratories, all yielding different PT results when applied to a certain sample. A suitable method will be selected by applying different geothermometer + geobarometer combinations to the EMP analyses of the M2 assemblage from different samples. Since all samples come from the same peridotite body, Scandian PT conditions must have been equal during metamorphism and any differences in PT conditions from geothermobarometry should reflect analytical errors/spread resulting from the applied method. Applying a geothermobarometric method to EMP analyses of mineral combinations from multiple samples will therefore be done to gain some insight in the amount of analytical spread that each method has. Afterwards a preferred method will be selected based on the amount of spread and by comparing the PT results with those from earlier studies (the

temperature contour map of Fig. 1.3). Pijpers (2012) already investigated the analytical spread of the different geothermobarometric methods, by using multiple linescan data points of a single opx, cpx or gnt crystal from a single sample as input for PTEXL. Using representative EMP analyses from different samples as input as done here, is however a different approach.

4.1. Selecting a suitable geothermobarometric method

The representative M2 mineral analyses used as input for PTEXL are listed in table 4.1. M2 garnet was only measured in 2 samples, which unfortunately limits the use of garnet involved thermometers and barometers to investigate analytical spread. 5 mineral combinations of orthopyroxene + clinopyroxene can however be used to determine the analytical spread of opx-cpx solvus thermometers, the single opx thermometer [OpxBK90] of Brey and Koehler (1998) and the Cr in cpx barometer of Nimis & Taylor (2000). Therefore these methods will be applied to the following M2 mineral combinations from the 4 samples: [02opx1, 02cpx3 & 02gnt1a]; [04opx1 & 04cpx2]; [11opx2, 11cpx2 & 11gnt3]; [12opx2 & 12cpx2]; [12opx5 & 12cpx3] (Table. 4.1).

	Garnet		Clinopyroxene					Orthopyroxene					
	02gnt1a (M2)	11gnt3 (M2)	02cpx3 (M2)	04cpx2 (M2)	11cpx2 (M2)	12cpx2 (M2)	12cpx3 (M2)	02opx1 (M2)	04opx1 (M2)	04opx3 (M2)	11opx2 (M2)	12opx2 (M2)	12opx5 (M2)
SiO2	41.15	40.18	53.89	54.10	54.62	54.80	54.80	57.18	56.41	56.52	57.26	57.09	56.95
TiO2	0.01	0.03	0.07	0.04	0.05	0.04	0.04	0.02	0.03	0.04	0.03	0.01	0.02
Al2O3	21.73	21.27	1.07	0.93	1.14	0.84	0.72	0.34	0.31	0.35	0.33	0.44	0.29
Cr2O3	1.36	1.70	0.43	0.50	0.67	0.36	0.25	0.04	0.08	0.05	0.10	0.09	0.04
FeO	14.18	15.61	2.22	2.60	2.58	2.57	2.49	8.35	9.88	9.87	9.49	9.61	10.51
MnO	0.57	0.63	0.04	0.07	0.03	0.06	0.04	0.10	0.14	0.14	0.12	0.12	0.12
MgO	15.04	14.51	16.63	16.11	16.27	16.65	16.99	32.57	32.24	32.30	32.53	32.69	31.73
CaO	5.36	5.10	23.69	23.43	23.04	23.73	24.11	0.13	0.11	0.13	0.11	0.11	0.09
Na2O	0.00	0.04	0.52	0.84	0.82	0.67	0.43	0.00	0.00	0.01	0.00	0.00	0.01
NiO	0.00	0.01	0.10	0.03	0.05	0.05	0.07	0.16	0.10	0.09	0.10	0.08	0.15
Sum	99.41	99.09	98.65	98.65	99.27	99.76	99.94	98.88	99.30	99.50	100.07	100.23	99.91

Table 4.1: Representative mineral EMP analyses for the M2 assemblage derived from linescans (see appendix: [02gnt1a] in Fig. A9{point#1-8}, [02cpx3] in Fig. A8, [02opx1] in Fig. A12, [04opx1] in Fig. A24, [04cpx2] in Fig. A21, [11opx2] in Fig. A56, [11cpx2] in Fig. A51, [11gnt3] in Fig. A54, [12opx2] in Fig. A69, [12cpx2] in Fig. A65, [12opx5] in Fig. A71{point#23-30}, [12cpx3] in Fig. A71{point#15-22}.

Applying the geothermometers of T[BKN90], T[Wells77], T[BM85], T[OpxBK90] & T[Taylor98] and the geobarometer of P[NimisTaylor00] to the 5 mineral combinations results in the PT diagram illustrated in figure 4.1. All thermometers except for T[OpxBK90] (purple lines in Fig. 4.1.) yield results with high temperature spreads of more than ±100 °C. For this reason the geothermometers of T[BKN90], T[Wells77], T[BM85] & T[Taylor98] are considered to be unreliable and combining them with the geobarometer of P[NimisTaylor00] results in high inaccuracies. T[OpxBK90] appears to be the best geothermometer to combine with the geobarometer of P[NimisTaylor00], since it has the least amount of spread. The best results from using the combination of T[OpxBK90] and P[NimisTaylor00] are illustrated by the shaded area in figure 4.1. The PT conditions estimated by using this combination should be somewhere in this shaded area: T=742±58 °C, P=38.5±9.5 kbar. The geobarometer of P[NimisTaylor00] leads to a high analytical spread of ±9.5 kbar when applied to the 5 mineral combinations of M2 opx and cpx, but this is the only applicable geobarometer that can be used for all samples, since it does not require the composition of gnt as input, however it does require to coexist with cpx.

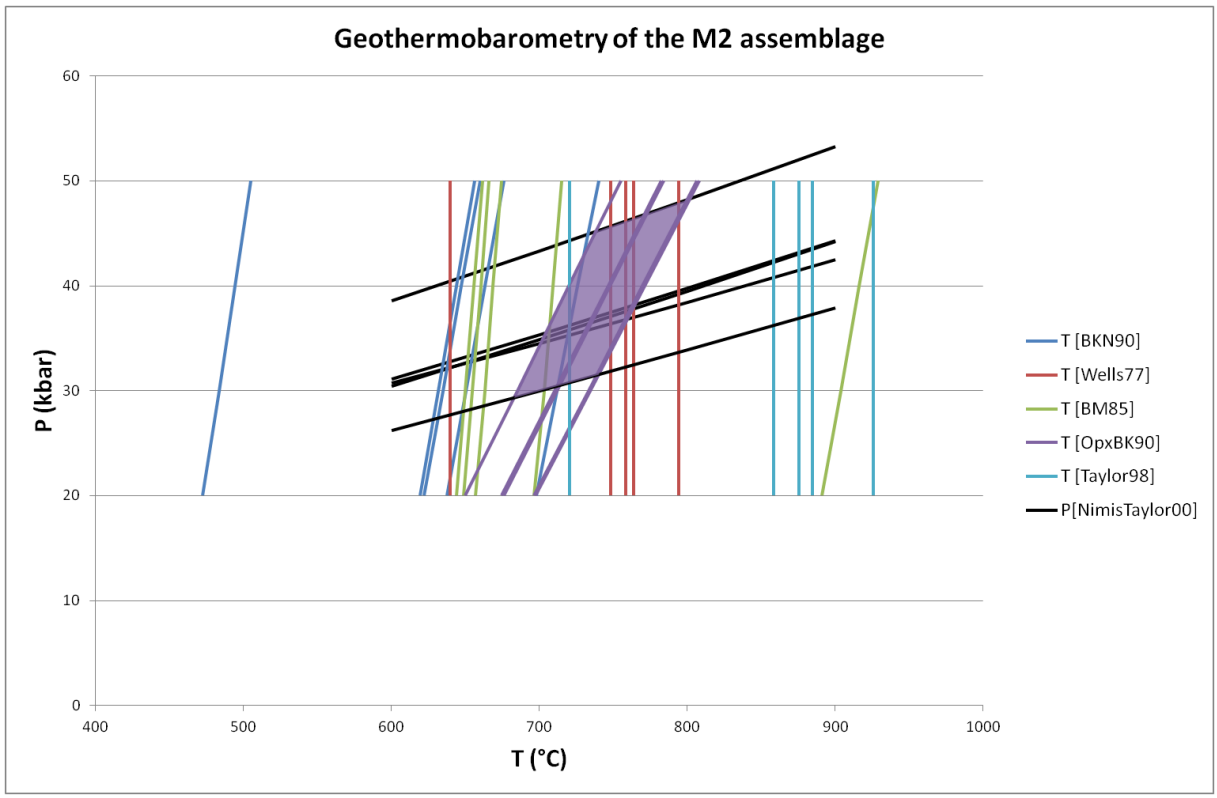

Figure 4.1: Geothermobarometry applied to the EMP analyses of 5 (M2) opx+cpx mineral combinations listed in table 4.1. Mineral combinations used: [02opx1, 02cpx3 & 02gnt1a]; [04opx1 & 04cpx2]; [11opx2, 11cpx2 & 11gnt3]; [12opx2 & 12cpx2]; [12opx5 & 12cpx3] (Table. 4.1). The shaded area indicates the best geothermobarometric method with the least amount of spread: T[OpxBK90] + P[NimisTaylor00].

Only the geothermometers and geobarometers that do not require the composition of garnet as input were used in figure 4.1. to estimate the PT conditions. This unfortunately eliminates the use of many widely applied and successful garnet involved methods. For this reason an attempt is made to additionally select a garnet involved geothermobarometric method. To do this the garnet involved geothermobarometric methods will be applied to EMP analyses of the M2 mineral combinations of [02opx1, 02cpx3 & 02gnt1a] and [11opx2, 11cpx2 & 11gnt3] (Table 4.1.). These mineral combinations are from sample 02 and sample 11, the only 2 samples in which M2 garnet was measured in garnet pyroxenite. The preferred garnet involved geothermometer and geobarometer will be selected based on consistency in results between the 2 samples and by comparing the results with those from earlier studies (the temperature contour map of figure 1.3).

Applying the garnet involved geothermometric methods to the mineral combinations of [02opx1, 02cpx3 & 02gnt1a] and [11opx2, 11cpx2 & 11gnt3](Table 4.1) yields the PT diagram illustrated in figure 4.2. The single-opx geothermometer of T[OpxBK90] was also applied here, because it proved to be successful in figure 4.1. According to figure 1.3. the APM is located at the 700 °C isotherm with a pressure of >24 kbar. When the temperature at a pressure of 30 kbar is considered in figure 4.2., the geothermometers that agree best with the 700 °C isotherm (Fig 1.3.) are T[OpxBK90] and T[EG79]. T[OpxBK90] yields a temperature of 722±12 °C at 30 kbar. T [EG79] yields a temperature of 704±24 °C at 30 kbar. Since the garnet involved geothermometers were only applied to 2 samples, the analytical spread does not mean much in figure 4.2., since it would require the application of the geothermometers to more samples to gain a better insight in the analytical spread. However, some geothermometric methods illustrated in figure 4.2 already have large spreads when applied to only 2

samples, indicating that they may become even more unreliable if they would be applied to more samples. Therefore the most consistent result will be preferred, meaning that T[OpxBK90] (722 ± 12 °C at 30 kbar) is preferred over T[EG79] (704 ± 24 °C at 30 kbar). Apparently the single opx thermometer T[OpxBK90] works better than the garnet involved thermometers.

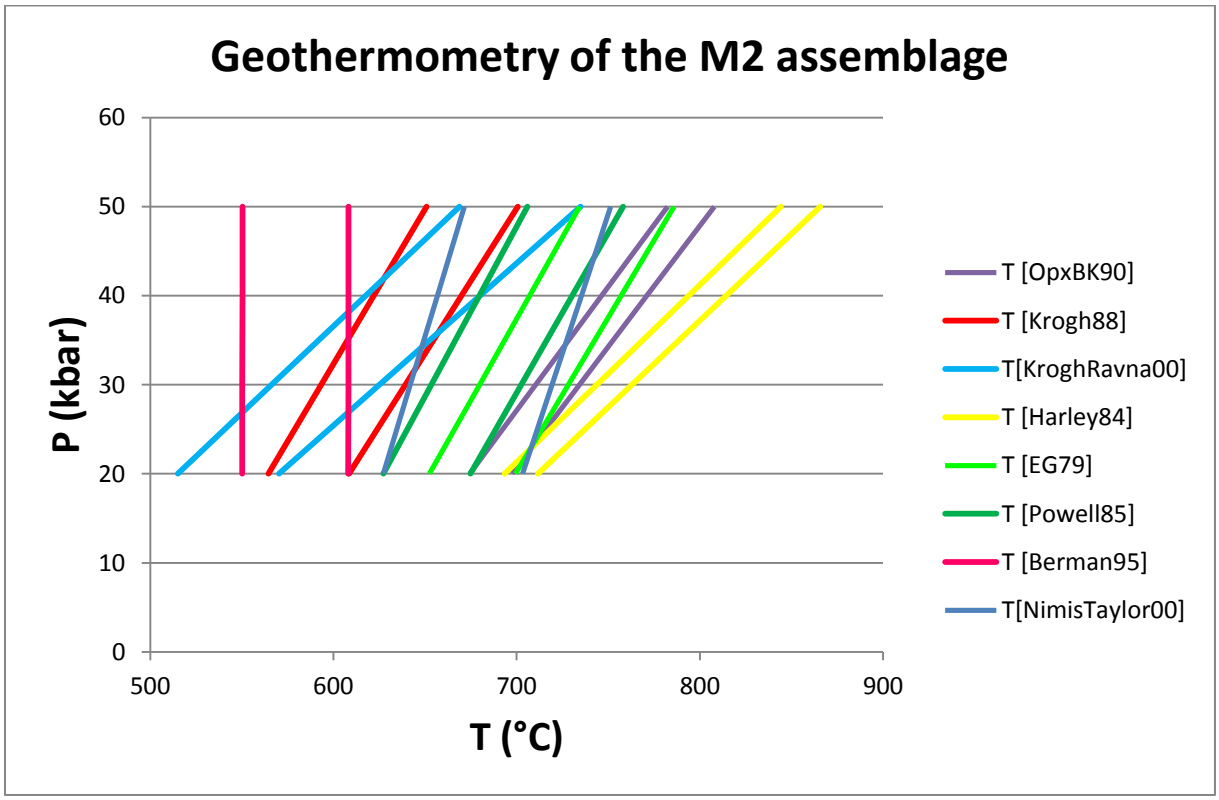

Figure 4.2: Geothermometry applied to the EMP analyses of (M2) gnt, opx and cpx from 2 samples. Mineral combinations used: [02opx1, 02cpx3 & 02gnt1a] and [11opx2, 11cpx2 & 11gnt3] (Table 4.1.).

Applying the garnet involved geobarometric methods to the mineral combinations of [02opx1, 02cpx3 & 02gnt1a] and [11opx2, 11cpx2 & 11gnt3](Table 4.1) yields the PT diagram illustrated in figure 4.3. When the pressure at 700 °C is considered, the pressure should be above 24 kbar according to figure 1.3. The exact pressure is however not known, making it hard to select a preferred geobarometer based on a reference pressure from earlier research for the APM. This means that any of the geobarometers listed in figure 4.3 might be applicable, except for P[RGP96], which yields a pressure below 24 kbar at 700 °C for 1 sample. The preferred barometric method will therefore be selected based on consistency between the pressure results of the 2 samples. P[MC79], P[BKN90] and P[BBG08] yield the most consistent results, since their lines overlap for both samples. Any of these methods may be successfully used for geothermobarometry of the M2 assemblage, but if one must be selected then p[BKN90] is preferred, because it yields intermediate pressures at 700 °C (P=32 kbar) with respect to p[BBG08]=27 kbar and p[MC74]=33.5 kbar. Additionally, p[BKN90] is developed by the same researchers and in the same lab as the earlier preferred geothermometer T[OpxBK90], which makes it likely that their combination leads to a reliable geothermobarometric method. The equations of the preferred geothermometer and geobarometers are given in Appendix: chapter 7, page 63.

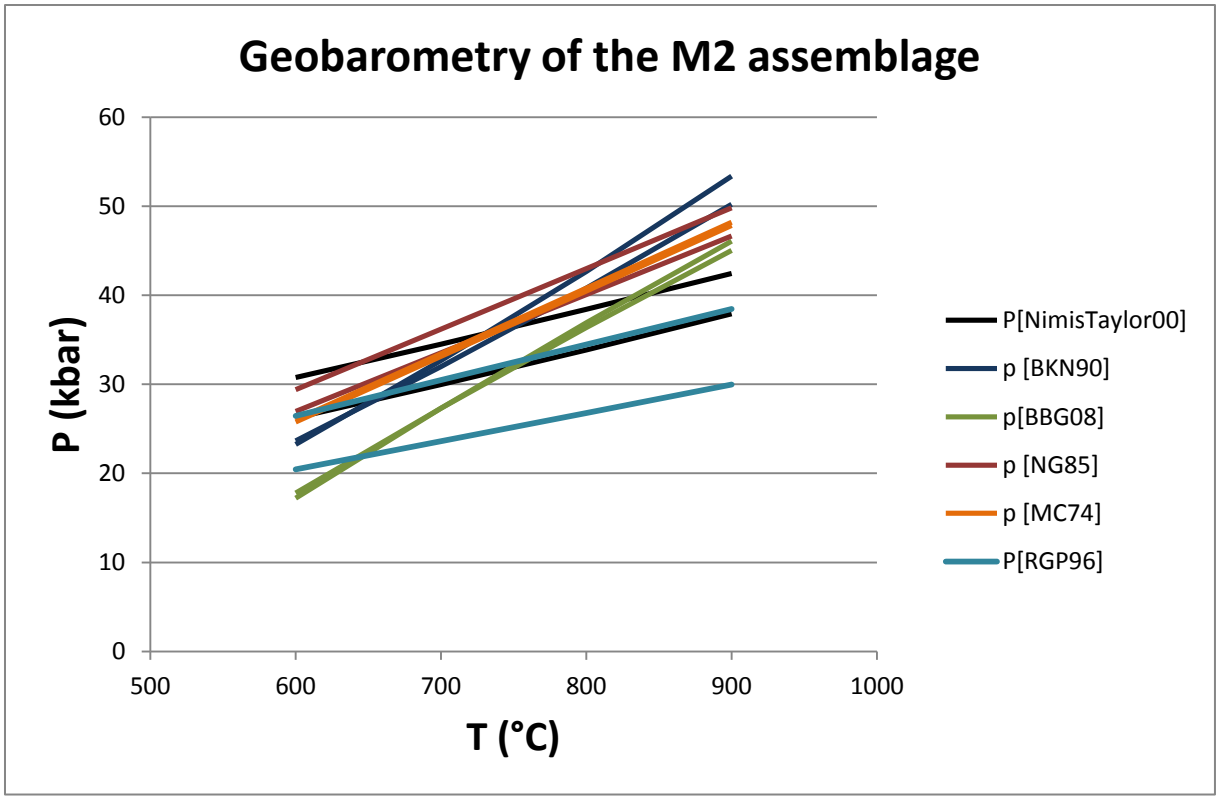

Figure 4.3: Geobarometry applied to the EMP analyses of (M2) gnt, opx and cpx from 2 samples. Mineral combinations used: [02opx1, 02cpx3 & 02gnt1a] and [11opx2, 11cpx2 & 11gnt3] (Table 4.1.).

4.2 Geothermobarometry of the M2 and M1 assemblages

Following from section 4.1 the preferred geothermometer/geobarometer combination is T[OpxBK90] + p[BKN90]. First the preferred geothermobarometric method will be applied to the M2 garnet bearing samples. The application of T[OpxBK90] and p[BKN90] to the mineral combinations [02opx1, 02cpx3 & 02gnt1a] and [11opx2, 11cpx2 & 11gnt3](Table 4.1) yields the PT diagram listed in figure 4.4. According to figure 4.4 the Scandian PT conditions of the APM are T=750±20 °C and P=37±3 kbar. The inaccuracies are however higher in reality, since the spread in figure 4.4 is the result of the application to just 2 mineral combinations from 2 samples.

The PT conditions following from the application of T[OpxBK90] and p[NimisTaylor00] to 5 mineral combinations give more insight in the analytical spread of these methods (shaded area in Fig. 4.1). These results are T=742±58 °C, P=38.5±9.5 kbar (Fig. 4.1.). The results from figure 4.4 (T=750±20 °C and P=37±3 kbar) fall within the this PT range. Apparently geothermobarometry applied to the Scandian M2 assemblage of the APM in this study estimates temperatures higher than 700 °C predicted by earlier studies (Fig. 1.3) and pressures reaching UHP conditions. Another question is if these PT conditions actually represent the maximum PT conditions during Scandian metamorphism of the APM, or if continued intragranular diffusion took place after peak metamorphism, because the temperature was higher than the blocking temperature of intragranular diffusion within minerals for some or all elements after peak metamorphism. This will be covered in the discussion section.

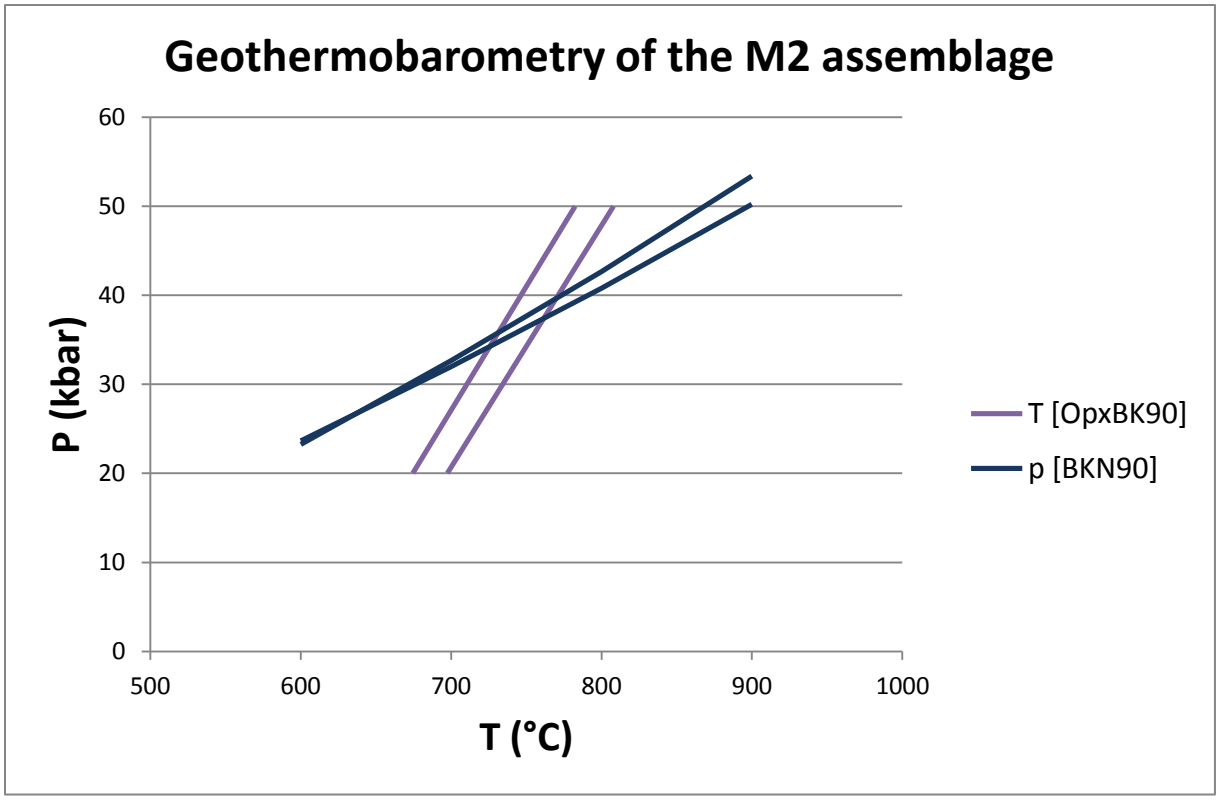

Figure 4.4: The preferred geothermobarometric methods of T[OpxBK90] + p[BKN90] applied to the EMP analyses of (M2) gnt, opx and cpx from 2 samples. Mineral combinations used: [02opx1, 02cpx3 & 02gnt1a] and [11opx2, 11cpx2 & 11gnt3] (Table 4.1.).

The results of geothermobarometry applied to the M2 assemblage must now be tested by applying the same geothermobarometric methods to the minerals from the M1 assemblage. Therefore the geothermobarometric methods of T[OpxBK90] + p[BKN90] (Fig. 4.5) and T[OpxBK90] + p[NimisTaylor00] (Fig 4.6) will be applied to the representative mineral EMP analyses for the M1 assemblage listed in table 4.2. The M1 mineral combinations to which geothermobarometry was applied are the following: [02gnt3, 02cpx2, 02opx2], [04gnt1, 04cpx1, 04opx2], [11gnt1, 11cpx1, 11opx1] and [12gnt1, 12cpx1, 12opx3].

	Garnet				Clinopyroxene				Orthopyroxene			
	02gnt3 (M1)	04gnt1 (M1)	11gnt1 (M1)	12gnt1 (M1)	02cpx2 (M1)	04cpx1 (M1)	11cpx1 (M1)	12cpx1 (M1)	02opx2 (M1)	04opx2 (M1)	11opx1 (M1)	12opx3 (M1)
SiO2	40.90	40.70	40.19	41.50	53.62	54.17	54.98	55.21	56.87	56.29	57.01	57.01
TiO2	0.08	0.08	0.06	0.05	0.08	0.02	0.05	0.06	0.03	0.03	0.02	0.02
Al2O3	20.56	20.24	20.51	21.20	1.12	0.98	1.50	1.35	0.67	0.53	0.78	0.58
Cr2O3	2.95	3.03	2.88	2.42	0.82	0.70	0.88	0.92	0.12	0.09	0.12	0.11
FeO	13.04	14.67	15.03	15.32	2.08	2.40	2.39	2.30	8.17	9.81	9.48	9.35
MnO	0.48	0.61	0.58	0.60	0.05	0.05	0.07	0.07	0.09	0.14	0.12	0.10
MgO	16.05	14.91	15.13	14.18	16.37	16.42	16.51	15.88	33.42	32.35	32.60	32.78
CaO	5.63	5.71	5.57	5.42	23.41	23.36	23.05	23.02	0.11	0.12	0.12	0.11
Na2O	0.00	0.03	0.00	0.03	0.80	0.76	1.00	0.83	0.00	0.00	0.00	0.00
NiO	0.01	0.00	0.00	0.00	0.09	0.04	0.04	0.03	0.17	0.08	0.05	0.14
Sum	99.70	99.98	99.96	99.66	98.42	98.91	100.48	100.73	99.67	99.44	100.29	100.21

Table 4.2: : Representative mineral EMP analyses for the M1 assemblage derived from linescans 02, 04, 11 and 12 (see appendix: [02cpx2] in Fig. A7, [02gnt3] in Fig. A11, [02opx2] in Fig. A13, [04gnt1] in Fig. A22, [04cpx1] in Fig. A20, [04opx2] in Fig. A25, [11gnt1] in Fig. A52, [11cpx1] in Fig. A50 and [11opx1] in Fig. A55) [12gnt1] in Fig. A66, [12cpx1] in Fig. A64, [12opx3] in Fig. A70.

Applying the geothermobarometric method of T[OpxBK90] + p[BKN90] to the minerals from the M1 assemblage (table 4.2) yields the PT diagram listed in figure 4.5. According to figure 4.5 the PT conditions of the M1 assemblage are T=656±18 °C and P=10±5 kbar. The temperature results show a higher consistency with a lower spread than the pressure results. The pressure results are significantly lower for the M1 assemblage (P=10±5 kbar) than for the M2 assemblage (P=37±3 kbar) when the method of T[OpxBK90] + p[BKN90] is used. The difference in pressure results using the p[BKN90] barometer are possibly because M2 opx has a lower Al core content than M1 opx (Table 3.2, Fig. 3.10, Fig. 3.11), since the barometer of p[BKN90] is dependent on the Al content of opx (Brey et al., 1990). Possible causes of the lower Al content in M2 opx will be treated in the discussion section. The low pressure estimate for the M1 assemblage when using T[OpxBK90] + p[BKN90] causes the temperature results to be lower, since the intersection will take place at lower pressures. However, when the temperature at 30 kbar is considered using only T[OpxBK90] the results are quite similar for the M1 assemblage (711±11 °C at 30 kbar (Fig. 4.5)) and the M2 assemblage (722±12 °C at 30 kbar (Fig. 4.4)).

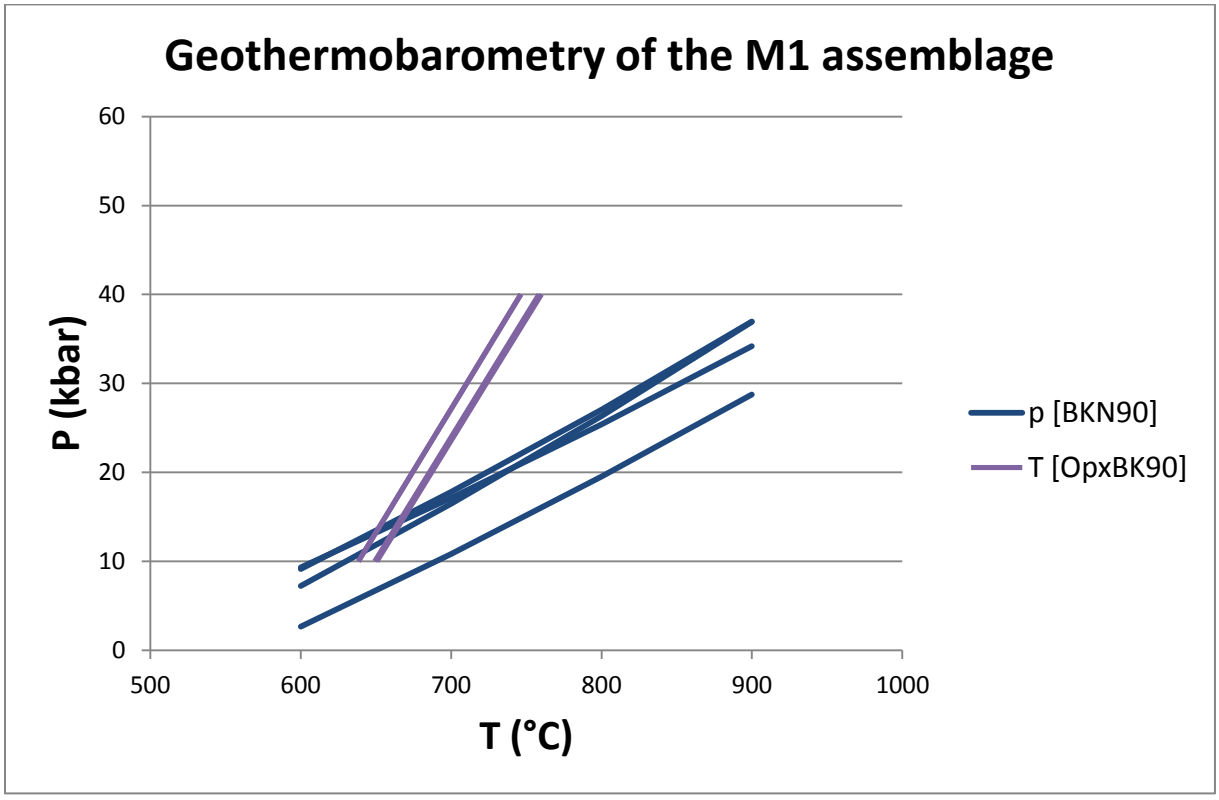

Figure 4.5: Geothermobarometric method of T[OpxBK90] + p[BKN90] applied to the EMP analyses of (M1) gnt, opx and cpx from 4 samples. Mineral combinations used: [02gnt3, 02cpx2, 02opx2], [04gnt1, 04cpx1, 04opx2], [11gnt1, 11cpx1, 11opx1] and [12gnt1, 12cpx1, 12opx3] (table 4.2).

Applying the geothermobarometric method of T[OpxBK90] + p[NimisTaylor00] to the minerals from the M1 assemblage (table 4.2) yields the PT diagram listed in figure 4.6. According to figure 4.6 the PT conditions of the M1 assemblage are T=735±15 °C and P=35.5±3.5 kbar. The method of T[OpxBK90] + p[NimisTaylor00] yields slightly lower average PT results for the M1 assemblage (T=735±15 °C and P=35.5±3.5 kbar) than for the M2 assemblage (T=750±20 °C and P=37±3 kbar), but the error margins show a large overlap.

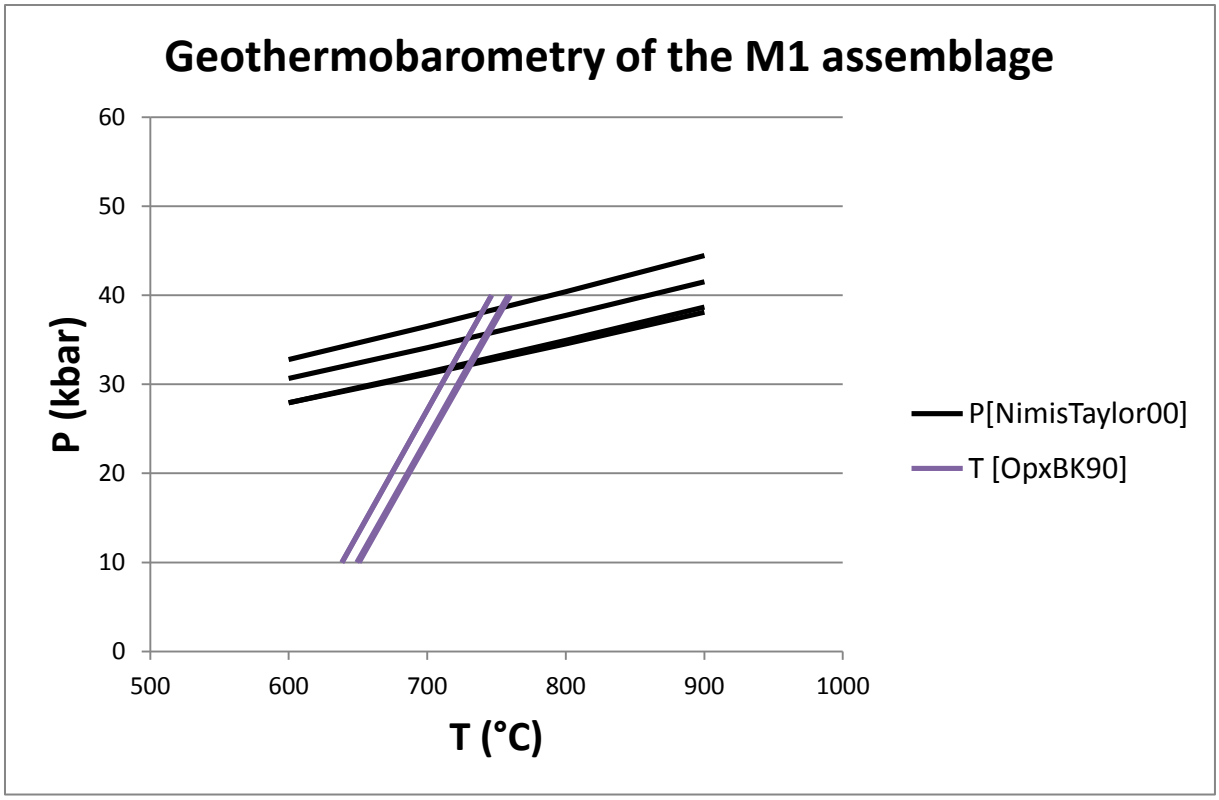

Figure 4.6: Geothermobarometric method of T[OpxBK90] + p[NimisTaylor00] applied to the EMP analyses of (M1) gnt, opx and cpx from 4 samples. Mineral combinations used: [02gnt3, 02cpx2, 02opx2], [04gnt1, 04cpx1, 04opx2], [11gnt1, 11cpx1, 11opx1] and [12gnt1, 12cpx1, 12opx3] (table 4.2).

4.3 Geothermobarometry summary

In table 4.3 the PT results from geothermobarometry are summarized. For the geothermobarometric method of T[OpxBK90] + p[NimisTaylor00] the results of M1 and M2 are in relatively good agreement. However, for the method of T[OpxBK90] + p[BKN90] the pressure estimate for the M1 assemblage is very low. This is because the barometer p[BNK90] uses the Al content of orthopyroxene to estimate pressure (Brey et al., 1990) and the Al content of M2 orthopyroxene is lower than M2 orthopyroxene (table 3.2). The temperature results for the M2 Scandian mineral assemblage are 750 ±50 °C for T[OpxBK90] + p[BKN90] and 742±58 °C for T[OpxBK90] + p[NimisTaylor00] which is a little higher than the 700 °C from earlier research (Fig. 1.3). This might be due to the high pressure estimate that comes with it of P=37±3 kbar and P=38.5±9.5 kbar. When the temperature results using only the geothermometers is used with a preset equilibrium pressure of 30 kbar, the results are closer to the 700 °C predicted by earlier research.

Table 4.3: Summarized PT results from geothermobarometry.

	T[OpxBK90] + p[BKN90]	T[OpxBK90] + p[NimisTaylor00]
M1 assemblage	T=656±18 °C, P=10±5 kbar	T=735±15 °C, P=35.5±3.5 kbar
M2 assemblage	T=750±20 °C, P=37±3 kbar	T=742±58 °C, P=38.5±9.5 kbar

5. Discussion

The amount of chemical re-equilibration can have a large effect on the PT estimates for the older M1 assemblage. Solid state diffusion may lead to re-equilibration of major elements within older proterozoic M1 crystals to compositions representing new temperature and pressure conditions at the formation of the younger Scandian M2 assemblage. The re-equilibration occurs if these conditions are above closure temperature for mobility of major elements within a mineral. Chemical re-equilibration of M1 may in fact have taken place in the garnet websterite samples for major elements like Fe and Mg, illustrated by the homogeneous chemical profiles throughout crystals of the M1 assemblage (Fig. 3.10, 3.13 & 3.17). The composition of these elements is similar in minerals from the M2 assemblage. Cr and Al however, appear to be less mobile, because they have varying core contents in M1 and M2 minerals illustrated by the lower amount of Al in M2 opx than in M1 opx (Fig. 3.10 & 3.11), by the lower amount of Cr in M2 cpx than in M1 cpx (Fig. 3.13 & 3.14) and by the lower amount of Cr in M2 garnet than in M1 garnet (Fig. 3.20). If Fe and Mg are more mobile within old assemblages than Al or Cr, the combination of barometer and thermometer may be erroneous. This is because the elements used in the geothermometric calculations (Fe and Mg) may have re-equilibrated completely, while the elements used in the geobarometric calculations (Al and Cr) may not have completely re-equilibrated. The intersection of thermometer and barometer will in this case yield a false PT estimate for the M1 assemblage.

The assumption that Cr is less mobile in garnet crystals than Fe and Mg, as well as the assumption that Al is less mobile in orthopyroxene is based on qualitative evidence regarding the observed chemical profiles throughout gnt/opx crystals in this study. Ideally quantitative evidence for elemental diffusion rates in garnet and orthopyroxene should back up these observations. However, reliable quantitative models for diffusion rates of Cr in garnet (and Al in opx) across various PT conditions with a compositional dependence are unavailable. The study done by Carlson (2006), in which diffusion rates in garnet are modeled across a range of PT conditions for Fe, Mg, Ca and Mn with a compositional dependence, should therefore be done in a similar way for Cr in garnet and Al in orthopyroxene in order to provide a quantitative argument.

In the case of the APM, the similar temperature results for the M1 and M2 assemblage suggest that the major elements Fe and Mg were completely re-equilibrated by intracrystalline diffusion during Scandian metamorphism, so that all temperature results reflect Scandian (M2) temperature conditions. The pressure estimates when using the p[NimisTaylor00] Cr in clinopyroxene geobarometer are also similar for the M1 and M2 assemblage, indicating that the small difference in Cr in clinopyroxene has no effect when using this barometer. The geobarometer p[BKN90] does however yield lower pressure estimates for the M1 assemblage than for the M2 assemblage (Table 4.3) due to the lower amount of Al in M2 orthopyroxene. This means that the combination of T[OpxBK90] and p[BKN90] yields a false PT result for the M1 assemblage, since it uses re-equilibrated elements to calculate temperature and un-equlibrated elements to calculate pressure.

According to Brueckner et al., 2010, a prograde metamorphic path is only present for the crustal emplacement of the peridotite bodies from the North-Western WGR, but not for those of the Central West where the APM is located (Fig. 1.3). The lower amount of Al in M2 orthopyroxene than in M1 orthopyroxene, together with the higher pressure estimate for the M2 assemblage when using the p[BKN90] barometer, imply that the peridotites of the Central West WGR may in fact have

experienced prograde metamorphism. The exact PT condition of the M1 assemblage prior to Scandian metamorphism is however not possible to determine using the geothermobarometric methodologies used in this study, due to the re-equilibration of temperature sensitive elements. This also holds for the possible lithospheric mantle evolution of the M1 assemblage prior to the Scandian orogeny as described by van Roermund, 2009a, b, Brueckner et al., 2010.

Pijpers (2012) concluded that the minerals from the M1 assemblage in garnet websterite were completely homogenized by intragranular diffusion during Scandian metamorphism, since they show homogeneous chemical profiles and the minerals from the M1 assemblage were completely re-equilibrated to the same chemical composition as the minerals from the M2 assemblage. Although the same results were obtained in this study for the major elements Fe, Mg, Ca, and Si in all minerals, a more detailed look in the chemical profiles of Al in orthopyroxene and Cr in garnet showed differences between minerals from the M1 and M2 assemblage. The lower amount of Cr in small garnet grains, located at the rims of garnet porphyroclasts or in the polygonal microstructure allowed to make a distinction between M1 and M2 garnet (Fig. 3.19). The high-Cr M1 garnet recrystallized to a low-Cr M2 garnet + M2 Cr-spinel during Scandian metamorphism. M2 garnet was not found by Pijpers (2012) and allowed a more detailed geothermobarometric investigation in terms of the M1 and M2 assemblages in this study.

The results from geothermobarometry applied to the M2 assemblage yielded temperature results higher than those from previous research (Fig. 1.3): T=750±20 °C, P=37±3 kbar for T[OpxBK90] + p[BKN90] and T=742±58 °C, P=38.5±9.5 kbar for T[OpxBK90] + p[NimisTaylor00]. However, the meaning of the resulting PT conditions must be discussed, since intragranular diffusion may continue after the maximum PT conditions are reached if these conditions are above the blocking temperature of intragranular diffusion. This means that the resulting PT conditions may reflect the blocking temperature of intragranular diffusion for the elements used in the calculations, rather than the maximum pressure and temperature reached during Scandian peak metamorphism if there is enough time for diffusion to occur after peak metamorphism. The PT results for Scandian metamorphism are already higher than those from previous research, even though they form a minimum estimate for the peak metamorphic conditions, since diffusion may continue after peak metamorphism. This means that either the exhumation after the subduction event and formation of the M2 was very rapid, so that non or very little diffusion occurred after peak metamorphism or the results from geothermobarometry for the M2 assemblage overestimate the peak metamorphic PT conditions. Another option is that the Scandian peak metamorphic conditions were underestimated in previous research.

The stable Scandian M2 mineral assemblage of opx, cpx, ol, spinel and garnet is complemented by a pseudosection made by Gilio et al., 2015, illustrated in figure 5.1. The M2 PT conditions indicated by the star in figure 5.1 are from a study on eclogites in the Friningen Garnet Peridotite done by Janák et al., 2013. Since these results are quite similar to those found in this study for the M2 assemblage it can be used to illustrated the PT conditions of the APM during Scandian metamorphism. According to figure 5.1 ol, gnt, cpx and opx are stable at UHPT lithospheric mantle conditions, which is where the M1 assemblage of the APM also originated and ol, gnt, cpx, opx and spinel are stable at the Scandian UHP metamorphic conditions around 750 °C and 3,0 GPa estimated by geothermobarometry applied to the M2 assemblage in this study. Therefore figure 5.1 complements the observed recrystallization of M1 garnet to M2 garnet + M2 spinel as a result of Scandian metamorphism (Fig. 3.19).

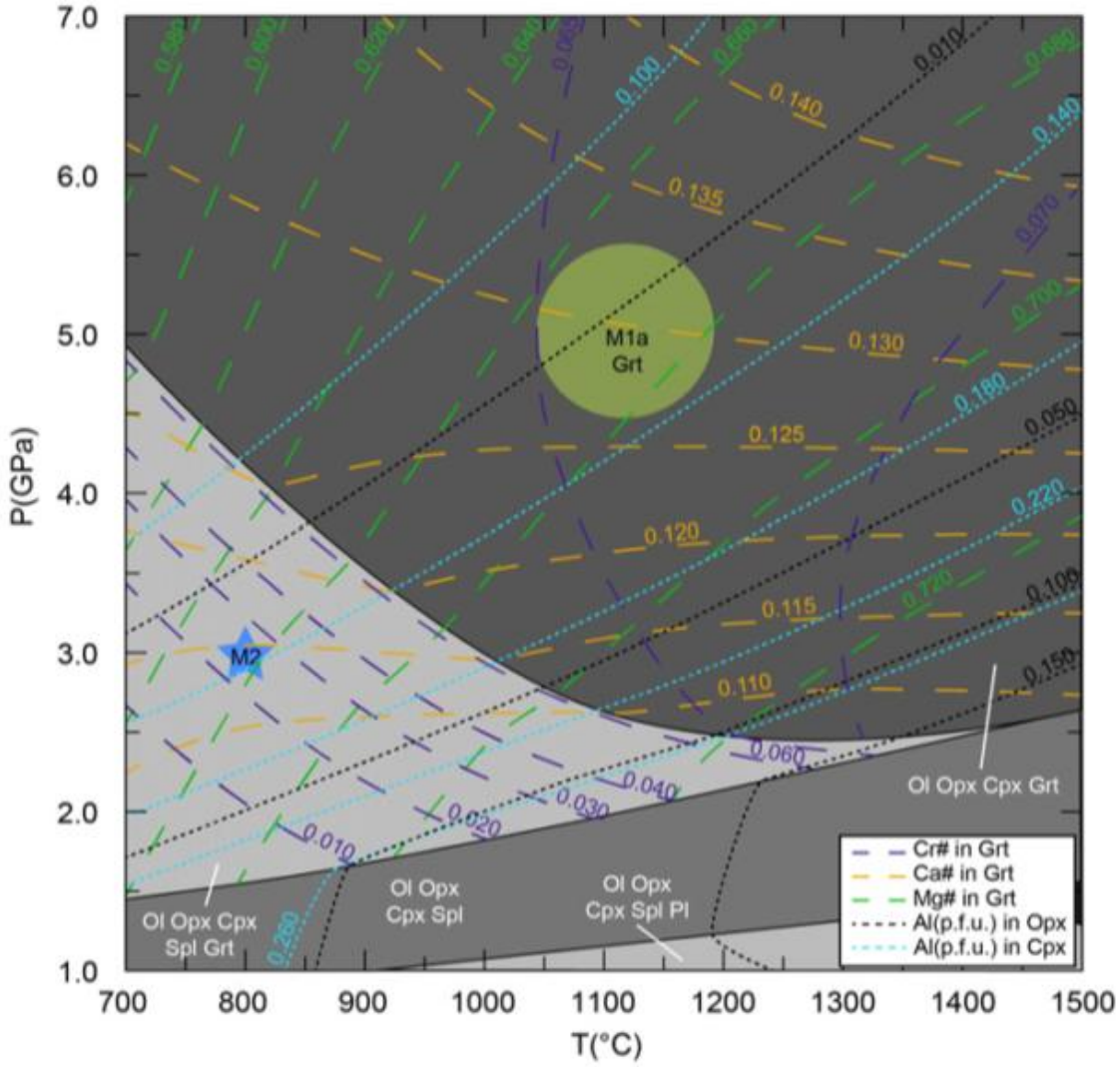

Figure 5.1: ***Gilio et al., 2015.*** **Pseudosection calculated with Perplex with Isopleths for Mg#, Ca# and Cr# in gnt and Al in opx. The star indicates a PT estimate for the M2 assemblage found in eclogites from the Friningen garnet peridotite from Janák et al., 2013, which is about similar to the PT estimate for the M2 mineral assemblage of the APM in this study. The shaded M1a area indicates the PT conditions of the lithospheric mantle M1a assemblage described in Gilio et al., 2015.**

Additional information that figure 5.1 provides are the Cr#, Ca#, Mg#, Al in opx and Al in cpx isopleths. Assuming that PT conditions for M1a and M2 in this study are similar to those plotted in figure 5.1, as well as assuming that the bulk rock composition is comparable, the plot would have similar isopleths for the AMP samples. The Mg# in grt isopleth is more or less parallel between M1a and M2, providing an additional explanation for the similar Mg content of M1 and M2 garnet found in the mineral-chemical analysis. According to figure 5.1 the Mg# of garnet hardly changes from M1a PT conditions towards M2 PT conditions. The Cr# in grt isopleth is however perpendicular relative to a straight path between M1a and M2, meaning that it changes drastically when going from M1a PT conditions towards M2 PT conditions. This explains the observed difference in Cr content between M1 and M2 garnet.

Future research regarding the PT conditions of the M1 proterozoic mantle and M2 Scandian mineral assemblages in the APM should focus on the analysis of bulk rock compositions of garnet-peridotite/-pyroxenite and eclogite samples to construct pseudosections like figure 5.1. Since garnet-peridotite/-pyroxenite has a different bulk rock composition than eclogite, separate pseudosections

should be created for both rock types. The comparison of eclogite pseudosections to garnet-peridotite/pyroxenite pseudosections could provide valuable information regarding the M1 proterozoic mantle and M2 Scandian peak-metamorphic PT conditions, as well as the differences between M1 and M2 mineral compositions in terms of elements.

6. Conclusion

The homogeneous chemical profiles for the elements Mg, Ca, Fe and Si (linescans) through minerals from the M1 assemblage most likely indicate that the most abundant elements were re-equilibrated by solid state diffusion during Scandian metamorphism. The assumed less mobile elements like Al in orthopyroxene and Cr in garnet were however not completely re-equilibrated, illustrated by lower amounts of Al in M2 orthopyroxene, Cr in M2 clinopyroxene and Cr in M2 garnet than in the same minerals from the M1 assemblage. New data from pseudosections however, show that Mg in garnet does not have to change in content when going from M1 proterozoic mantle to M2 scandian peak-metamorphic PT conditions. Suitable geothermometer/geobarometer combinations were selected based on the amount of spread they produced when applied to the M2 assemblage from different samples. The physical conditions (in terms of pressure and temperature) operating in the mantle rocks of the APM during crustal emplacement, when the coarse grained mantle wedge M1 porphyroclast assemblage recrystallized into a finer grained M2 assemblage are estimated to be 750±20 °C and 37±3 kbar using the geothermometer-geobarometer combination of T[OpxBK90] + p[BKN90] and T=742±58 °C, P=38.5±9.5 kbar using the combination of T[OpxBK90] + p[NimisTaylor00]. These PT conditions were derived by applying geothermobarometric calculations to the Scandian M2 recrystallized mineral assemblage. Applying the same geothermobarometric methods to the M1 assemblage yields similar results for the thermometers, but different results for the Al in orthopyroxene barometer of p[BKN90]. This leads to mismatch in PT results from geothermobarometry for the M1 assemblage and proves that the exact pre-Scandian PT conditions of the APM cannot be calculated using this method. The lower amount of Al in M2 opx than in M1 opx, combined with Al in opx geobarometry implies that the pre-Scandian pressure conditions in the APM were lower, indicating a possible prograde metamorphic path for the minerals in the APM after crustal emplacement during Scandian metamorphism. Cr in garnet was used to distinguish between M1 and M2 garnet: high-Cr M1 garnet recrystallized into low-Cr M2 garnet + M2 Cr-Spinel.

Acknowledgements

I would like to thank Herman L.M. van Roermund for supervising this MSc thesis and for helping me with any questions I had while working on this thesis. I would also like to thank M.J.C. Bouten for her help with the EMP analyses.

References

Beyer, E. E. (2006). Transformation of Archaean Lithospheric Mantle by Refertilization: Evidence from Exposed Peridotites in the Western Gneiss Region, Norway. *Journal of Petrology*, *47*(8), 1611–1636. doi:10.1093/petrology/egl022

Beyer, E. E., Brueckner, H. K., Griffin, W. L., & O'Reilly, S. Y. (2012). Laurentian Provenance of Archean Mantle Fragments in the Proterozoic Baltic Crust of the Norwegian Caledonides. *Journal of Petrology*, *53*(7), 1357–1383. doi:10.1093/petrology/egs019

Brey, G.P. & Koehler, T. (1990). Geothermobarometry in four-phase lherzolites II. New thermobarometers, and practical assessment of existing thermobarometers. Journal of Petrology 31, 1353–1378.

Brey, G. P., Koehler, T. & Nickel, K. G. (1990). Geothermobarometry in four-phase lherzolites I. Experimental results from 10 to 60 kbar. Journal of Petrology 31, 1313-1352

Brueckner, H. K. (1969). Timing of ultramafic intrusion in the Caledonides of Western Norway.pdf.

Brueckner, H. K., Carswell, D. a., & Griffin, W. L. (2010). The mantle and crustal evolution of two garnet peridotite suites from the Western Gneiss Region, Norwegian Caledonides: an isotopic investigation. *Lithos*, *117*(1-4), 1–19. doi:10.1016/j.lithos.2010.01.011

Brueckner, H. K., & van Roermund, H. L. M. (2004). Dunk tectonics: A multiple subduction/eduction model for the evolution of the Scandinavian Caledonides. *Tectonics*, *23*(2), n/a–n/a. doi:10.1029/2003TC001502

Brueckner, H., & Medaris, L. (2000). A general model for the intrusion and evolution of "mantle"garnet peridotites in high-pressure and ultra-high-pressure metamorphic terranes. *Journal of Metamorphic Geology*, 123–133. Retrieved from

Butler, J. P., Jamieson, R. a., Steenkamp, H. M., & Robinson, P. (2013). Discovery of coesite-eclogite from the Nordøyane UHP domain, Western Gneiss Region, Norway: field relations, metamorphic history, and tectonic significance. *Journal of Metamorphic Geology*, *31*(2), 147–163. doi:10.1111/jmg.12004

Carlson, W. D. (2006). Rates of Fe, Mg, Mn, and Ca diffusion in garnet. *American Mineralogist*, *91*(1), 1–11. doi:10.2138/am.2006.2043

Carswell, D. a. (1986). The metamorphic evolution of Mg□Cr type Norwegian garnet peridotites. *Lithos*, *19*(3-4), 279–297. doi:10.1016/0024-4937(86)90028-9

Cordellier, F. Boudier, F. & Boullier, A. M. (1981). Structural study of the Almklovdalen Peridotite Massif (Southern Norway), *Tectonophisics*, *77*, 257–281.

Dobrzhinetskaya, L., Eide, E., & Larsen, R. (1995). Microdiamond in high-grade metamorphic rocks of the Western Gneiss Region, Norway. …. doi:10.1130/0091-7613(1995)023<0597

Ellis, D.J. & Green, D.H. (1979). An experimental study of the effect of Ca upon garnet-clinopyroxene Fe-Mg exchange equilibria. Contributions to Mineralogy and Petrology 71, 13-22

Gee, D., Fossen, H., Henriksen, N., & Higgins, A. (2008). From the early Paleozoic platforms of Baltica and Laurentia to the Caledonide Orogen of Scandinavia and Greenland. *Episodes*, (March), 44–51.

Graham, D., & Midgley, N. (2000). TECHNICAL COMMUNICATION-Graphical Representation of Particle Shape using Triangular Diagrams: An Excel Spreadsheet Method. *Earth Surface Processes and …*, *1477*, 1473–1477.

Griffin, W.L. and Carswell, D.A. (1985). In situ metamorphism of Norwegian eclogites: an example. (In: *The Caledonide Orogen: Scandinavia and related areas*). Wiley. Pp. 813-822.

Griffin, W.L. and Qvale, H. (1985). Superferrian eclogites and the crustal origin of garnet peridotites, Almklovdalen, Norway. (In: *The Caledonide Orogen: Scandinavia and related areas*). Wiley. Pp. 803-812.

Hacker, B. (2007). Ascent of the ultrahigh-pressure Western Gneiss region, Norway. *Geological Society of America Special …*. doi:10.1130/2006.2419(09).

Hacker, B., & Andersen, T. (2010). High-temperature deformation during continental-margin subduction & exhumation: The ultrahigh-pressure Western Gneiss Region of Norway. *Tectonophysics*, *480*(1-4), 149–171. doi:10.1016/j.tecto.2009.08.012

Harley, S.L. (1984). An experimental study of the partitioning of Fe and Mg between garnet and orthopyroxene. Contributions to Mineralogy and Petrology 86, 353–373.

Hartz, E., & Torsvik, T. (2002). Baltica upside down: a new plate tectonic model for Rodinia and the Iapetus Ocean. *Geology*. doi:10.1130/0091-7613(2002)030<0255

Janák, M., Van Roermund, H., Majka, J., & Gee, D. (2013). UHP metamorphism recorded by kyanite-bearing eclogite in the Seve Nappe Complex of northern Jämtland, Swedish Caledonides. *Gondwana Research*, *23*(3), 865–879. doi:10.1016/j.gr.2012.06.012

Kostenko, O., Jamtveit, B., Austrheim, H., Pollok, K., & Putnis, C. (2002). The mechanism of fluid infiltration in peridotites at Almklovdalen, western Norway. *Geofluids*, *2*(3), 203–215. doi:10.1046/j.1468-8123.2002.00038.x

Krogh Ravna & Paquin (2003). Thermobarometric methodologies applicable to eclogites and garnet ultrabasites. *EMU notes on Mineralogy*. Vol. 5 (2003), chapter 8, 229-259.

Krogh Ravna, E. J., & Terry, M. P. (2004). Geothermobarometry of UHP and HP eclogites and schists - an evaluation of equilibria among garnet-clinopyroxene-kyanite-phengite-

coesite/quartz. *Journal of Metamorphic Geology*, *22*(6), 579–592. doi:10.1111/j.1525-1314.2004.00534.x

Kylander-Clark, A., & Hacker, B. (2007). Coupled Lu–Hf and Sm–Nd geochronology constrains prograde and exhumation histories of high-and ultrahigh-pressure eclogites from western Norway. *Chemical …*, *242*(1-2), 137–154. doi:10.1016/j.chemgeo.2007.03.006

Kylander-Clark, A. R. C., Hacker, B. R., Johnson, C. M., Beard, B. L., & Mahlen, N. J. (2009). Slow subduction of a thick ultrahigh-pressure terrane. *Tectonics*, *28*(2), n/a–n/a. doi:10.1029/2007TC002251

Kylander-Clark, A. R. C., Hacker, B. R., & Mattinson, J. M. (2008). Slow exhumation of UHP terranes: Titanite and rutile ages of the Western Gneiss Region, Norway. *Earth and Planetary Science Letters*, *272*(3-4), 531–540. doi:10.1016/j.epsl.2008.05.019

Lappin, M.A. (1974). Eclogites from the Sunndal-Grubse Ultramafic Mass, Almklovdalen, Norway and the T-P History of the Almklovdalen Masses *J. Petrology* (1974) 15 (3): 567-601 doi:10.1093/petrology/15.3.567

Medaris, L. G. (1980). Petrogenesis of the Lien peridotite and associated eclogites, Almklovdalen, Norway. *Lithos* 13, 339-353.

Medaris, L. M. (1984). A geothermobarometric investigation of garnet peridotites in the Western Gneiss Region of Norway. *Contributions to Mineralogy and Petrology*, 72–86. Retrieved from http://link.springer.com/article/10.1007/BF00371404

Medaris, L. G. (1999). Garnet Peridotites in Eurasian High-Pressure and Ultrahigh-Pressure Terranes: A Diversity of Origins and Thermal Histories. *International Geology Review*, *41*(9), 799–815. doi:10.1080/00206819909465170

Nimis, P., & Taylor, W. R. (2000). Single clinopyroxene thermobarometry for garnet peridotites. Part I. Calibration and testing of a Cr-in-Cpx barometer and an enstatite-in-Cpx thermometer. *Contributions to Mineralogy and Petrology*, *139*(5), 541–554. doi:10.1007/s004100000156

Nickel, K.G. & Green, D.H. (1985). Empirical geothermobarometry for garnet peridotites and implications for the nature of the lithosphere, kimberlites and diamonds. Earth Planetary Science Letters 73, 158–170.

Osland. (1997). Modelling of variations in Norwegian olivine deposits; Causes of variation and estimation of key quality factors. *NTU Trondheim.*

Pijpers, J. (2012). Refertilisation of the Almklovdalen dunite body at the north of Gusdal Quarry locality, Western Gneiss Region, Norway., (3221660).

Powell, R. (1985). Regression diagnostics and robust regression in geothermometer/geobarometer calibration: the garnet-clinopyroxenc geothennometer revisited. Journal of Metamorphic Geology 3, 231-43.

Prelicz, R. M. (2005). Seismic anisotropy in peridotites from the Western Gneiss Region (Norway) DISS. ETH Nr.16176.

Roberts, D. (2003). The Scandinavian Caledonides: event chronology, palaeogeographic settings and likely modern analogues. *Tectonophysics*, *365*(1-4), 283–299. doi:10.1016/S0040-1951(03)00026-X

Rosenthal, A., Yaxley, G. M., Green, D. H., Hoefer, H. E., Hermann, J., & Spandler, C. S. (2008). New insights into the genesis of peridotite-pyroxenite layers : Western Gneiss Region , Norway, (9), 3–5.

Scambelluri, M., Van Roermund, H. L. M., & Pettke, T. (2010). Mantle wedge peridotites: Fossil reservoirs of deep subduction zone processes. *Lithos*, *120*(1-2), 186–201. doi:10.1016/j.lithos.2010.03.001

Smith, D. C., & Godard, G. (2013). A Raman spectroscopic study of diamond and disordered sp 3 -carbon in the coesite-bearing Straumen Eclogite Pod, Norway. *Journal of Metamorphic Geology*, *31*(1), 19–33. doi:10.1111/jmg.12007

Spengler, D., & Brueckner, H. (2009). Long-lived, cold burial of Baltica to 200 km depth. *Earth and Planetary …*, *281*(1-2), 27–35. doi:10.1016/j.epsl.2009.02.001

Spengler, D., Roermund, H. Van, & Drury, M. (2006). Deep origin and hot melting of an Archaean orogenic peridotite massif in Norway. *Nature*, *440*(7086), 913–917. doi:10.1038/nature04644

Van Roermund, H.L.M. (1998). Ultra-high pressure (P> 6 GPa) garnet peridotites in Western Norway: exhumation of mantle rocks from> 185 km depth. *Terra Nova*, 295–301.

Van Roermund, H.L.M. (2009). Mantle-wedge garnet peridotites from the northernmost ultra-high pressure domain of the Western Gneiss Region, SW Norway. *European Journal of Mineralogy*, *21*(6), 1085–1096. doi:10.1127/0935-1221/2009/0021-1976

Van Roermund, H.L.M. (2009). progress in Scandian ultrahigh-pressure metamorphism in the northernmost domain of the Western Gneiss Complex, SW Norway: continental subduction down to 180. *Journal of the Geological Society*, *166*(4), 739–751. doi:10.1144/0016-76492008-020

Van Roermund, H.L.M. & Carswell, D. (2002). Microdiamonds in a megacrystic garnet websterite pod from Bardane on the island of Fjørtoft, western Norway: evidence for diamond formation in mantle rocks during deep continental. …. doi:10.1130/0091-7613(2002)030<0959

Vrijmoed, J. C., Smith, D. C., & van Roermund, H. L. M. (2008). Raman confirmation of microdiamond in the Svartberget Fe-Ti type garnet peridotite, Western Gneiss Region, Western Norway. *Terra Nova*, *20*(4), 295–301. doi:10.1111/j.1365-3121.2008.00820.x

Wang, Q., Xia, Q.-K., O'Reilly, S. Y., Griffin, W. L., Beyer, E. E., & Brueckner, H. K. (2013). Pressure- and stress-induced fabric transition in olivine from peridotites in the Western Gneiss Region (Norway): implications for mantle seismic anisotropy. *Journal of Metamorphic Geology*, *31*(1), 93–111. doi:10.1111/jmg.12011